

**Experimental and Numerical Study on Mode II
Delamination Behavior of Stitched CFRP Laminate**

縫合 CFRP 複合材のモード II 層間剥離についての実験
および数値解析的研究

Jonny Herwan

Department of Aerospace Engineering

Graduate School of System Design

Tokyo Metropolitan University

March 2016

Experimental and Numerical Study on Mode II Delamination Behavior of Stitched
CFRP Laminate

縫合 CFRP 複合材のモード II 層間剥離についての実験
および数値解析的研究

by

Jonny Herwan
Student ID 12991571

Submitted to the Department of Aerospace Engineering,
Graduate School of System Design,
in partial fulfillment of the requirements for the degree of
Doctor of Philosophy in Aerospace Engineering
at
TOKYO METROPOLITAN UNIVERSITY
March 2016

Certified by advisor

Professor Naoyuki Watanabe
Department of Aerospace Engineering
Graduate School of System Design
Tokyo Metropolitan University

Doctoral thesis committee:

Professor Naoyuki Watanabe
Professor Hiroshi Suemasu
Professor Koichi Kitazono
Professor Satoshi Kobayashi

Tokyo Metropolitan University (Chairman)
Sophia University
Tokyo Metropolitan University
Tokyo Metropolitan University

Abstract

Carbon fiber reinforced plastics (CFRP) possess a superb strength and stiffness to weight ratio, thus have been used increasingly for light weight structures. However, conventional CFRP are very weak in the thickness direction and prone to be delaminated on interlaminar surfaces. To overcome this issue, stitching technique has been attracted a lot of attention. This dissertation aims to evaluate mode II (shear mode) delamination of stitched composites through experiment and finite element simulation. Based on literature review, evaluating mode II delamination behavior of stitched composites is facing a serious problem. The testing specimens were failed before crack propagation. Considering this issue, a modified method called tabbed end notched flexure (TENF) test is proposed and the effects of stitching parameters are investigated. It is found that the laminate with maximum stitch density and stitch thread thickness in this study have energy release rate 2.4 times of those unstitched one. To understand the crack bridging mechanism, a single stitched laminate under shear loading has also been investigated using a novel test called interlaminar shear test (IST). Based on this test, finite element simulation of TENF test has been developed. Using cohesive element (to simulate crack propagation plane) and spring connector element (to present the stitch thread), high accuracy of finite element modeling was achieved. Finally, the finite element model is extended to understand stitched laminate behavior under four point end notched flexure (4ENF) and quasi static indentation test.

Keywords: Mode II delamination, energy release rates, end notched flexure test, 3D reinforcement, stitching, finite element modelling, cohesive zone model

Contents

Abstract	iii
Contents	iv
List of Figures	vii
List of Tables	xi
Nomenclature	xiii
Chapter 1	1
Introduction	1
1.1 Background and Literature Review	1
1.1.1 Suppressing Delamination by Stitch Threads	3
1.1.2 Mode II Delamination Testing of Stitched Composites.....	4
1.1.3 Numerical Study of Mode II Delamination Testing	6
1.1.4 Finite Element Simulation of Low Velocity Impact Induced Delamination of Stitched Composites.....	7
1.2 Objectives of Dissertation	8
1.3 Layout of Dissertation.....	9
Chapter 2	11
Effect of stitching parameters on mode II delamination behavior of stitched composites	11
2.1 Overview	11
2.2 Experimental Work	11
2.2.1 Material and Specimen Preparation.....	11
2.2.2 Test Method	14
2.2.3 Data Reduction	18
2.2.4 Measurement of Local Fiber Volume Fraction	19
2.2.4.1 Fiber Compaction due to Stitching Process	19
2.2.4.2 Effect of Local Fiber Volume Fraction on Energy Release Rates ...	20
2.2.4.3 Measurement Method of Local Fiber Volume Fraction.....	21
2.3 Results and Discussion.....	22
2.3.1 Load-displacement Curves	22
2.3.2 Energy Release Rates	25
2.3.3 Fiber Compaction Effects	33
2.4 Conclusions	34
Chapter 3	35
Finite Element Analysis of Tabbed End Notched Flexure (TENF) Test	35
3.1 Overview	35
3.2 Interlaminar Shear Test (IST).....	35
3.2.1 Experimental Method	35
3.2.2 Finite Element Simulation of Interlaminar Shear Test	37
3.3 Finite Element Simulation of Tabbed End Notched Flexure Test.....	39
3.4 Results and Discussion.....	43
3.5 Conclusions	60
Chapter 4	61
Feasibility Study of Using Four Point End Notched Flexure (4ENF) Test for	

Stitched Laminate Application	61
4.1 Overview	61
4.2 Modeling Techniques	61
4.2.1 Finite Element Model	61
4.2.2 Investigating Laminate Failure during 4ENF Test	64
4.2.3 Predicting of Energy Release Rates	65
4.3 Results and Discussions	65
4.3.1 Load-displacement Curves	65
4.3.2 Laminate Failure Possibility during 4ENF Test	72
4.3.3 Energy Release Rates Prediction	79
4.4 Conclusions	80
Chapter 5	83
Conclusions and Recommendations	83
5.1 Conclusions	83
5.2 Recommendations	83
References	87
Appendix A. Predicting Damage in Stitched Composites under Quasi Static Indentation Test	101
A.1 Overview	101
A.2 Modelling Techniques	101
A.3 Results and Discussions	104
A.4 Conclusions	113
Appendix B. User Subroutine for Matrix Crack Simulation	114
Appendix C. Derivation of Equation 2.2	115
Acknowledgements	117

List of Figures

Figure 1.1: Composites as primary structure of Boeing 787 Dreamliner.....	1
Figure 1.2: CFRP body frame of BMW – 7 Series.....	2
Figure 1.3: (a) Stitching process by Toyota Industries. Co. Ltd. [11], (b) Cross-section of typical final product of stitched laminate	3
Figure 1.4: Types of delamination modes.....	4
Figure 1.5: Types of mode II delamination test; (a) End notched flexure (ENF), (b) Stabilized end notched flexure (SENF), (c) End loaded split (ELS), (d) Four point end notched flexure (4ENF).....	5
Figure 1.6: Types of impact loading [49]	8
Figure 2.1: Modified-lock stitching (a) Schematic pattern, (b) A 3×3 mm stitched composite laminate with ENF specimen cutting position	13
Figure 2.2: A schematic premature failure of stitched composite during ENF test (courtesy of JAXA)	15
Figure 2.3: Tabbed end notched flexure (TENF) specimen set-up with a specific crack tip position.....	16
Figure 2.4: Mode II delamination test set-up	17
Figure 2.5: Normalized maximum interface shear stress at the loaded fibers end of a pull-out test simulation (data from: Fu <i>et al.</i> [82]).....	21
Figure 2.6: Schematic of the cutting method used for sample burn-off tests.....	22
Figure 2.7: Typical load–displacement pattern for (a)Unstitched laminate (b)Stitched 6x6 200D (c)Stitched 6x6 500D (d)Stitched 3x3 200D and (e)Stitched 3x3 500D	23
Figure 2.8: Tested specimen of stitched 6×6 mm and 500 denier thread thickness	24
Figure 2.9: Crack propagation planes of all specimen types at pre-crack regions	25
Figure 2.10: Typical specimen compliance curve in terms of C/C_0 versus $(a/L)^3$	26
Figure 2.11: R curves for (a)Unstitched laminate (b)Stitched 6x6 200D (c)Stitched 6x6 500D (d)Stitched 3x3 200D and (e)Stitched 3x3 500D	31
Figure 2.12: Average values of critical energy release rates (G_{IIc}) for crack lengths of 25 mm and 45 mm.....	32
Figure 2.13: Local fiber volume fractions (V_{fl}) for each specimen type obtained by burn-off tests.....	33
Figure 3.1: Interlaminar shear test specimen.....	37

Figure 3.2: Interlaminar shear test set-up	37
Figure 3.3: Cross-sectional of stitch thread composites at the interface of middle layers	38
Figure 3.4: Half model (lower part) of IST specimen	39
Figure 3.5: Convergence check of the elements sizes	39
Figure 3.6: TENF experimental set up	41
Figure 3.7: TENF modeling geometry	42
Figure 3.8: Load-displacement curve obtained by IST of single stitched laminate	44
Figure 3.9: Fracture surface of interlaminar shear test specimen.....	44
Figure 3.10: Stitching process with Kapton film at the middle layer.....	45
Figure 3.11: Micro-CT image of IST specimen after different loading	45
Figure 3.12: Load displacement curve of experimental and numerical results.....	47
Figure 3.13: Global coordinate system of IST simulation.....	47
Figure 3.14: Displacement and stress distribution at delaminated surface (90° layer) of the moving part, under 10.5 N loading (a)Displacement in x-direction (b)Normal stress along fibers direction (c)In-plane shear stress (d)Normal stress perpendicular to fibers direction	48
Figure 3.15: Displacement and stress distribution at delaminated surface (90° layer) of moving part, under 21.3 N loading (a)Displacement in x-direction (b)Normal stress along fibers direction (c)In-plane shear stress (d)Normal stress perpendicular to fibers direction	49
Figure 3.16: Displacement and stress distribution at delaminated surface (90° layer) of moving part, under 180.5 N loading (a)Displacement in x-direction (b)Normal stress along fibers direction (c)In-plane shear stress (d)Normal stress perpendicular to fibers direction	50
Figure 3.17: Effects of critical interfacial strength.....	51
Figure 3.18: Effects of viscosity coefficient of the cohesive element.....	52
Figure 3.19: Effects of interfacial stiffness.....	53
Figure 3.20: Effects of number of stitch rows at the crack region	54
Figure 3.21: Load displacement curve with number of active stitch thread at crack region.....	55
Figure 3.22: Crack propagation length vs. displacement	56
Figure 3.23: Delamination indicator (a) At the crack length of 38 mm (b) At the crack length of 50 mm	56
Figure 3.24: Finite element simulation of TENF at the crack length of 50 mm (a) Deflection- U_3 (b) Normal stress along fiber direction- S_{11}	57

Figure 3.25: Finite element simulation of TENF at the crack length of 50 mm (a) Normal stress perpendicular to fiber direction- S_{22} (b) In-plane shear stress- S_{12}	58
Figure 3.26: Predicting stitch thread deformation during TENF test	59
Figure 4.1: Set-up of tabbed 4ENF test	62
Figure 4.2: Finite element model of Tabbed 4ENF test.....	63
Figure 4.3: Detail modelling techniques of Tabbed 4ENF test	64
Figure 4.4: Predicted load-displacement curve of unstitched unidirectional laminate under 4ENF test.....	66
Figure 4.5: Simulation results of unstitched unidirectional laminate under 4ENF test (a) Deformation (b) Delamination propagated till 48.5 mm length	66
Figure 4.6: Predicted load-displacement curve of unstitched multidirectional laminate under 4ENF test.....	67
Figure 4.7: Simulation results of unstitched multidirectional laminate under 4ENF test (a) Deformation (b) Delamination propagated till 48.5 mm length	67
Figure 4.8: Predicted load-displacement curve of stitched laminate under 4ENF test...	69
Figure 4.9: Simulation results of stitched multidirectional laminate under 4ENF test (a) Deformation (b) Delamination propagated till 48.5 mm length	69
Figure 4.10: Predicting stitch thread deformation during 4ENF test	70
Figure 4.11: Predicted load-displacement curve of stitched laminate under Tabbed 4ENF	70
Figure 4.12: Simulation results of stitched multidirectional laminate under T4ENF test (a) Deformation (b) Delamination propagated till 48.5 mm length	71
Figure 4.13: Predicting stitch thread deformation during T4ENF test	72
Figure 4.14: Normal stress along fiber direction (σ_{xx}) of unstitched unidirectional laminate	73
Figure 4.15: Normal stress perpendicular to fiber direction (σ_{yy}) of unstitched unidirectional laminate.....	74
Figure 4.16: In plane shear stress (σ_{xy}) of unstitched unidirectional laminate	74
Figure 4.17: Normal stresses perpendicular to fibers direction- S_{22} (a) Stitched laminate without tabs (b) Stitched laminate with tabs	76
Figure 4.18: Normal stress perpendicular to fiber direction at each layer	76
Figure 4.19: In-plane shear stresses- S_{12} (a) Stitched laminate without tabs (b) Stitched laminate with tabs	77
Figure 4.20: In-plane shear stress at each layer.....	77
Figure 4.21: Normal stresses along fibers direction- S_{11} (a) Stitched laminate without	

tabs (b) Stitched laminate with tabs	78
Figure 4.22: Normal stress in fiber direction.....	79
Figure 4.23: Compliance vs. crack length	80
Figure A.1: Finite element model of quasi static indentation.....	103
Figure A.2: Finite element model of open-hole tension test	104
Figure A.3: Open hole simulation of unidirectional 0° laminate (a) Normal stress along fibers direction (b) Normal stress perpendicular to fibers direction (c) Matrix crack	105
Figure A.4: Open hole simulation of unidirectional 90° laminate (a) Normal stress along fibers direction (b) Normal stress perpendicular to fibers direction (c) Matrix crack	106
Figure A.5: QSI simulation results of unstitched laminate (a) Deformation (b) Normal stress along fibers direction (c) In-plane shear stress (d) Normal stress perpendicular to fiber direction	108
Figure A.6: QSI simulation results of stitched laminate (a) Deformation (b) Normal stress along fibers direction (c) In-plane shear stress (d) Normal stress perpendicular to fiber direction	109
Figure A.7: Load-displacement of quasi static indentation results.....	110
Figure A.8: Delamination area at indentation depth of 1.8 mm (a) Experiment [61], ..	111
Figure A.9: Effect of matrix tensile strength on QSI results	112
Figure A.10: Effect of materials degradation rule on QSI results	113

List of Tables

Table 2.1: Types of test specimens	14
Table 2.2: Parametric study of tab thickness	16
Table 2.3: Detail data of each specimens	28
Table 3.1: Mechanical properties of matrix and carbon fiber.....	36
Table 4.1: Mechanical properties of laminae.....	62
Table 4.2: Parametric study of matrix crack.....	78
Table 4.3: Energy release rate prediction	80
Table A.1: Mechanical properties of lamina [108]	102
Table A.2: Cohesive contact parameters [69].....	104

Nomenclature

E	Elastic modulus
G	Shear modulus
ν	Poisson's ratio
SD	Stitch density
Sp	Stitch pitch
Ss	Stitch space
V_f	Fiber volume fraction of composites
V_{fl}	Local fiber volume fraction of tow
G_{II}	Mode II energy release rates
P	Load
C	Specimen compliance at certain crack length
C_0	Specimen compliance without crack
m	Slope of compliance vs. crack length
a	Crack length
w	Specimen width
L	Half-length of testing span
σ_i	Stress component under pure modes I, II and III
σ_i^0	Critical interfacial strength under pure modes I, II and III
G_n	Energy release rates in normal (mode I) direction
G_s	Energy release rates in shear (mode II) direction
G_t	Energy release rates in tearing (mode III) direction
G_i^c	Critical energy release rate in i - direction (mode I, II, or III)
K	Stiffness of cohesive element or cohesive contact
μ	Viscosity coefficient of cohesive zone element
Y_T	Matrix tensile strength
S_{xy}	Matrix in-plane shear strength
S_{yz}	Matrix out of plane shear strength

Chapter 1

Introduction

1.1 Background and Literature Review

Carbon fiber reinforced plastics (CFRP) possess a superb strength and stiffness to weight ratio. These exceptional properties meet the requirement for more economic fuel consumption. Therefore, the use of CFRP for main structures is increasing tremendously, particularly in aircraft and automotive structures (Figure 1.1 and 1.2).

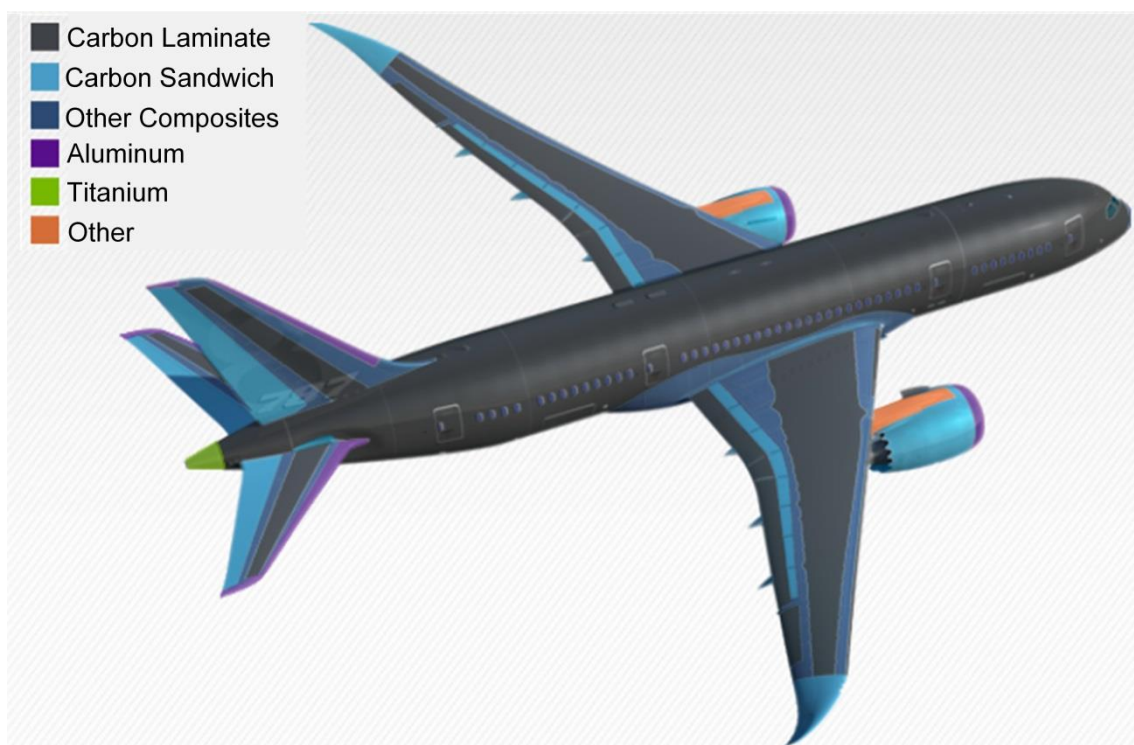


Figure 1.1. Composites as primary structure of Boeing 787 Dreamliner

However, CFRP laminate are very weak in the thickness direction and prone to be delaminated at interlaminar. To overcome this issue, 3D reinforcements [1, 2] such as

braiding [1, 3], knitting [4], stitching [5-7] and z-pinning [8, 9] were attracted a lot of attention. Stitching is one of promising method which conducted by insertion of threads into the preforms in the thickness direction prior to resin infusion and consolidation, as shown in Figure 1.3(a). A cross section of typical final product of stitched laminate manufactured by Toyota Industries Co. Ltd. is depicted in Figure 1.3(b). Although 3D reinforcement has negative effect on in-plane properties, due to resin rich region at vicinity of 3D reinforcements, latest review by Mouritz and Cox [6] concluded that stitching has less negative effect on in-plane properties compared to z-pinning. Furthermore, Scarponi et al. [10] evaluate compression after impact performance of composite laminate with stitching, tufting and z-pinning, and concluded that stitching performs the best damage tolerance to manufacturing cost ratio.



Figure 1.2. CFRP (the black portions) on body frame of BMW – 7 Series

(Provided by BMW)

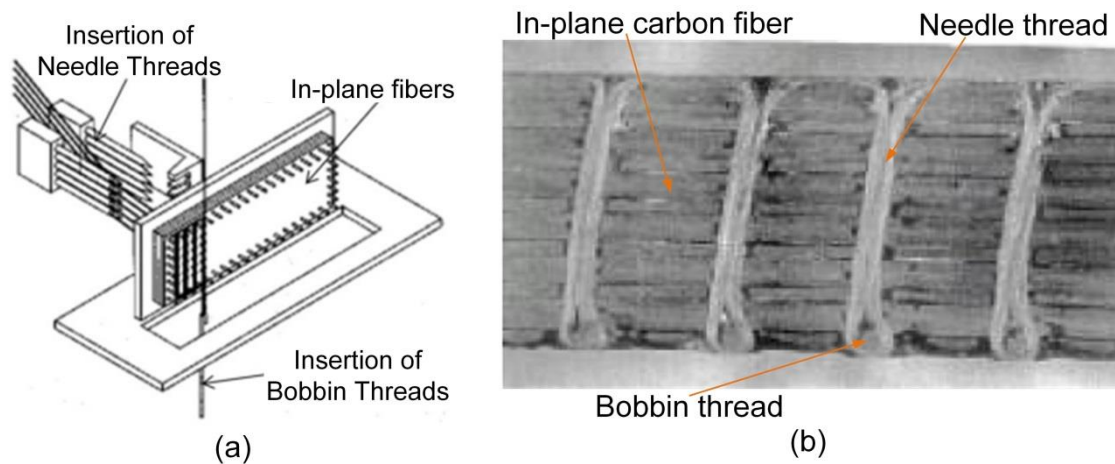


Figure 1.3. (a) Stitching process by Toyota Industries. Co. Ltd. [11], (b) Cross-section of typical final product of stitched laminate

1.1.1 Suppressing Delamination by Stitch Threads

The existence of stitch threads in composite laminates increases opening mode delamination toughness by shielding the crack tip from full effect of crack opening stress, thus reduces the crack propagation zone [12-18]. Mode I (opening mode) energy release rate (G_{IC}) in stitched laminate could reach 15 times that of unstitched laminate, depending on the type and diameter of the stitch thread, stitch density, and stitch distribution. In case of mode II delamination, stitch threads retain the sliding displacement, thereby increase the energy release rate (G_{IIC}) [19-25]. Moreover, stitching is also proven to be an effective reinforcement of composite laminates subjected to mixed mode loading [26-28]. A brief description of delamination modes are depicted in Figure 1.4.

Although stitched laminate shows a slight decreasing on in-plane mechanical properties [6, 29], the extensive improvement on delamination toughness surpasses this minor drawback. Therefore, many researchers are interesting on further applications of stitching, such as T-joints [30-32], and lap-joints [33-36].

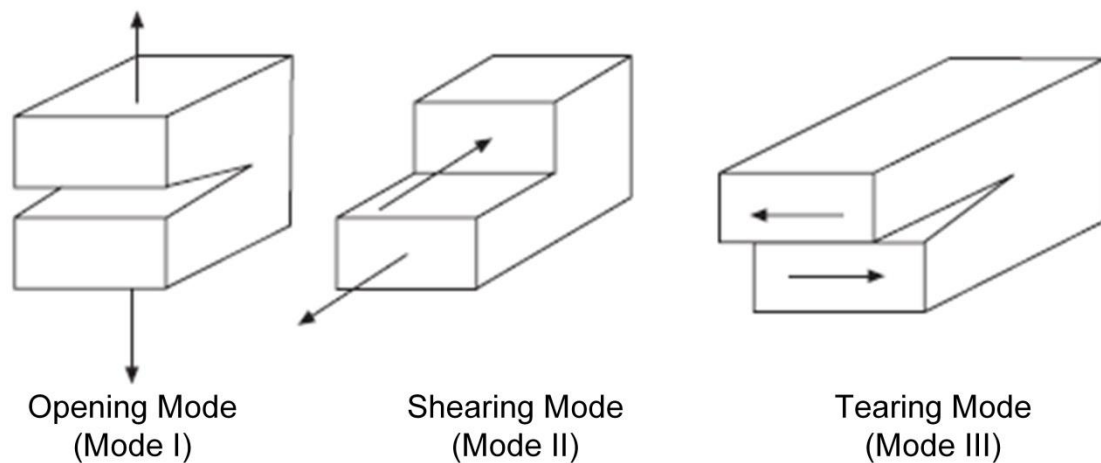


Figure 1.4. Types of delamination modes

1.1.2 Mode II Delamination Testing of Stitched Composites

It is important to be noted that international consensus on the standard procedure of mode II delamination testing of composite laminate has not been achieved, even though collaborative work has been conducted in 1996 by ESIS (European Structural Integrity Society), JIS (Japan Industrial Standards) group, ASTM (American Society for Testing and Materials) [37]. In this international round robin, four types of shear mode delamination testing were investigated in term of results consistency, simplicity of test configuration and crack propagation stability. Those four testing methods (Figure 1.5) are end notched flexure (ENF), stabilized end notched flexure (SENF), end loaded split (ELS), and four point end notched flexure (4ENF) test. The team summarized that ENF is simple but unstable, on the other hand ELS and SENF provide stable crack but not simple. Finally 4ENF showed good stability and simplicity, but still has little experience. Therefore, the situation in 2003 seemed clear that 4ENF test become the standard test. However, the group (Martin and Davidson) who proposed the 4ENF test [38] continued their work particularly on evaluating four factors; loading roller diameter, specimen

geometry, friction, and fixture compliance. Latest review on those prospective standard procedures has also been reported by Brunner *et al.* [39]. Up to now only a local standard method already existed which is Japanese Industrial Standard JIS K 7086) [40]. Meanwhile, European Structural Integrity Society has proposed a draft European Standard called EN 6034. Both of JIS K 7086 and draft EN 6034 are using ENF testing method.

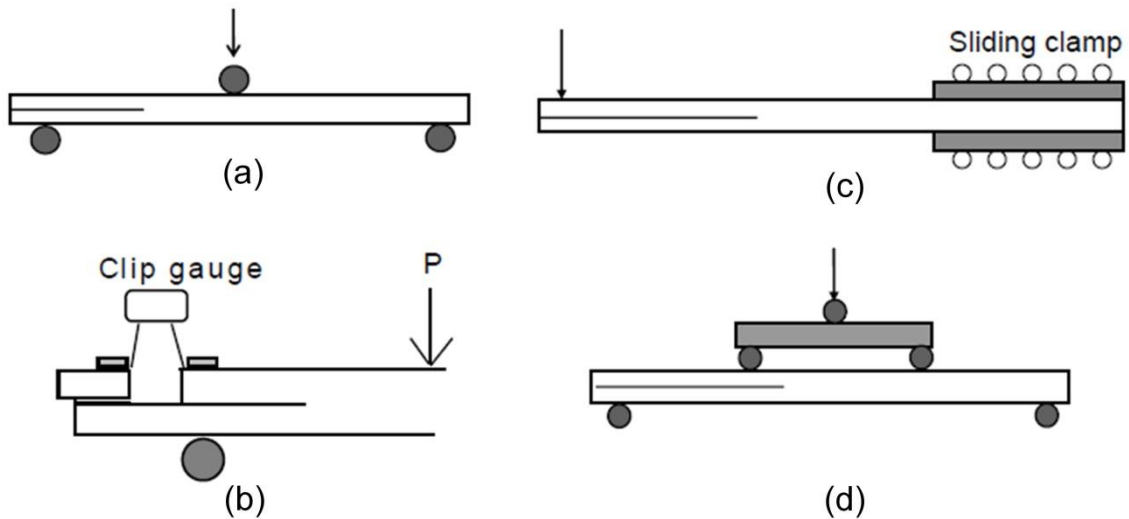


Figure 1.5. Types of mode II delamination test; (a) End notched flexure (ENF), (b) Stabilized end notched flexure (SENF), (c) End loaded split (ELS), (d) Four point end notched flexure (4ENF)

Despite of no international consensus on standard test method, a few works on evaluating mode II delamination of stitched composites have been reported. The first experimental work on stitched composites was reported by Sankar and Sharma [21]. Kevlar and glass fibers were used as stitch threads in unidirectional CFRPs, and the existence of stitch threads increased the energy release rates (G_{IIC}) by between five and eight times. Generally, G_{IIC} values increased with increasing stitch density, except for

Glass-750 stitch thread, where optimum stitch density was probably achieved at the level 2.48 stitches/cm². The area method with compliance of the unloading curve was applied to calculate G_{IIC} . Jain *et al.* [22] reported that the G_{IIC} values were improved by up to 3.3 times when Kevlar and Carbon T-900 were used as stitch threads. Stitch density and stitch thread thickness did not affect G_{IIRi} (initial energy release rate) but had considerable effects on G_{IIRs} (steady-state energy release rate). It was also reported that, in some specimens, compression failure occurred at the stitch lines closest to the central loading pin. To avoid premature failure, Wood *et al.* [24] used tabbed end notch flexural (TENF) specimens, embedding aluminum 2024 T3 sheets of 2 mm thickness at both the upper and lower surfaces of specimens. In their experiment, liquid crystal polymers (1500 denier) were stitched on satin weave carbon fibers with epoxy matrices. They reported that the energy release rates of stitched composites were 2.25 times those of unstitched composites, and were negligibly affected by stitch distribution.

1.1.3 Numerical Study of Mode II Delamination Testing

Predicting delamination behavior of stitched composites using finite element simulation has also attracted a lot of attention. Chen *et al.* [41] predicted the effective energy release rate of stitched composites under mode II loading using a J-integral contour. The interaction of a stitch with the surrounding laminates was idealized as an elastic–perfectly plastic relationship and represented by very short bar elements in a three-dimensional finite element model. It was concluded that the effective energy release rate depends strongly on the crack length and the number of stitches in the bridging zone. However, the predicted energy release rates were not compared with experimental data. Another numerical study was reported by Wood *et al.* [24] who used

a method called the virtual crack closure technique (VCCT). A stitch was modelled as a spring–damper system composed of three connected rods. A numerical parametric study was conducted to obtain the force–displacement relationship for single-stitched laminates under pure shear loading. The stitch thread and matrix properties were taken as input. This parametric study considered stitch failure at the surface loop, so the frictional force of thread pull-out was taken into account. The predicted energy release rates were close to those determined experimentally (with an error less than 9%). It is important to be noted that the force-displacement relationship of single stitched proposed by Wood *et al.* [24] had different bridging mechanism with the one reported by Chen *et al.* [41].

During the last two decades, the use of the cohesive zone model (CZM) to simulate damage in composite materials has expanded rapidly. Compared with VCCT, CZM can predict both damage initiation and propagation, whereas VCCT can only be used to simulate damage propagation. Therefore, CZM has become widely used to simulate not only all the modes of delamination testing [42-44], but also composite structures (e.g. π and T joints [45, 46]), damage in open hole testing [47, 48] and many other situations. However, modeling of mode II delamination test of stitched composites using CZM has not been reported yet.

1.1.4 Finite Element Simulation of Low Velocity Impact Induced Delamination of Stitched Composites

Serge Abrate [49] classifies types of impact loading into low, intermediate, and high velocity impact (ballistic impact) as shown in Figure 1.6. In case of low velocity impact loading, the damage mechanisms are usually can be understood through quasi

static indentation test.

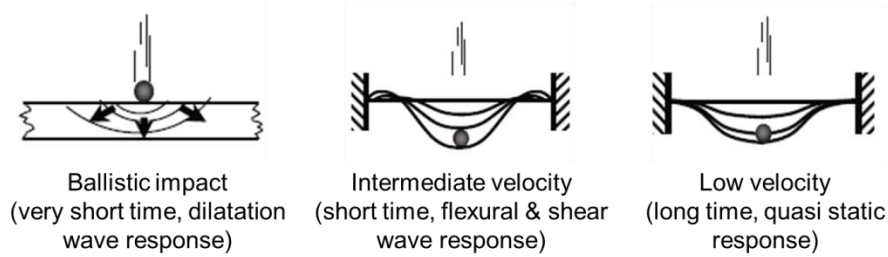


Figure 1.6. Types of impact loading [49]

Both quasi static indentation (QSI) and low velocity impact (LVI) of stitched composites have already investigated experimentally [50-60]. However, the numerical study of such testing for stitched laminate is very limited. In case of unstitched laminate, many approaches have been proposed to simulate QSI and LVI [61-69]. Among them, the latest report [68, 69] seems to be an effective and efficient approach which use surface based cohesive contact to predict delamination area. Cohesive contact models reduce time consuming because it omits special elements for cohesive zone, and it can be combined with friction contact simultaneously. It is worth noted that the friction force is useful to capture the influence of through thickness compressive stresses during LVI or QSI.

1.2 Objectives of Dissertation

This dissertation aims to understand the effectiveness of stitching process on improving mode II delamination behavior of composite laminate.

The detail objectives of this dissertation are listed below:

1. To establish an experimental method for mode II delamination test that can

overcome the problem of specimen premature failure during the test

2. To investigate the effect of stitching parameters on mode II energy release rates (G_{IIC}), particularly for stitch thread materials called Vectran
3. To understand crack bridging mechanism, deformation and fracture of single stitched laminate under pure shear loading
4. To provide reliable finite element model that can be used as general tools to evaluate any related testing on mode II delamination behavior of stitched laminates such as end notched flexure (ENF), four point end notched flexure (4ENF), and quasi static indentation test.

1.3 Layout of Dissertation

This dissertation is presented in five chapters as follows:

The current chapter, Chapter 1, presents an introduction including literature review, background and objectives of this dissertation. Literature study focuses on stitch bridging mechanism to increase delamination toughness, experimental and numerical study on mode II delamination test, and finite element analysis of low velocity impact induced delamination of stitched composites.

Chapter 2 describes investigation on the effects of stitching parameters (stitch density and stitch thread thickness) on mode II delamination behavior. A relatively new stitch threads material namely Vectran is used. To avoid premature failure of specimens, a modified method called tabbed end notched flexure (TENF) test is used. Furthermore, considering the strong relation between fiber volume fractions and energy release rate, burn-off test is also conducted to measure local fiber volume fraction.

Chapter 3 demonstrates a finite element simulation of tabbed end notched

flexure (TENF) test. In this FE model, the interaction between stitch threads and composite laminate become most important. Therefore, a novel interlaminar shear test (IST) of single stitched laminate is performed. The load displacement curve that obtained by IST is then applied to FE model using spring connector element. Moreover, cohesive zone elements are used to simulate crack propagation. A parametric study is also conducted to find suitable cohesive zone parameters. Finally, the simulation results are verified with the experimental data.

Chapter 4 presents a numerical study of using four point end notched flexure (4ENF) test for stitched laminate application. Adopting the modeling techniques in the previous chapter, the capability of using 4ENF test with and without tabs is evaluated. The results accuracy of tabbed 4ENF is also investigated by comparing the predicted energy release rates with the results of simulation without tabs.

Chapter 5 summarizes the dissertation with conclusion and recommendation for future research.

Additionally, a numerical study on delamination behavior of stitched laminate under quasi static indentation is also reported in appendix. This simulation is the extension of the main topic where mode II delamination behavior plays the main rule of damage propagation.

Chapter 2

Effect of stitching parameters on mode II delamination behavior of stitched composites

2.1 Overview

This chapter aims to investigate the effect of stitch thread density and stitch thread thickness for particular stitch thread material namely Vectran. In order to avoid premature failure of specimen during testing, tabbed end notched flexure (TENF) specimen is used. TENF specimens are manufactured by embedded aluminum plates Al 7075-T6 at top and bottom side of the specimen. Four types of stitched laminate are tested with two different stitch densities (3 x 3 mm and 6 x 6 mm) and two different stitched thread thicknesses (200 and 500 denier). Unstitched laminates are also fabricated for comparison. Furthermore, the effect of local fiber volume fraction on mode II delamination behavior is also investigated. The local fiber volume fractions of stitched and unstitched specimen are measured using burn-off test.

2.2 Experimental Work

2.2.1 Material and Specimen Preparation

Both unstitched and stitched composite laminates used in this test were made with T800SC-24K (Toray Industry), and follow the same lay-up as our group's previous work on mode I delamination testing [15], which is 24-ply quasi-isotropic (+45/0/-45/90)_{3S}. Toyota Industries Corporation fabricated the stitched composite laminates using their patented modified lock stitching process [11], as shown in Figure

1.3(a). Using this technique, multi-directional (MD) laminate is preferable because it exhibits minimal fiber waviness compared with unidirectional (UD) laminate. The multi-directional preformed fibers can be stretched in many directions during the stitching process to restrain the fiber waviness. It is worth minimizing the fiber waviness in mode II delamination test specimens because it affects the results by slip-locking [70] and emerging mode I processes. Therefore, quasi-isotropic laminates were used in this experimental work.

To investigate the effect of stitch thread thickness, two fibers linear densities were used (200 denier and 500 denier, equal to 0.0158 mm² and 0.0394 mm² cross-sectional areas, respectively). Meanwhile the effects of stitch density were evaluated by manufacturing different types of specimens: so-called moderately and densely stitched laminates. Both types have different stitch spacing (S_s) and stitch pitch (S_p), as illustrated in Figure 2.1(a). These moderately and densely stitched laminates had $S_s \times S_p$ values of 6 × 6 mm, and 3 × 3 mm, respectively. The stitch density (SD) of the laminates can be calculated using the following expression:

$$SD = \frac{1}{S_s \times S_p} \quad (2.1)$$

Kapton film was inserted between the middle layers of the laminates to facilitate the initial crack, and stitching did not occur in the specimen area where the film was inserted, as described in Figure 2.1(b).

After the stitching process, XNR/H6813 Denatite resin (Nagase Chemtex Corp.) was used to consolidate the composite laminates using a vacuum-assisted resin transfer molding technique. The same process was used to manufacture the unstitched laminates, but a wider area was left unstitched, so that the total thickness remained similar between the stitched and unstitched laminates (the average thickness was 5.16 mm).

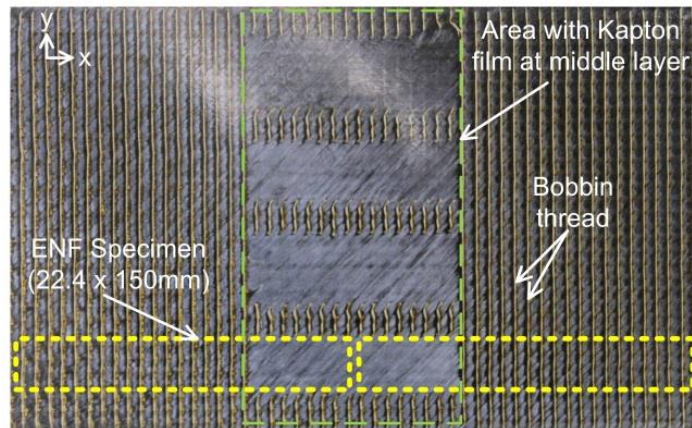
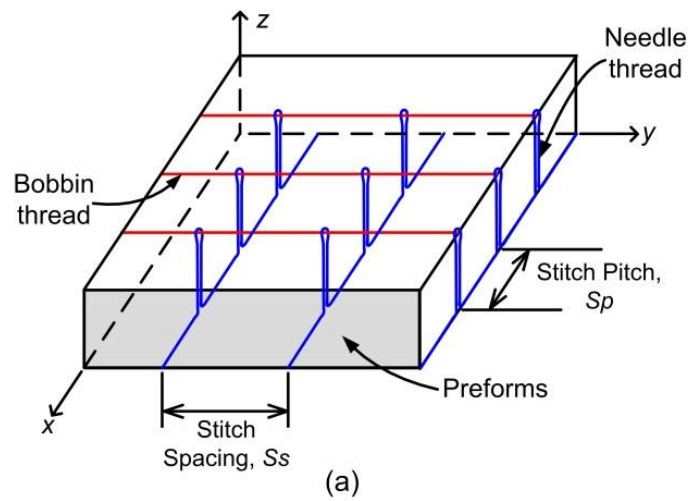


Figure 2.1: Modified-lock stitching (a) Schematic pattern, (b) A 3×3 mm stitched composite laminate with ENF specimen cutting position

The specimens were cut from the plates using a water-cooled cutting machine (AC-400CF, Maruto) and were 22.4 mm wide and 150 mm long. Five types of specimens were prepared (Table 2.1).

Table 2.1: Types of test specimens

Specimen Type	Unstitched	Stitched 6 × 6		Stitched 3 × 3	
		200d	500d	200d	500d
Code	Unstitched	6D2	6D5	3D2	3D5
Stitch pitch (mm)	...	6	6	3	3
Stitch spacing (mm)	...	6	6	3	3
Stitch density (cm ⁻²)	...	2.78	2.78	11.11	11.11
Stitch thread thickness (denier)	...	200	500	200	500
Fiber volume fraction (%)	53.9	53.7	54.2	54.4	54.9
Number of needle thread lines in the width direction	...	4	4	8	8
Number of specimens	6	6	6	6	6

2.2.2 Test Method

Until now, international consensus on the standard procedure of mode II delamination testing has not been achieved, even though collaborative work has been conducted by ESIS (European Structural Integrity Society), JIS (Japan Industrial Standards) group, ASTM (American Society for Testing and Materials) [37]. A review on prospective standard procedures has been reported by Brunner *et al.* [39]. However, a local standard method already existed (Japanese Industrial Standard JIS K 7086) [40] and a draft European Standard EN 6034 has been proposed.

In this experimental work, the ENF test adopted refers to JIS K7086, mainly for the test fixtures and specimen sizes. Modifications have been conducted to overcome many problems on stitched composites. Based on our preliminary test and those of many other reported works [22, 24], stitched composite laminates are prone to failure before crack propagation during ENF testing. To avoid this, tab plates were embedded in top and bottom side of the specimen. However, many problems are still remained such as failure of tab plates and de-bonding between tabs and stitched composites as shown in Figure 2.2.

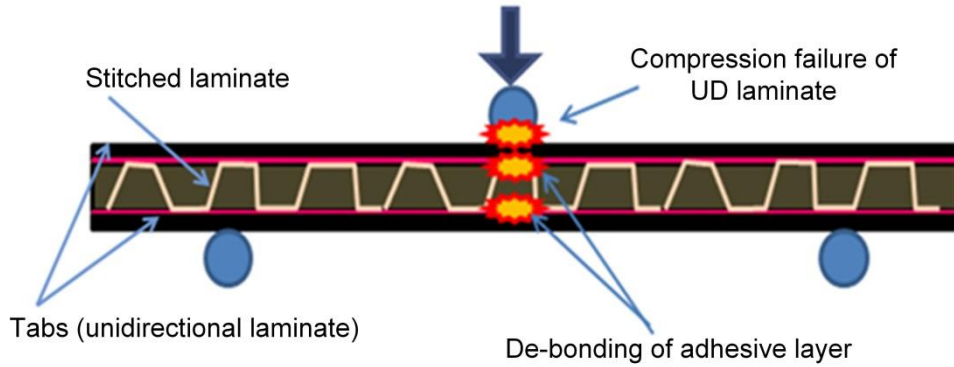


Figure 2.2: A schematic premature failure of stitched composite during ENF test

(courtesy of JAXA)

A comprehensive design consideration is required to decide tabs material and thickness. Modulus elasticity or flexural modulus of the tab plates should be closed to the modulus elasticity (E_x) of stitched laminate. In case of multidirectional stitched laminate with quasi isotropic orientation (E_x between 50 GPa and 80 GPa), aluminum alloy with highest yield strength is the best choice for tab material. Therefore Al-7075 T6 (yield strength about 500 MPa) was chosen in this study.

In order to avoid tabs de-bonding, the shear stress at the adhesive bonding area (between tab and laminate) should be much lower than the shear stress at the delamination interface (middle layer). The following equation could be used as reference to estimate the comparison of shear stress at the two critical positions. The derivation of this equation is written in Appendix B.

$$\frac{\tau_{int}}{\tau_{mid}} = \frac{a(a+b)}{(a+b/2)^2} \quad (2.2)$$

where τ_{int} is the shear stress at adhesive bonding between tab and composite laminate, τ_{mid} is interlaminar shear stress at the middle layer. Symbols a , b are the thickness of tab plate and composite laminate, respectively.

A parametric study is conducted to select appropriate thickness for particular stitched composite as shown in Table 2.2. Considering the lowest stress at bonding region, aluminum tab with 1 mm thickness is selected in this experiment.

Table 2.2: Parametric study of tab thickness

Thickness of laminate (mm)	Thickness of tab (mm)	τ_{int} / τ_{mid}
5.1	1	0.48
	1.5	0.60
	2	0.69
4.1	1	0.55
	1.5	0.67
	2	0.74

Aluminium tabs were embedded at the upper and bottom surfaces of the specimen using high-strength epoxy (Hysol EA 9309.3NA from Henkel Corporation) [71]. This type of epoxy contains 0.13 mm glass beads for bond-line thickness control, so that the total thickness of TENF specimens can be kept constant at $7.39 \text{ mm} \pm 0.03 \text{ mm}$. A detailed description of the TENF specimen set-up is given in Figure 2.3.

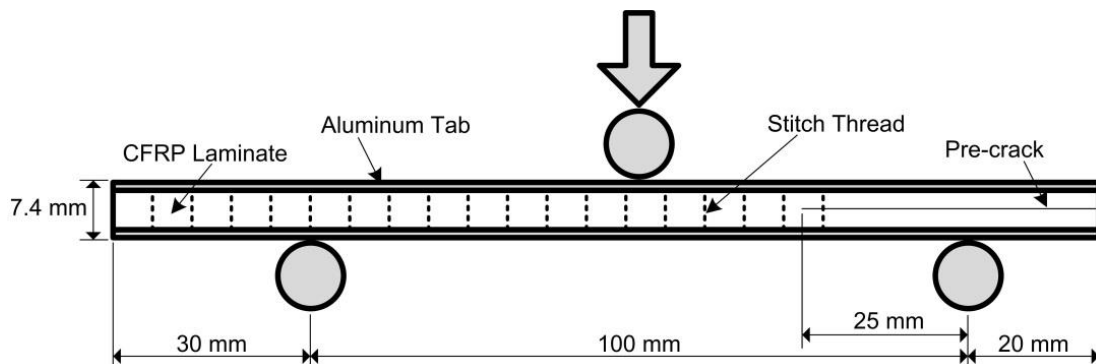


Figure 2.3: Tabbed end notched flexure (TENF) specimen set-up with a specific crack tip position

Additionally, the crack tip was developed using a pre-cracking process.

Pre-crack greatly influence the energy release rates of composite laminates [72, 73] because it removes resin pockets at the end of the inserted film. These resin pockets create a blunt crack tip and increase the crack's propagation resistance. Prior to ENF testing, a crack opening that was a few millimetres long was created using a sharp, thin razor blade. Then, three-point bend loading was used to propagate the crack to a position between 1 and 3 mm beyond the end of the Kapton film. This pre-ENF test was conducted with a half-span length of 40–45 mm, and the loading point was placed exactly in between the first and second stitch row. Because this pre-ENF test was conducted in the unstitched region, unstable crack propagation occurred, and stopped exactly below the loading point. The greatest advantage of using this pre-cracking process was that the crack tip position was located at the same region for all specimens (between the first and second stitch row), as shown in Figure 2.3. Furthermore, to enhance the contrast of the crack tip, brittle white paint was applied to both edges of the specimens.

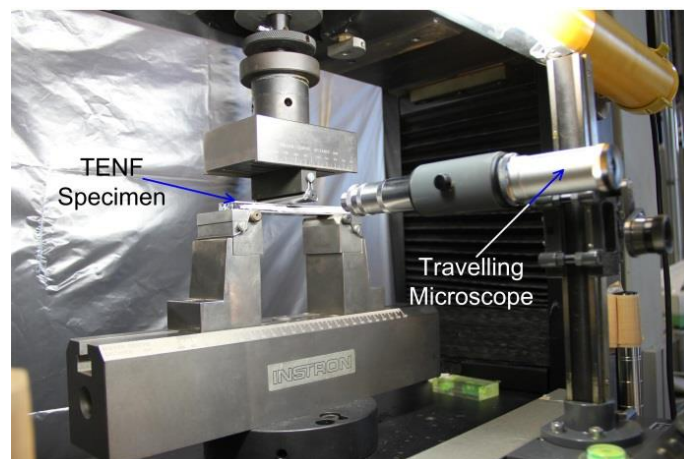


Figure 2.4: Mode II delamination test set-up

Subsequently, TENS tests were conducted using a 4505 series Instron machine with a 10 kN load cell over a total span of 100 mm (Figure 2.3). The specimens were

loaded at a constant crosshead speed of 0.5 mm/min until 1 kN was reached, then the crosshead speed was reduced to 0.1 mm/min to enable slow crack propagation. After unloading, the new crack length was measured using a travelling microscope at 25 × magnification and 0.01 mm reading accuracy.

2.2.3 Data Reduction

The energy release rate (G_{II}) was calculated using the compliance calibration method of Carlsson and Gillespie [72, 74]. This method was selected because it can accommodate tabs being on the specimen without any modifications to the basic G_{II} calculation [75]. The energy release rate can be evaluated by differentiation of compliances with respect to crack lengths when there is no plastic deformation and no damage except for interlaminar fracture. Prior to TENF testing, the specimen compliance was measured for five crack lengths (0, 10, 20, 30 and 40 mm) by applying small loadings until 600 N (0.1 mm/min crosshead speed). Similar procedures were repeated at each specific point where the energy release rate was being measured. Placement of the specimens was adjusted to obtain a new compliance data, depending on the available space. For example, to measure G_{IIC} at a typical crack length of 45 mm, the compliances were measured at crack tip positions of 37, 41, 45 and 49 mm from the right supporting pin. Then, compliance values were plotted in terms of C/C_0 versus $(a/L)^3$, and the slope (m) of the curve was measured.

Energy release rates were calculated as follows:

$$G_{II} = \frac{3mP^2a^2C_0}{2wL^3} \quad (2.3)$$

where C_0 is the compliance of the specimen without any crack along the span, a is the crack length and P is the peak load at which the crack starts to propagate. Parameters w

and L are the width of the specimen and half-length of the span, respectively. It is important to note that the slope (m) in equation (2.3) is specific for each crack length on the specimen to be tested.

To investigate the effects of stitch thread thickness and stitch density, G_{IIC} values were determined for crack lengths of 25 mm and 45 mm for all specimens. These crack lengths were close to the initial and steady-state points given by Jain *et al.* [22]. In the present work, steady-states (flat portions of R curves) were not achieved in some type of specimens, therefore a crack length of 45 mm was chosen. In between the two crack lengths, only one or two other G_{IIC} values could be measured for each specimen due to the limited space available. However, the R curve (G_{II} versus crack length) could still be determined for each type of specimen.

2.2.4 Measurement of Local Fiber Volume Fraction

This sub-topic was added into the experimental work based on preliminary results of TENF tests and related references [76, 77] which raised queries about correlations between fiber volume fraction and G_{IIC} values. To address this issue, the explanation is separated as detailed in the following.

2.2.4.1 Fiber Compaction due to Stitching Process

It has been reported that fiber compaction during the stitching process increased the local fiber volume fraction (V_{fl}) through numerous steps [78]. First, the insertion of the stitch fiber moves the preformed fibers laterally. The fibers between the two stitch lines are then deflected, causing a local increase in the volume fraction. Second, the tension forces created during the stitching process enhance fiber compaction. Finally,

the pressure applied to stitched fibers during laminate consolidation also increases V_{fl} , especially in the area under the stitched threads. These three factors are inevitable characteristics of stitched composite laminates [79].

2.2.4.2 Effect of Local Fiber Volume Fraction on Energy Release Rates

The effects of V_{fl} on mode I and mode II delamination properties of 5 harness satin (5HS) woven carbon fiber/epoxy resin composites have been investigated [76]. However, it was difficult to measure these effects in mode II delamination testing due to the serious influence of friction and interlocking between delamination surfaces. Work on similar case was carried out by Feret *et al.* [77] using a mixed-mode delamination test. They concluded that at the high mode II ratio, the total crack propagation energy was decreased by increasing V_{fl} .

The above reported works used fabric/woven carbon fibers. To enhance the hypothesis on non-fabric composites, a mode II static fracture mechanism may be the best approach. Hojo *et al.* [80] reported that during static ENF testing, micro-cracks initiated first at the fiber/matrix interfaces, followed by matrix cracking between the fibers. These micro-cracks appeared when the shear stress at the fiber/matrix interface near the crack tip reached a certain value (called the critical shear stress) [81]. Furthermore, in relation to the maximum shear stress at fiber/matrix interfaces, multi fibers pull-out study at different V_{fl} [82] was adopted. Quantitatively, this numerical study explained that the maximum shear stress at the interface will increase with increasing V_{fl} , following the curve shown in Figure 2.5.

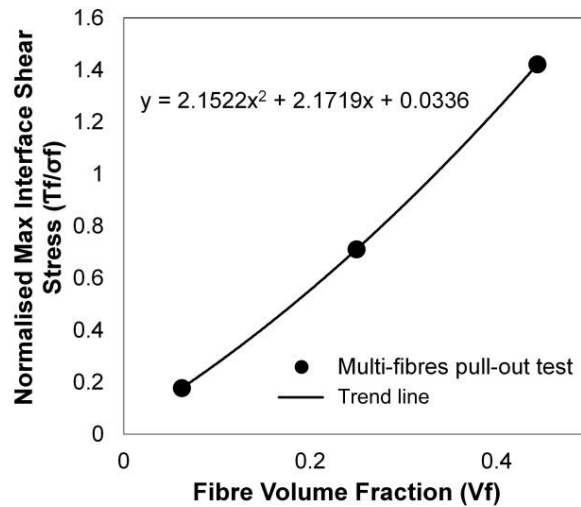


Figure 2.5: Normalized maximum interface shear stress at the loaded fibers end of a pull-out test simulation (data from: Fu *et al.* [82])

2.2.4.3 Measurement Method of Local Fiber Volume Fraction

JIS K7075-1991 [83] was referred to when conducting burn-off tests to measure fiber volume fraction. The measurement was performed as follows: (1) the sample mass was measured, (2) the sample was burned with a gas torch, (3) the mass of the burned sample was re-measured and (4) the fiber volume fraction was calculated. Prior to burning, the masses of each specimen were measured in open air and under water so that the densities of the samples could be calculated.

To measure local volume fraction at the position where it increases as a result of the stitching process, the specimens were cut as shown in Figure 2.6. This cutting position mostly excluded the resin-rich region, and the three main factors related to fiber compaction (discussed above) were encountered. For the stitched laminates of 6×6 mm, the length (a) and width (b) were 10 mm and 4 mm, respectively. For the unstitched and stitched laminates of 3×3 mm, the dimensions were 10×2 mm. After cutting was

complete and prior to the burn-off tests, the remaining needle thread was sanded off using emery paper. The average thickness (t) of all specimens was 4.88 mm. Five to six burn-off specimens from each type of laminate were investigated.

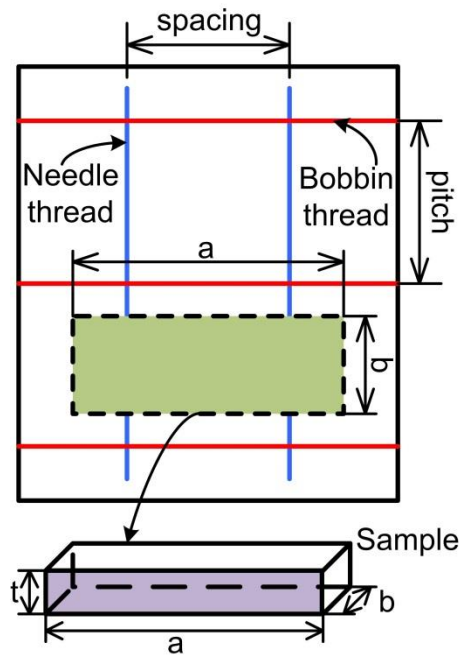


Figure 2.6: Schematic of the cutting method used for sample burn-off tests

2.3 Results and Discussion

2.3.1 Load-displacement Curves

Typical load–displacement curves for all types of specimens that resulted from TENS tests are displayed in Figure 2.7. Detail data for each specimen are compiled in Table 2.3. In the case of unstitched and moderately stitched specimens, it is evident in Figure 2.7(*a–c*) that the cracks suddenly propagated to the center of the loading pin. The densely stitched laminates (Figure 2.7(*d, e*)) could detain crack propagation, and their load–displacement curves consist of two or three steps until the cracks reach the center of the loading pin.

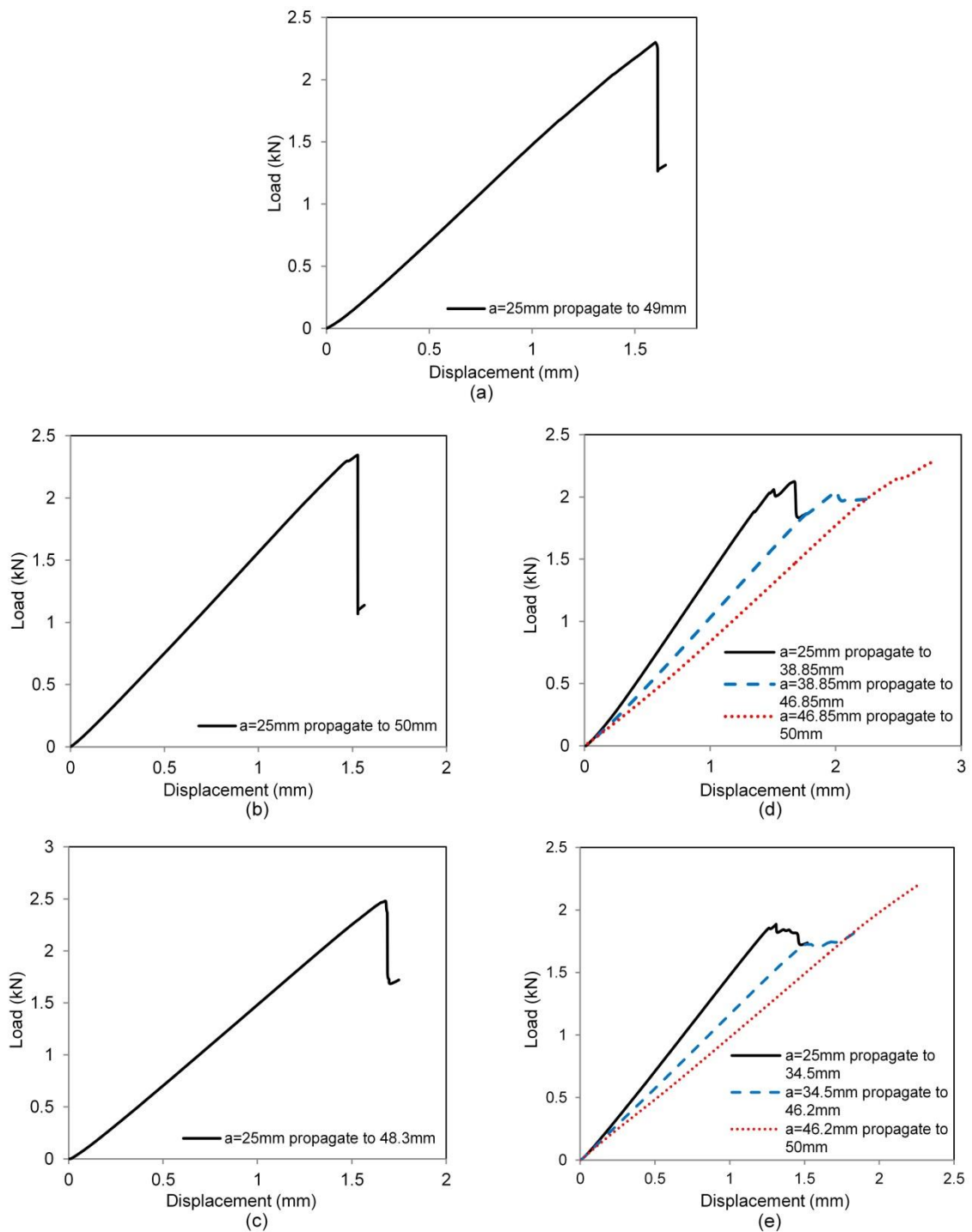


Figure 2.7: Typical load–displacement pattern for (a)Unstitched laminate (b)Stitched 6x6 200D (c)Stitched 6x6 500D (d)Stitched 3x3 200D and (e)Stitched 3x3 500D

After completion of the TENF tests, all specimens were visually inspected to determine whether any plastic deformation of the specimens or delamination occurred at the interfaces between the composite laminates and the aluminum tabs. Neither plastic deformation nor delamination was observed (Figure 2.8), guaranteeing that the energy lost during the tests was only due to interlaminar crack extension.

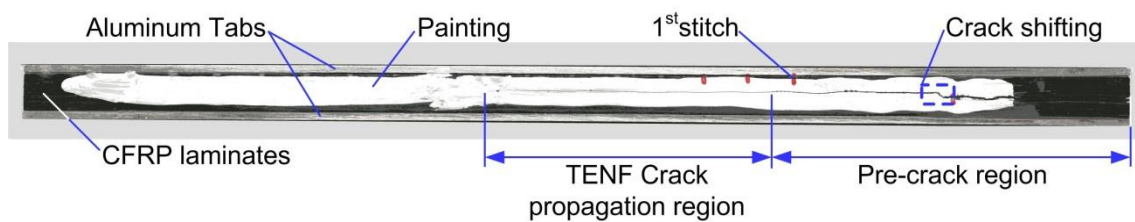


Figure 2.8: Tested specimen of stitched 6×6 mm and 500 denier thread thickness

Additionally, Figure 2.8 also reveals that the crack shifted from the center (between the $90^\circ/90^\circ$ layer) to the interface between the $-45^\circ/0^\circ$ layers. This occurred during the pre-cracking process, which used either a sharp razor blade (at the beginning) or the three-point bending fixture, as described previously. This behavior appeared on all types of specimens as demonstrated in Figure 2.9. Other researchers have also reported that cracks shift to the closest 0° layer on the compressive side [84-86].

During the TENF tests, the cracks propagated at the interface between $-45^\circ/0^\circ$ layers without crack shifting (Figures 2.8 and 2.9). Some comparison studies have been proposed to address these issues. Polaha *et al.* [86]. investigated carbon/epoxy laminates with $\theta/-\theta$ delaminated interfaces where $\theta = 0^\circ, 15^\circ,$ and 30° . They concluded that the effect of θ on G_{IIC} was negligible. However, De Morais [87] conducted numerical analysis on several multi-directional laminates, and reported that in the case of the $0^\circ/45^\circ$ delamination interface, mode III and mode I processes arose by 3% and 1% of

the total energy release rate, respectively. Additionally, related to asymmetry crack plane, Mollon *et al.* [88] concluded that it has no significant effects on G_{II} . Therefore, the results obtained in this experimental work are quite reasonable. All of the specimen types show similar crack behaviors (Figure 2.9), and the disadvantages of delaminated interfaces and crack planes were universal to all specimens and should not affect the comparative study.

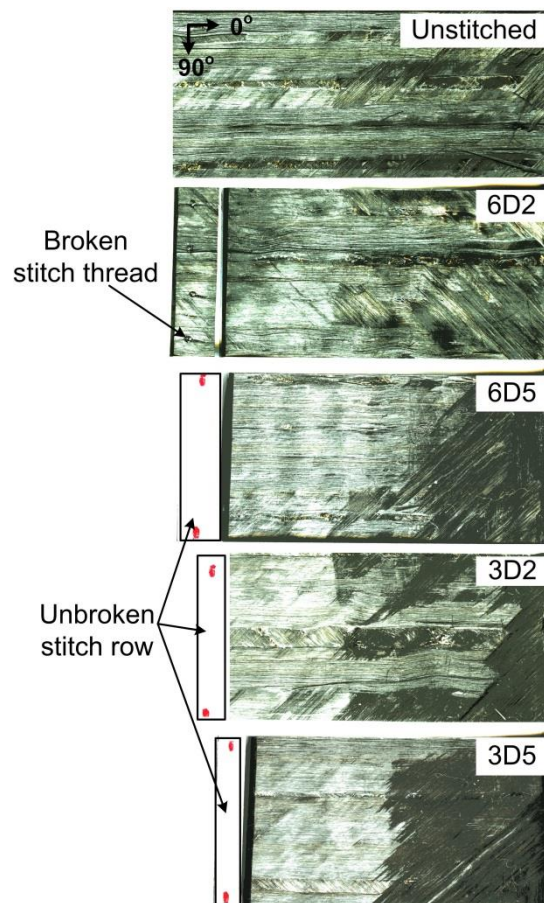


Figure 2.9: Crack propagation planes of all specimen types at pre-crack regions

2.3.2 Energy Release Rates

Each point of the G_{II} data has a specific value of slope (m), as mentioned in

equation (2.2). A typical C/C_0 versus $(a/L)^3$ curve is plotted in Figure 2.10, and the slope (m) was calculated from this curve. Furthermore, G_{II} values were calculated (Table 2.3) and R curves were plotted as shown in Figure 2.11. In general, the unstitched and moderately stitched specimens presented similar R curves. The steady-state regions (the flat regions) appeared for both unstitched and stitched laminates of 6×6 mm, 200 denier. To support this evidence, stitched specimens were cut into small pieces in between two stitched rows, so that one stitched row was present on each part, then separated slowly by hand. It was found that in the stitched sample of 6×6 mm 200 denier, the first and second rows of stitch threads were broken, as illustrated in Figure 2.9. The maximum energy bridged by the stitch fiber was achieved, after which the energy release rate did not increase with further increases in the crack length. In stitched specimens of 6×6 mm 500 denier, no stitch fiber was broken, and the steady-state zone was not obviously observed.

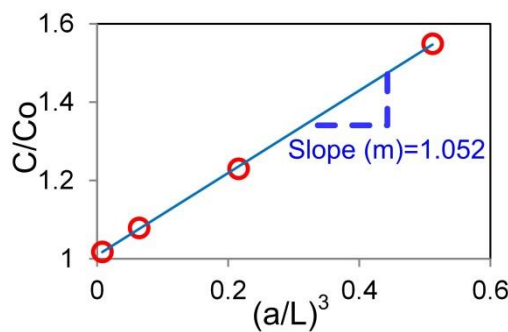


Figure 2.10: Typical specimen compliance curve in terms of C/C_0 versus $(a/L)^3$

Furthermore, the densely stitched specimens showed desirable mode II delamination properties. Based on the cutting results described in Figure 2.9, the stitch fibers were not broken during the test, so steady-state regions were not attained.

To quantitatively evaluate the effect of stitching, the G_{IIC} values at the crack

lengths (a) of 25 mm and 45 mm from each type of specimen are plotted in Figure 2.11. It is worth noting that at a crack length of 25 mm, only one stitched row was present in the crack region, and it represented the crack tip was placed in the stitching environment (Figure 2.3). Conversely, at a crack length of 45 mm, the crack region was fully stitched and the left overhang on Fig. 2.3 is only about 9–13 mm. There were, on average, 8 and 15 stitch rows in the crack zone for stitched specimens of 6×6 mm and 3×3 mm, respectively.

At a crack length of 25 mm, all types of stitched specimens yielded lower G_{IIC} values (by approximately 13.4%) compared to the unstitched ones. One plausible reason why these G_{IIC} values were lower is that fiber compaction during the stitching process increased the local fiber volume fraction. A detailed explanation will be presented in the next section.

At a crack length of 45 mm, the moderately stitched specimens showed negligible increases in G_{IIC} compared to the unstitched ones (1.3% and 3.8% for specimens with stitched thread thicknesses of 200 denier and 500 denier, respectively). Even though a certain amount of energy was absorbed by the stitch threads, G_{IIC} values were most affected by the stitching process itself, which reduced the G_{IIC} values as discussed above.

On the other hand, the densely stitched specimens underwent a significant improvement in G_{IIC} compared to the unstitched ones (64.8% and 140.3% increases for the specimens with stitch thread thicknesses of 200 denier and 500 denier, respectively). In this case, the energy absorbed by the existence of the stitch threads significantly increased the G_{IIC} values.

Table 2.3: Detail data of each specimens

Specimen type	Specimen No.	Crack length (mm)	Slope- m , Equation-2.3	Load, crack start to propagate (N)	G_{IIC} (kJ/m ²)	
Unstitched	1	25	1.38	1941.39	0.99	
		41	1.38	1433.54	1.46	
		45	1.38	1310.05	1.47	
	2	25	1.07	2299.78	1.08	
		40.2	1.07	1480.82	1.16	
		45	1.07	1472.00	1.43	
	3	25	1.20	2086.69	0.97	
		45	1.20	1380.87	1.38	
	4	25	0.87	2567.18	1.10	
		30	0.59	2650.24	1.13	
		5	25	0.97	2259.66	0.93
	5	33	0.68	2390.19	1.27	
		45	0.78	1791.06	1.52	
		6	25	1.18	2201.10	1.08
	6	45	1.11	1218.66	1.23	
		6D2	25	1.07	2153.3	0.98
	1		33	0.97	1885.92	1.19
			45	0.79	1676.61	1.43
2		25	1.26	1921.77	0.99	
	35	1.01	1560.47	1.02		
	45	0.77	1595.19	1.35		
3	25	1.41	1698.06	0.81		
	38	1.23	1529.26	1.32		
	45	0.89	1605.13	1.48		
4	25	0.84	2344.56	0.91		
	45	1.19	1371.65	1.43		
5	25	1.46	1702.68	0.84		
	30	1.17	1636.44	0.89		
6	25	1.02	1959.72	0.76		
	33	1.21	1829.65	1.38		

Specimen type	Specimen No.	Crack length (mm)	Slope- m , Equation-2.3	Load, crack start to propagate (N)	G_{IIc} (kJ/m ²)	
6D5	1	25	1.15	2153.00	1.05	
		42	1.19	1382.71	1.27	
		45	1.00	1499.20	1.43	
	2	25	1.23	1945.59	0.91	
		35	1.29	1373.14	0.93	
		45	1.02	1550.75	1.55	
	3	25	1.04	1939.54	0.89	
		38	0.95	1476.97	1.08	
		45	0.73	1434.11	1.10	
	4	25	1.02	1996.24	0.82	
		30	0.73	1887.02	0.76	
		45	0.48	2150.56	1.45	
	5	25	0.56	2492.15	0.76	
	6	25	0.61	2479.67	0.96	
		43	0.80	1547.7	1.47	
	3D2	1	25	1.21	1898.71	0.87
			38.85	1.08	1867.00	1.83
			45	0.61	2371.12	2.24
2		25	1.06	2111.59	0.94	
		37	0.84	2431.78	2.15	
		46	0.89	2127.21	2.70	
3		25	1.10	1989.99	0.90	
		45	0.79	2072.60	2.30	
4		25	0.77	2390.74	0.87	
		45	0.43	2841.95	2.24	
5		25	1.05	1956.93	0.90	
		35	0.78	1904.79	1.24	
		43	0.77	2038.89	2.14	
6		25	0.79	2304.08	0.85	
		45	0.84	2120.91	2.48	

Specimen type	Specimen No.	Crack length (mm)	Slope- m , Equation-2.3	Load, crack start to propagate (N)	G_{IIc} (kJ/m ²)
3D5	1	25	1.19	2075.20	1.01
		32.5	1.20	1851.71	1.37
		35.9	1.17	1915.49	1.74
		45	1.11	2211.09	3.45
	2	25	0.98	1948.89	0.80
		37.1	0.91	1788.55	1.37
		45	0.96	2278.06	3.47
	3	25	0.79	2284.05	0.84
		45	0.46	3288.76	3.25
	4	25	0.95	2070.59	0.82
		45	0.98	2265.09	3.2
	5	25	0.70	2626.15	0.98
		38	0.53	2860.45	2.06
		46	0.54	2823.45	3.01
	6	25	1.08	1965.95	0.85
		25 (7 active stitch)	0.96	2625.45	1.35

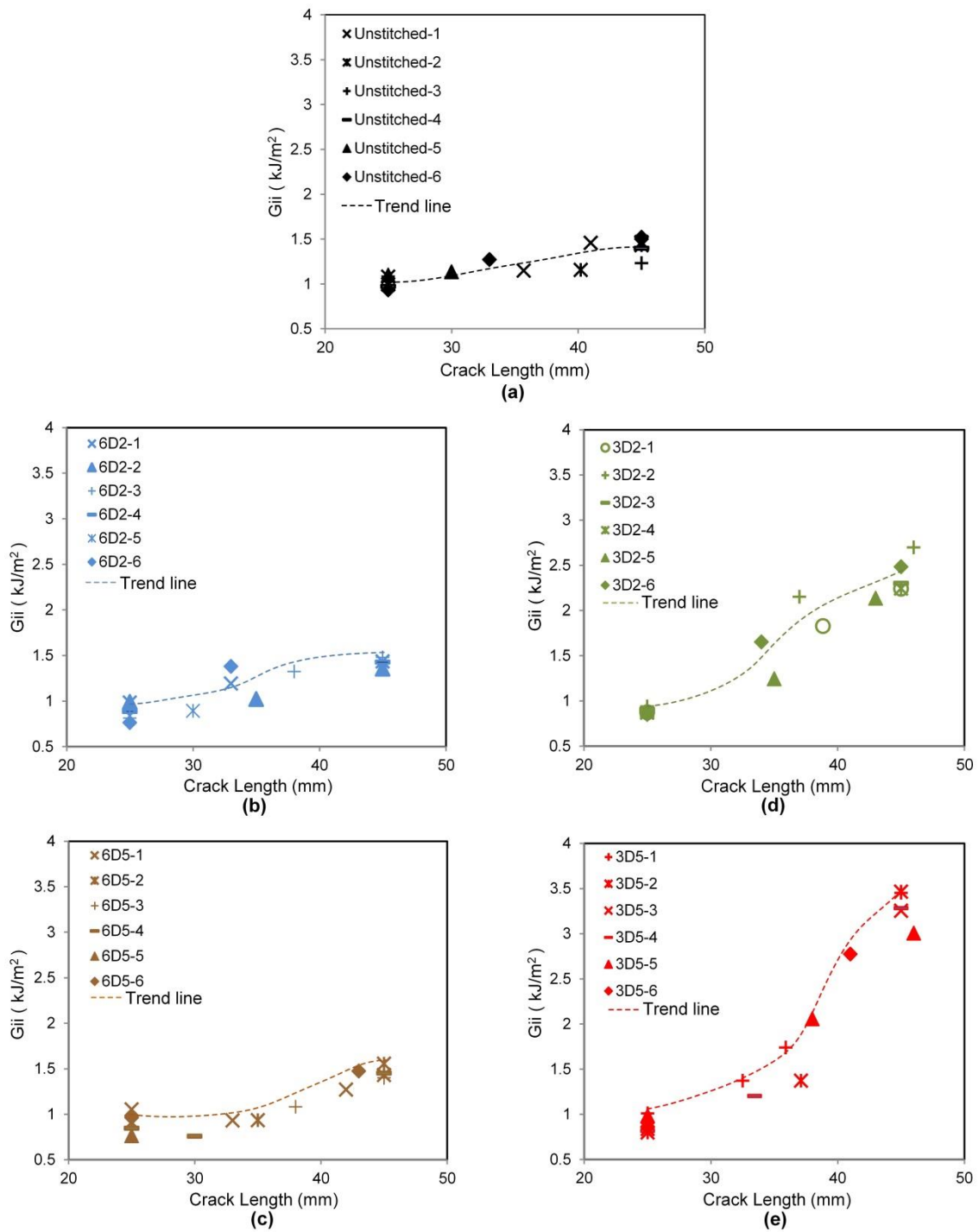


Figure 2.11: R curves for (a)Unstitched laminate (b)Stitched 6x6 200D (c)Stitched 6x6 500D (d)Stitched 3x3 200D and (e)Stitched 3x3 500D

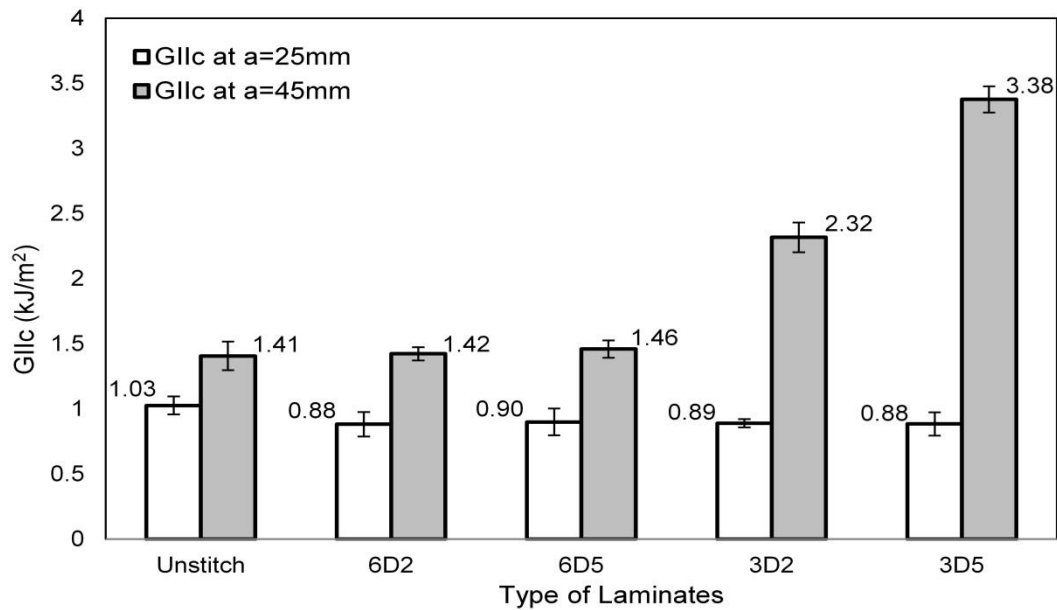


Figure 2.12: Average values of critical energy release rates (G_{IIC}) for crack lengths of 25 mm and 45 mm

Based on the above G_{IIC} data at crack lengths of 25 and 45 mm, particularly for densely stitched specimens, we recognize that the number of stitch threads at the crack area significantly determines the effectivity of delamination growth suppression. The G_{IIC} values at a crack length of 25 mm could be higher if more stitch threads are in the crack area. This issue could not be verified in more detail in this work due to the limited space available in the specimens. However, our group previous work on damage progression of stitched composites under out-of-plane loading[53] could explain the delamination growth rate after small damage was initiated. In this case, the crack area was fully stitched (unlike in mode II specimens). It was observed that delamination growth in moderately stitched specimens was slightly slower than in unstitched ones, and delamination growth was suppressed significantly in densely stitched specimens.

The effect of stitch thread thickness is relatively small in the case of moderately stitched specimens (3%). In densely stitched specimens, thicker stitch threads (500

denier) exhibited G_{IIC} values that were 1.46 times those of thinner stitch threads (200 denier). This clearly showed that thicker stitch threads could absorb more energy during the test.

2.3.3 Fiber Compaction Effects

Local fiber volume fractions were plotted for each type of specimen (Figure 2.13). Fiber compaction during the stitching process increased local fiber volume fractions by averages of 3% and 3.8% for moderately and densely stitched laminates, respectively. These increments generate higher levels of maximum shear stress at the crack tip during ENF testing. Quantitatively, using the trend line in Figure 2.5, these higher local fiber volume fractions could increase the maximum shear stress at the fiber/matrix interface around the crack tip by up to 9.9%. Furthermore, higher shear stresses around the crack tips allow for easier crack propagation and alleviate the values for G_{IIC} as reported previously.

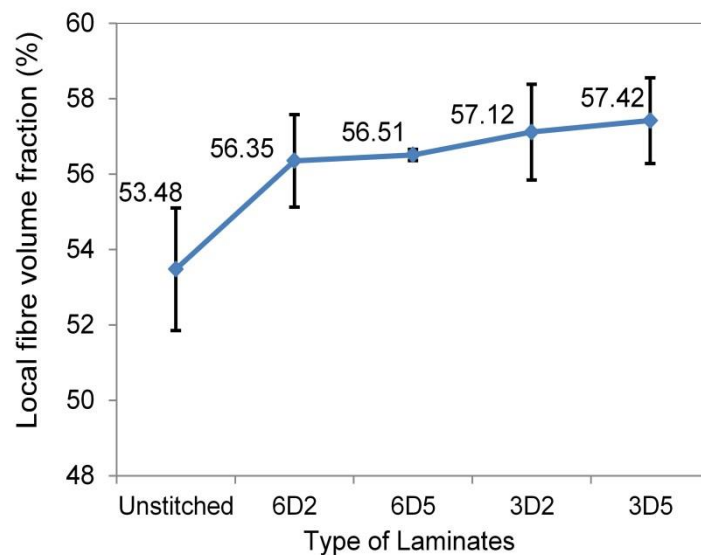


Figure 2.13: Local fiber volume fractions (V_{fl}) for each specimen type obtained by burn-off tests

2.4 Conclusions

TENF specimens exhibited a strong capability to prevent compression failure around a loading pin during mode II delamination tests. Thin aluminum tabs (1 mm in thickness) were enough to avoid plastic deformation, and created a low shear stress at the tabs/laminate interface; hence, there was no tab de-bonding.

The test results revealed that low stitch density ($SD\ 2.78\ \text{cm}^{-2}$) affected G_{IIC} insignificantly. In this case, the energy absorbed by the stitch threads at the crack area was almost equal to the decreasing G_{IIC} values due to fiber compaction. Therefore, there is almost no increment obtained in moderately stitched laminate (low stitch density). Crack bridging due to stitch threads was significantly perceived for densely stitched specimens ($SD\ 11.11\ \text{cm}^{-2}$) with the increment of G_{IIC} reaching 2.4 times that of unstitched specimens. The effect of SD also could be observed from load–displacement curves, where in the unstitched and moderately stitched laminates, the load dropped drastically, but it did not drop in densely stitched laminates.

The effect of stitch thread thickness for moderately stitched specimens was relatively small (3%). However, for densely stitched laminates, specimens with a stitch thread thickness of 500 denier presented G_{IIC} values that were 1.5 times those of specimens with a stitch thread thickness of 200 denier.

Chapter 3

Finite Element Analysis of Tabbed End Notched Flexure

(TENF) Test

3.1 Overview

This chapter demonstrates a finite element simulation of tabbed end notched flexure (TENF) test of stitched composites. In this simulation, the interaction between stitch threads and composite laminate become most important. Therefore, a novel experimental test called interlaminar shear test (IST) is introduced to understand the bridging mechanism of single stitched laminate under pure shear loading. The load displacement curve that obtained by IST is then applied to FE model using spring connector element. Furthermore, cohesive zone elements are used to simulate crack propagation. A parametric study to find suitable cohesive zone parameters is conducted and the previous experimental results are used for comparison. The limitation of previous experimental condition, where only one stitch thread in delaminated region at the initial state, are also covered by increasing number of stitch threads at delaminated region. Finally, the model is then verified with different laminate lay-up configuration to check reliability of the modeling techniques.

3.2 Interlaminar Shear Test (IST)

3.2.1 Experimental Method

Interlaminar shear test (IST) is a novel test method used to investigate the behavior of single stitch thread under pure shear loading. The specimens were cut

according to the dimensions shown in Figure 3.1. The laminates contained 24 plies of quasi-isotropic $(+45/0/-45/90)_{3S}$ carbon fibers (T800SC-24K, Toray Industry) and epoxy (XNR/H6813, Nagase Chemtex Corp.) as the matrix. Mechanical properties of epoxy [89] and carbon fiber [90] are listed in Table 3.1. Kapton film is inserted in the middle layers. Vectran thread (Kuraray) was used as the stitch thread, with a fiber linear density of 500 denier (equivalent to 0.0394 mm^2 cross-sectional area). The details of laminates fabrication have been described in the previous chapter. It is worth noting that the single stitch was in the stitching environment (connected with other stitches). The other eight stitch threads were located at all of the edges had already been cut in the middle layer using a sharp, thin razor. Similar conditions have been used in interlaminar tension testing to avoid sudden pull-out of the stitch thread during the test [91]. Because there is no standard testing fixture for this specific application, a special jig was designed to be fitted with a standard Iosipescu fixture as shown in Figure 3.2. The specimen was held by the special jig and placed in the Iosipescu fixture, before being tested using a tensile test machine (Instron 4505 series). A small load cell (10 kN) was used, with a crosshead speed of $0.025 \text{ mm min}^{-1}$. The tests were conducted until the stitch thread broke.

Table 3.1: Mechanical properties of matrix and carbon fiber

Epoxy matrix	Carbon fiber
Tensile strength = 50 MPa	Tensile strength = 5,880 MPa
Flexural strength = 120 MPa	Tensile modulus 294 GPa
Flexural Modulus = 2.8 GPa	Laminae tensile modulus (60% V_f) = 154 MPa
	Laminae tensile strength = 2,950 MPa

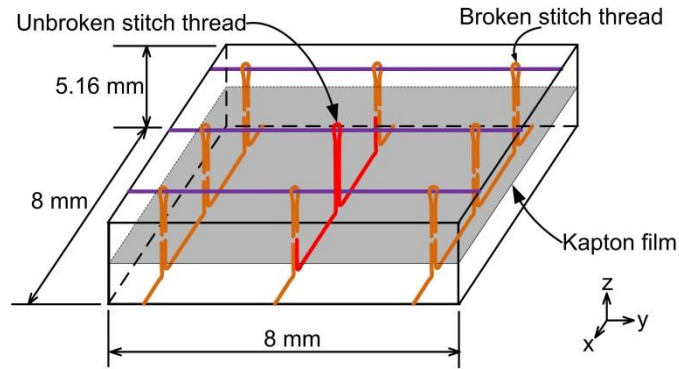


Figure 3.1: Interlaminar shear test specimen

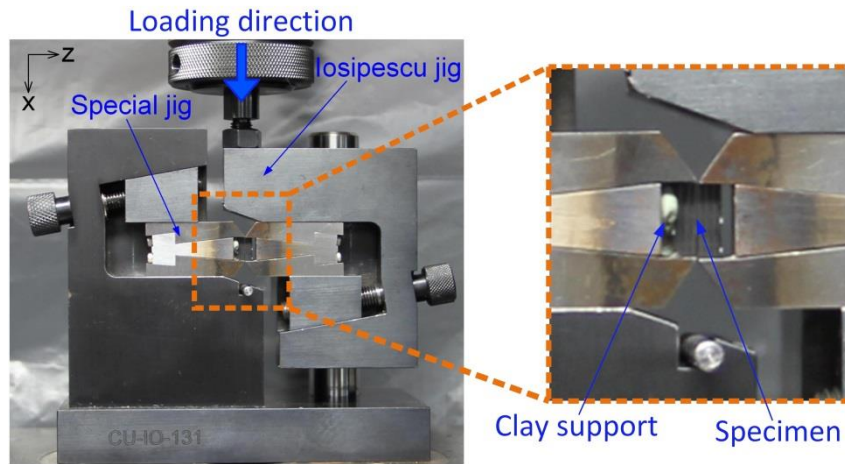


Figure 3.2: Interlaminar shear test set-up

3.2.2 Finite Element Simulation of Interlaminar Shear Test

To simulate the ENF test, IST of a single-stitched specimen was first modelled and verified. Finite element modelling was conducted using ABAQUS commercial software. The stitch thread was modelled as a spring connector with a user-defined force–displacement relationship. The spring was connected to the laminates through multiple-point constraints (MPCs). The size and shape of the connection points (the MPC area) were based on the stitch cross-sectional area as shown in Figure 3.3. The stitches resembled composite materials containing two stitch threads (Figure 3.1) with

epoxy resin as the matrix. Generally, the cross-sectional areas of the stitches were close to elliptical as a result of the compaction and pre-tensioning of the two threads during fabrication. The major and minor axes of the ellipse were measured from seven specimens.

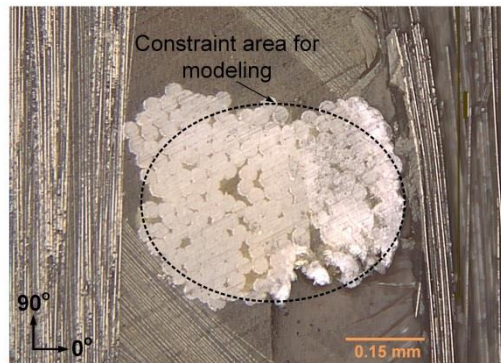


Figure 3.3: Cross-sectional of stitch thread composites at the interface of middle layers

The geometry of the IST model is shown in Figure 3.4. The area close to the MPC area was also modelled as an ellipse, with axis lengths and element sizes twice those in the MPC area. Taking account of the stress concentrations existing between the stitch thread and the surrounding laminates, the convergence of the element sizes was investigated. Several combinations of element sizes were simulated to check mesh convergence (Figure 3.5).

Each layer of laminates was modelled using continuum shell elements, with one element in each thickness of the layer. All of the layers were connected by sharing of nodes. Prior to computation, the element shape and compatibility errors were checked using the ABAQUS package. The laminae properties listed in Table 1 were used which calculated using in-house simulation codes based on the homogenization method [92]. Input properties such as fiber and matrix properties were obtained from the

manufacturers.

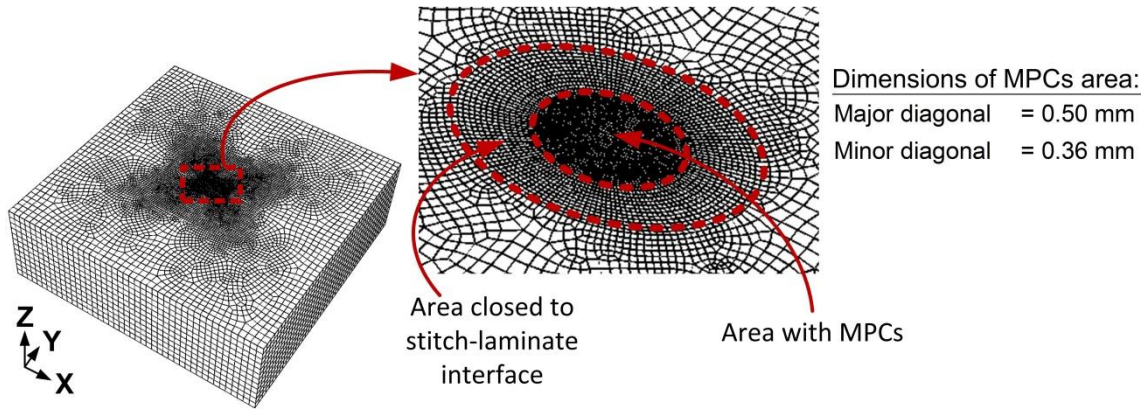


Figure 3.4: Half model (lower part) of IST specimen

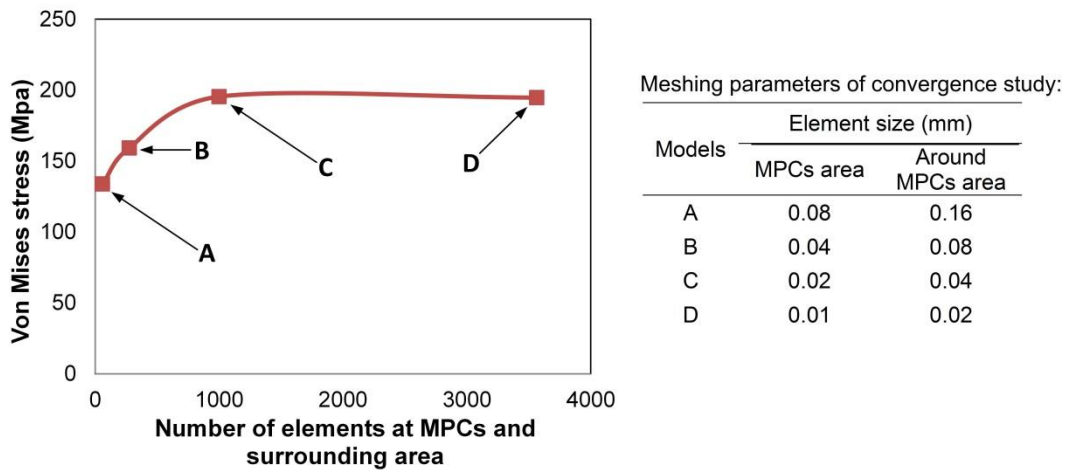


Figure 3.5: Convergence check of the elements sizes

3.3 Finite Element Simulation of Tabbed End Notched Flexure Test

Mode II delamination tests of multidirectional stitched composites were reported in the previous chapter. A tabbed end notched flexure (TENF) specimen was used to avoid matrix cracking in the loading area during the test (Figure 3.6). Therefore, in this finite element simulation, the TENF test was modelled, rather than the ENF test. The

modelling and meshing techniques for the laminates (including the stitched thread) from the IST simulation were adopted.

Additional aluminum tabs and adhesive bonding were connected to the laminates by node sharing. The crack propagation plane was modelled using cohesive zone elements with a traction separation response. The cohesive zone elements were inserted at positions where an actual crack occurred in the previous experiments (at the interface of the $-45/0$ layers, on the compression side). To select appropriate parameters for the cohesive zone elements, a parametric study was conducted. These CZM parameters were the initial interface stiffness K_0 , the interface strength σ_i and the viscosity coefficient μ . Zhao *et al.* [42] have summarized typical values of K_0 and $\sigma_{I, II}$ obtained by many investigators through trial-and-error methods (in many types of application). It seems that most investigators have preferred to use an initial stiffness between 10^{12} and 10^{15} N m^{-3} . Values that are too large can create unexpected oscillations, while values that are too small can give unreasonable compliance of the models.

Unlike interface stiffness, there is no specific suggested value for interface strength. Some results indicated that lower values can help computational convergence, but extremely low values can affect accuracy [93]. Computational convergence has become a serious problem in simulation of mode II delamination tests. To overcome this, viscous damping techniques are commonly used [94]. The optimal viscosity coefficient should be determined, taking account of computational costs and the effect on the accuracy of the results [95]. In the present work, various values of K_0 , σ_i^0 and μ were tested and an appropriate value of each parameter was then recommended.

Furthermore, a quadratic stress failure criterion was applied to evaluate the

initial damage according to the following equation:

$$\left\{ \frac{(\sigma_I)}{\sigma_I^o} \right\}^2 + \left\{ \frac{\sigma_{II}}{\sigma_{II}^o} \right\}^2 + \left\{ \frac{\sigma_{III}}{\sigma_{III}^o} \right\}^2 = 1 \quad (3.1)$$

where σ_i and σ_i^o ($i = I, II, III$) are respectively the stress components and the critical interfacial strength under pure modes I, II and III.

Delamination growth was controlled by an exponential softening fracture-based method. A mixed mode fracture energy criterion with power-law interaction was applied according to the following equation:

$$\left\{ \frac{G_n}{G_n^c} \right\}^\alpha + \left\{ \frac{G_s}{G_s^c} \right\}^\alpha + \left\{ \frac{G_t}{G_t^c} \right\}^\alpha = 1 \quad (3.2)$$

The normal critical strain energy release rates G_n^c and shear critical strain energy release rates G_s^c , G_t^c were 450 and 880 J m⁻², respectively, which were obtained from literature [15, 88] and the previous experiments. The value of α was assumed to be 1. To reduce the simulation time, a half-slice model was used instead of the full model. Each half-slice was equal to one-sixteenth of the full model and consisted of only half of the stitch thread in the width direction, as shown in Figure 3.7. The symmetric boundary condition was applied at the side where the half-stitch was placed.

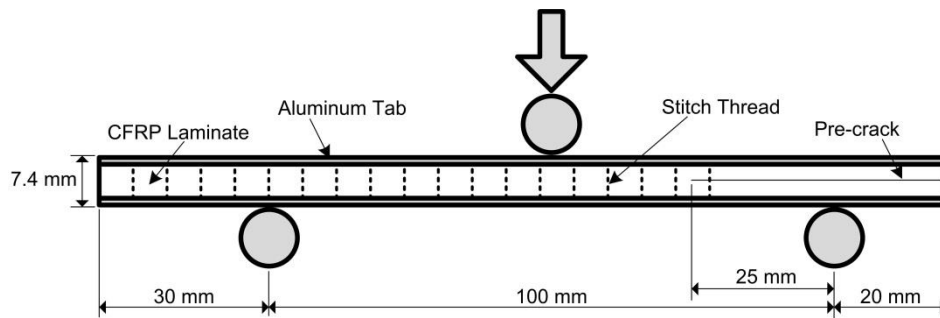


Figure 3.6: TENSILE EXPERIMENTAL SET UP

Another issue that has to be addressed in modelling stitched multidirectional laminates is the interaction between the stitch and matrix for different layer orientations. The interlaminar shear tests of a single stitch in the previous section were conducted with the crack between the $90^\circ/90^\circ$ layers. In this case, during the test, the stitch penetrates the surrounding laminates in the x -direction (Figure 3.1 and 3.2), which is perpendicular to the 90° layer as shown in Figure 3.3. The force–displacement curve of a single stitch will be different if the stitch penetrates the laminates with another orientation. To deal with this issue, the elastic modulus E of the elements in the vicinity of the stitch threads (Figure 3.4) was varied, depending on the orientation of each laminate (at the position where the spring connector was applied). It was assumed to be 4.6 GPa (equal to E_2 of the laminate), 2.8 GPa (equal to E_{matrix} of the matrix) and 3.7 GPa (the average of E_2 and E_{matrix}) for the cases in which the spring was connected to the laminate with orientations of 90° , 0° and 45° , respectively. These adjustments of properties were applied only at those layers where a crack plane existed, because the penetration of the stitch through the laminate was negligible at other layers.

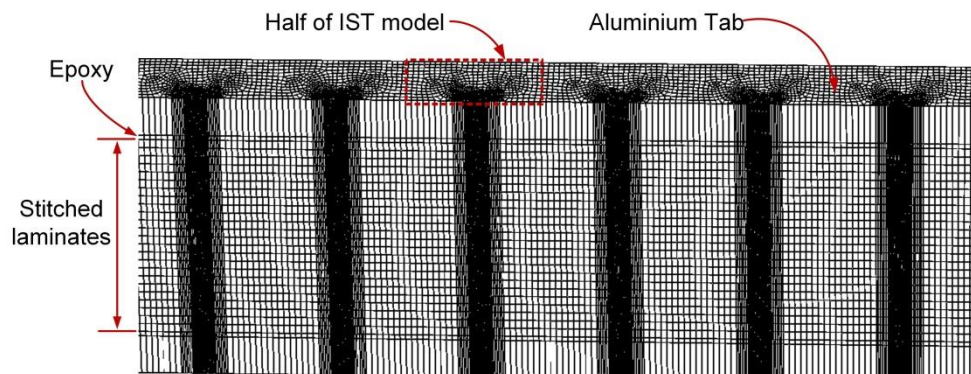


Figure 3.7: TENS modeling geometry

Using similar techniques, the effects of the number of stitch thread rows on mode II delamination properties were investigated. It should be noted that this issue could not be investigated in previous experimental work, where the TENS testing for a crack length a of 25 mm was conducted with only one stitch thread in the crack region (Figure 3.6). The experimental work showed that the G_{IIc} of stitched composites (at $a = 25\text{mm}$) were even lower than the values for unstitched composites, because of the increasing local fiber volume fraction in the stitched laminates. Several models with different numbers of stitch rows in the crack region were analyzed, and a model of unstitched laminates was also presented for comparison.

3.4 Results and Discussion

3.4.1 Experimental and Simulation Results of Interlaminar Shear Test

Interlaminar shear test results of single stitched laminate are plotted in Figure 3.8. At initial displacement (up to 0.2 mm), a disturbance in load-displacement curve occurred due to the sticky interface and in-plane fiber bridging. Although Kapton film was inserted at the middle layer, the interlaminar surfaces still stick each other. The fracture surface (Figure 3.9) shows that the delamination was not occurred smoothly at the Kapton film interface, but in some region delamination occurred in between fibers. The Kapton film was not worked properly due to some reasons. Some damage could be created on the film during needle penetration into the preform as shown in Figure 3.10. Noted that the release film was inserted into the preform before stitching and resin infusing. In addition, the film itself was in contact with the in-plane fibers under pre-tension during stitching process, hence the film surface might not be perfectly flat.

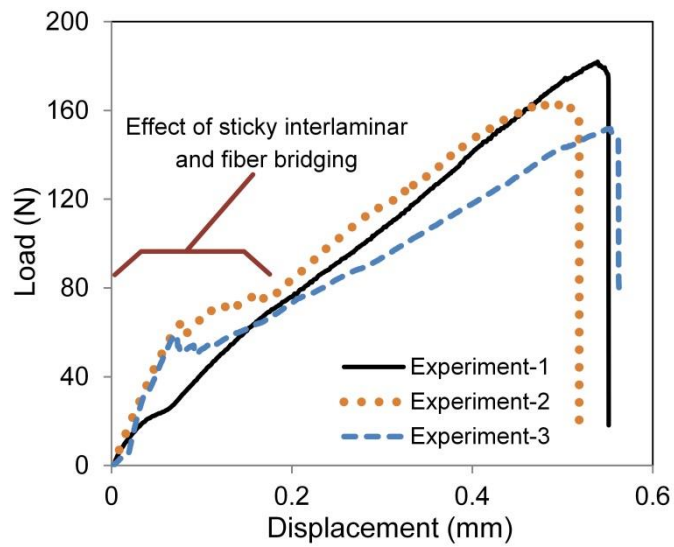


Figure 3.8: Load-displacement curve obtained by IST of single stitched laminate

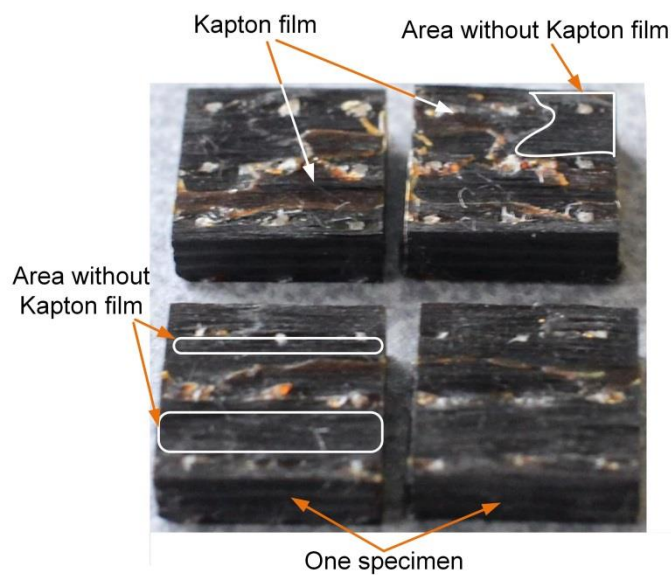


Figure 3.9: Fracture surface of interlaminar shear test specimen

In order to understand the stitch thread bridging mechanism under shear loading, micro-computed tomography images of IST specimens at different loading condition are

presented in Figure 3.11. After completely delaminated, with a small load (21 N) the stitch thread is de-bonded from surrounding laminate. The load increase almost linearly and the stitch thread starts to plough the surrounding laminate particularly at the region close to delaminated area. It is reported [96] that there were internal damage of the stitch thread before the final failure, but it could not be captured in this study.

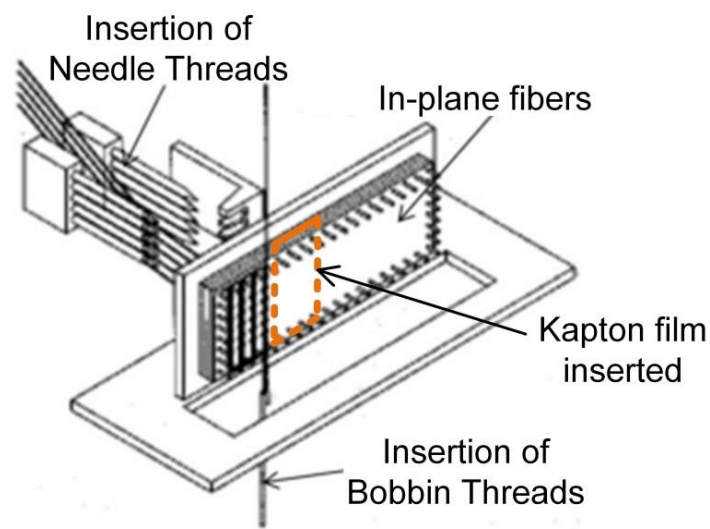


Figure 3.10: Stitching process with Kapton film at the middle layer

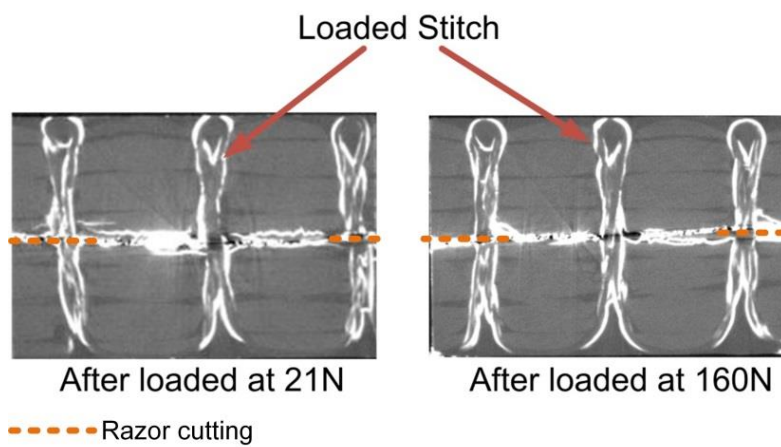


Figure 3.11: Micro-CT image of IST specimen after different loading

Furthermore, the fracture surface (Figure 3.9) also showed that the stitch thread broken at the mid-layer where delamination occurred. It revealed that the frictional force between stitch thread and surrounding laminates could be neglected because of the absence of fiber pull-out. The situation was different in the opening-mode case [97], where the stitch threads broke mostly at the upper side of the threads and the frictional force (after stitch breakage) played an important role in the energy release rate. Therefore, in shear-mode loading, the energy dissipated by stitch bridging is mostly due to stitch de-bonding, penetration of the stitch into the laminates (ploughing), deformation and fracture of the stitch threads.

The simulation results (Figure 3.12) was obtained from the model with element sizes 0.02 and 0.04 mm in the MPC area and the surrounding area, respectively. These element sizes were selected for the single-stitch model on the basis of the element convergence check (Figure 3.5), where mesh-independent results had already been obtained with these typical element sizes. Figure 3.12 presents a parametric study of spring connector properties. The spring constant of 450 N/mm seems to be fit well with the experimental results. Hence this spring constant is used in modeling mode II delamination test of stitched composites.

In order to analyze the stresses at various step of loading, three components of stresses (S_{11} , S_{22} , and S_{12}) are taken at the delaminated surface (90° layer) of the moving part of IST specimen as shown in Figure 3.13. The stresses are plotted in Figure 3.14-16 with loading of 10.5, 21.3, and 180.5 N (before broken), respectively. It is worth to be noted that the stresses distribution are in local coordinate of 90° layer, so that S_{11} means normal stress along fiber direction (y-axis in global coordinate system) and S_{22} is normal stress perpendicular to fiber direction (x-axis in global coordinate system).

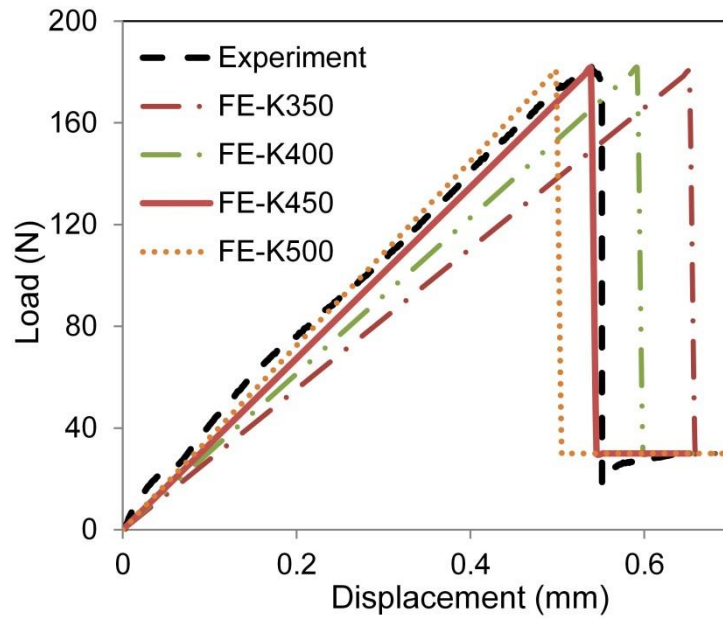


Figure 3.12: Load displacement curve of experimental and numerical results

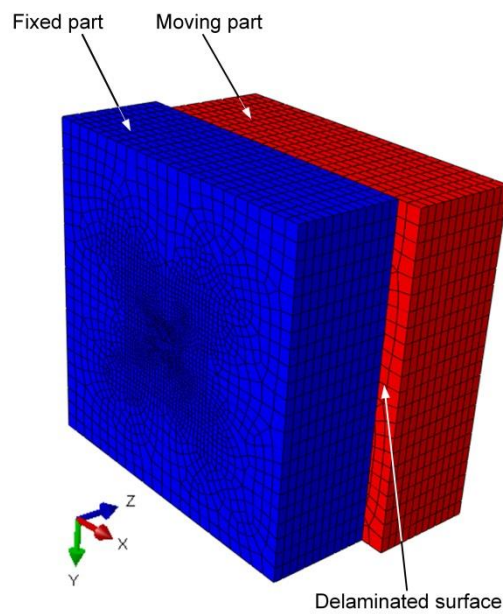


Figure 3.13: Global coordinate system of IST simulation

Figure 3.14 shows that with small load (10.5 N), S_{22} reach the value above the matrix tensile strength (50 MPa) which indicate the possibility of matrix crack around

the stitch fibers. Furthermore, with 21.3 N of load, S_{12} almost reach the matrix shear strength (120 MPa). Hence matrix surrounding the stitch will start to be damage (de-bonding) and by increasing the load, the de-bonding could be extended along the stitch thread.

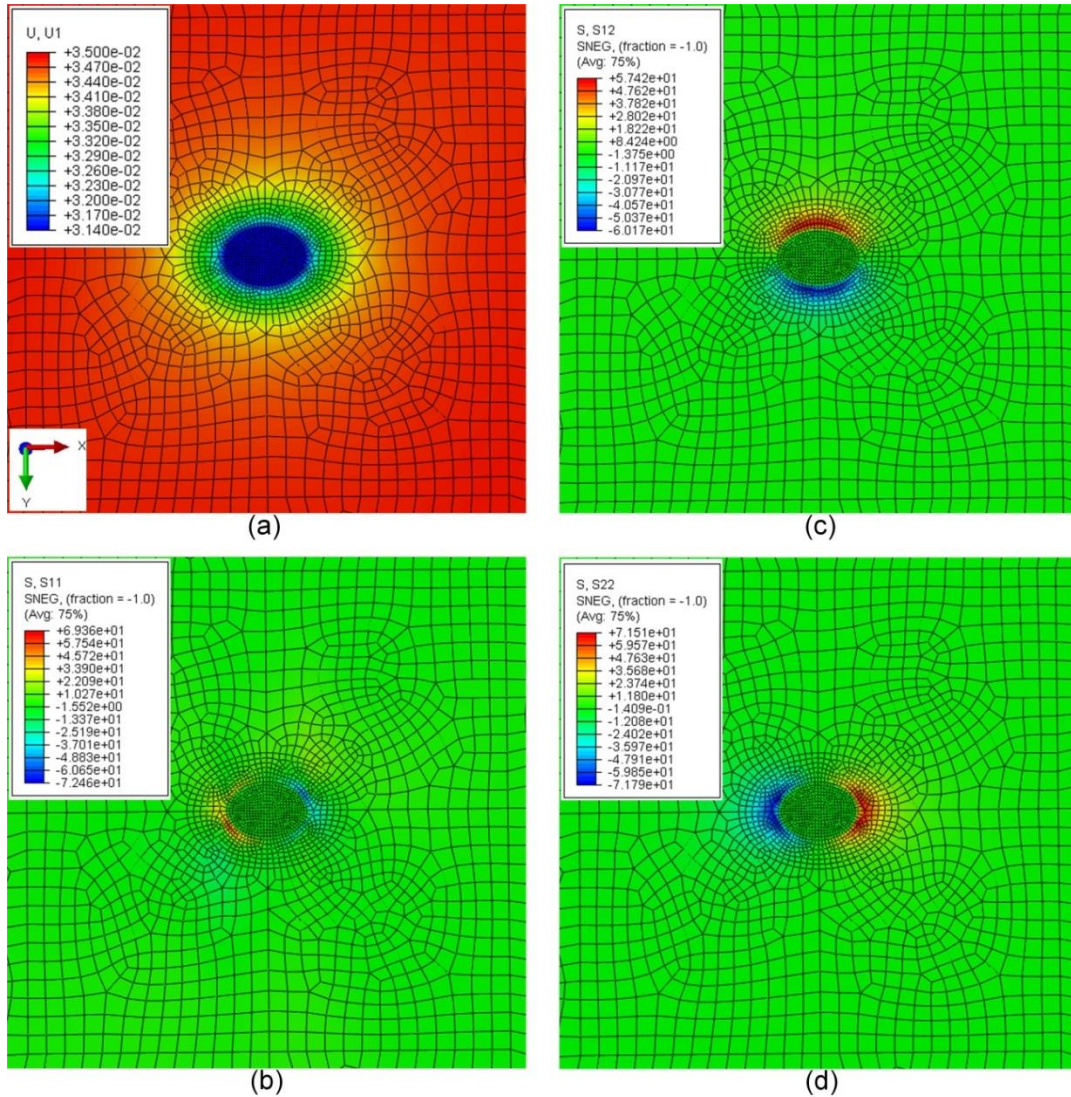


Figure 3.14: Displacement and stress distribution at delaminated surface (90° layer) of the moving part, under 10.5 N loading (a)Displacement in x-direction (b)Normal stress along fibers direction (c)In-plane shear stress (d)Normal stress perpendicular to fibers direction

The results agree with experimental results where stitch threads de-bonded at lower load. The relative displacement between stitch thread and surrounding laminate (Figure 3.16(a)) also exhibit the stitch thread penetrates the laminate.

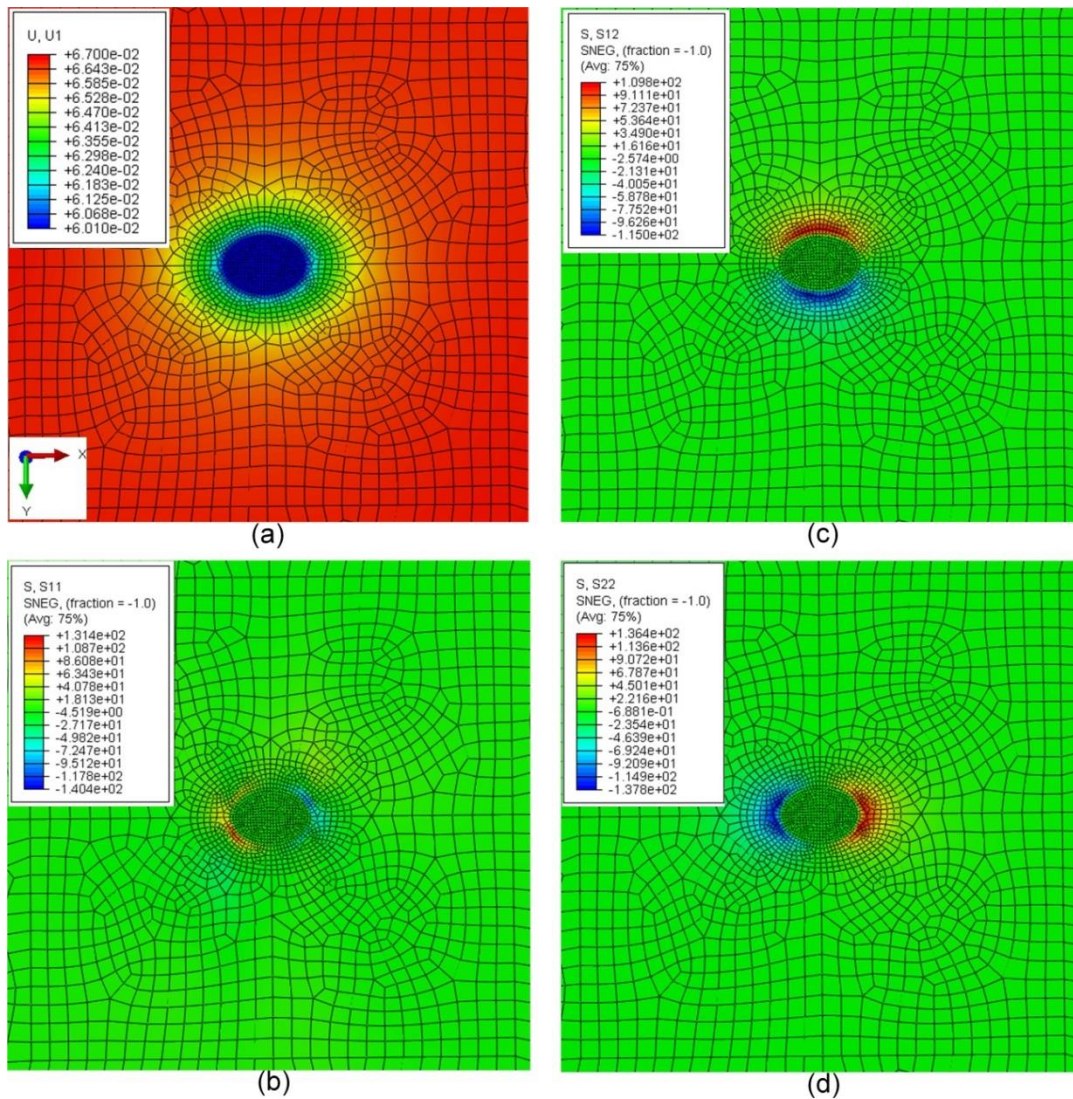


Figure 3.15: Displacement and stress distribution at delaminated surface (90° layer) of moving part, under 21.3 N loading (a) Displacement in x-direction (b) Normal stress along fibers direction (c) In-plane shear stress (d) Normal stress perpendicular to fibers direction

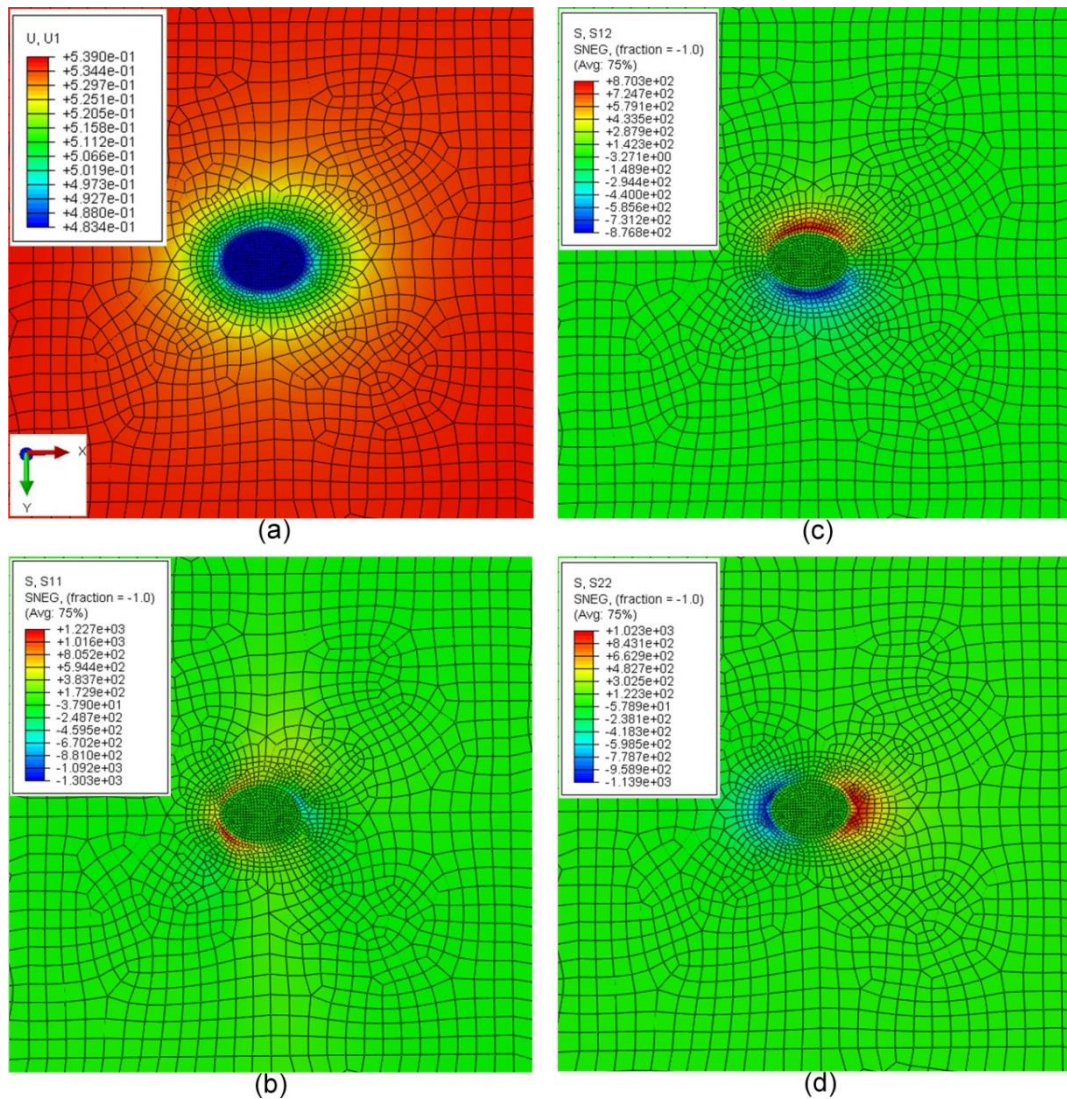


Figure 3.16: Displacement and stress distribution at delaminated surface (90° layer) of moving part, under 180.5 N loading (a) Displacement in x-direction (b) Normal stress along fibers direction (c) In-plane shear stress (d) Normal stress perpendicular to fibers direction

3.4.2 Cohesive Zone Modeling Parameters

The results of the parametric study of interfacial strength, viscosity coefficient and interfacial stiffness are plotted in Figures 3.17-19, respectively. All of these figures show the load–displacement curves until the initial crack starts to propagate (indicated

by the drop in load). Beyond this point, the simulation will run relatively slowly. Considering the computational time and the energy release rate calculation method, which were based on the peak load [98], the simulations were stopped a few millimeters beyond the load drop point.

Figure 3.17 shows that variation in interfacial strength did not affect the peak load significantly. It could affect the length of delamination during crack propagation process. However, the experimental data [98] were mainly taken until the peak load obtained, and delamination process do not continue until the center of loading point. Therefore additional verification of the model by considering the crack length propagation is needed and reported at the end of this chapter.

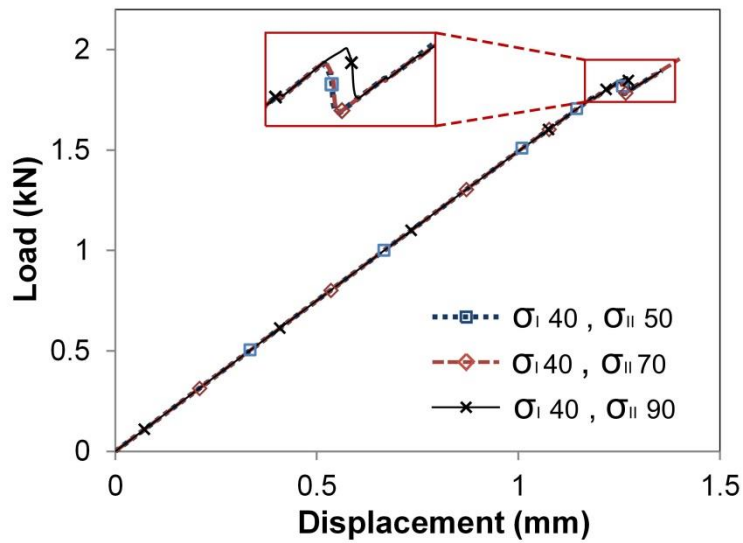


Figure 3.17: Effects of critical interfacial strength

For the sake of computational convergence, as already discussed, interfacial strengths of 40 and 70 MPa were selected for σ_I^o and σ_{II}^o , respectively. In this work, σ_{III}^o was assumed to be the same as σ_{II}^o .

Unlike the interfacial strength, the viscosity coefficient had a notable effect on the peak load (Figure 3.18) and on computational convergence. When a viscosity coefficient was not applied, the simulation stopped before crack propagation. On the other hand, the use of a high value of the viscosity coefficient ($\mu = 10^{-3}$) led to a lower computational cost, but the peak load was far above the experimental result. Taking account of the need for both accuracy and computational efficiency, a range of μ from 10^{-5} to 10^{-4} seems to be most appropriate for this particular simulation.

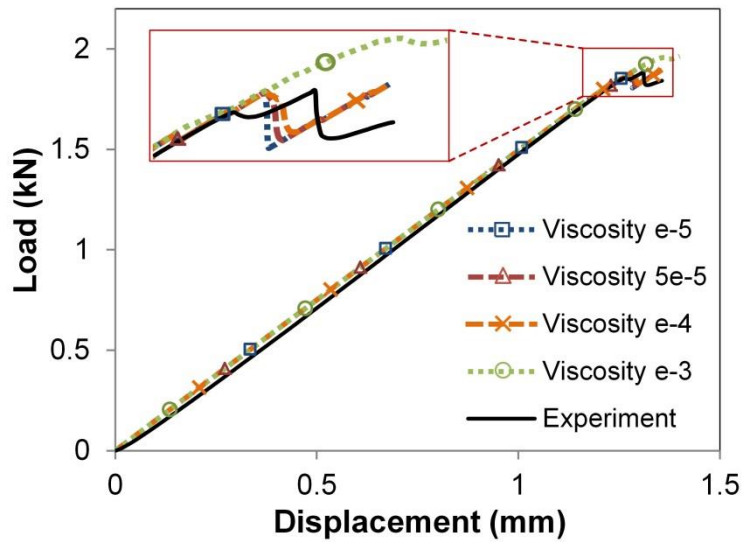


Figure 3.18: Effects of viscosity coefficient of the cohesive element

Finally, the interfacial stiffness has a remarkable influence on the simulation results (Figure 3.19). It shows that the upper limit (10^{15} N m^{-3}) suggested by many investigators is not appropriate in this type of simulation, because the peak load is far above the experimental value. A relatively low stiffness helps convergence but leads to inaccurate results. On the basis of the results in Figure 3.19, an interfacial stiffness between 4.25×10^{14} and $4.5 \times 10^{14} \text{ N m}^{-3}$ should be selected.

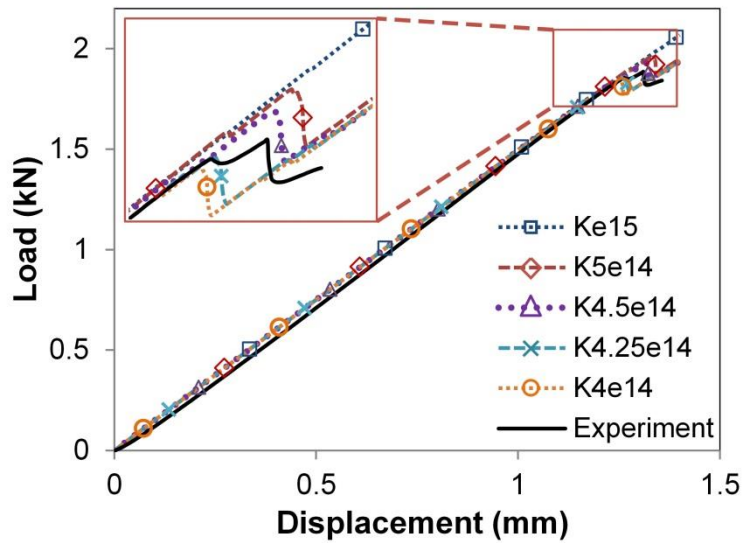


Figure 3.19: Effects of interfacial stiffness

3.4.3 Effects of Number of Stitch Rows in the Crack Region

As discussed previously, the TENF testing was done using an initial condition with only one stitch row in the crack region. Because of the limited specimen length, a test with more stitch rows in the crack region could not be conducted properly. The finite element analysis here investigates the effect of stitch rows in the crack region. The load–displacement curve (Figure 3.20) reveals a significant effect of the number of stitch rows on the peak load. The more stitch rows there were in the crack region, the greater was the load needed to initiate propagation of delamination. However, an increasing load could not be considered as equivalent to an increasing energy release rate, because the compliance of the laminates also changed owing to stitch bridging. To address this issue, further work is needed to understand the energy dissipated by the stitch during loading. The energy dissipation due to stitch penetration of the laminate, to plastic deformation of the stitch thread and to fracture should be quantified clearly.

Furthermore, all of the stitched laminate models showed semi-stable crack propagation, even with no stitch row in the crack region. It should be noted that the absence of a stitch row in the crack region means that the model has stitch rows in the non-cracked region (and is not equivalent to a totally unstitched laminate model). The delamination behavior is called semi-stable because propagation occurred when a step (a small drop in load) appeared in the load–displacement curve. Conversely, in the case of a totally unstitched laminate model, the load dropped drastically once delamination started to propagate. This showed that stitched laminates could suppress propagation of delamination.

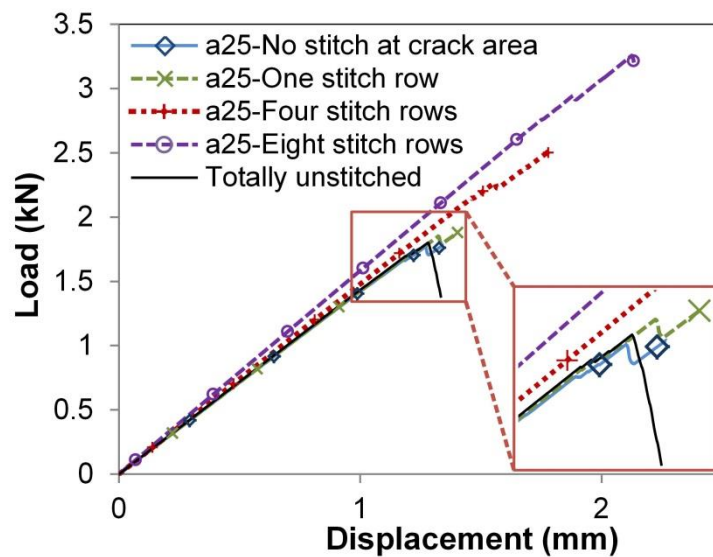


Figure 3.20: Effects of number of stitch rows at the crack region

3.4.4 Finite Element Validation using other Laminate Orientation

In order to confirm reliability of the developed finite element model, particularly on cohesive zone parameter as discussed previously, another validation with different specimen lay-up were conducted. Additional experiment with stitched laminate lay-up

of $[45/90/-45/0/0/45/90/90/-45/0]_s$ were tested continuously until the delamination reach the central loading pin. Load-displacement curve with number of active stitch threads from both experiment and finite element simulation are plotted in Figure 3.21. The finite element result shows strong agreement with the experimental ones (with 5% error in the peak load). The crack propagation length vs. loading pin displacement also observed as shown in Figure 3.22. The simulation of crack propagation exhibits similar results with the experimental data, thus confirm the reliability of modeling techniques and a proper selection of cohesive zone parameters.

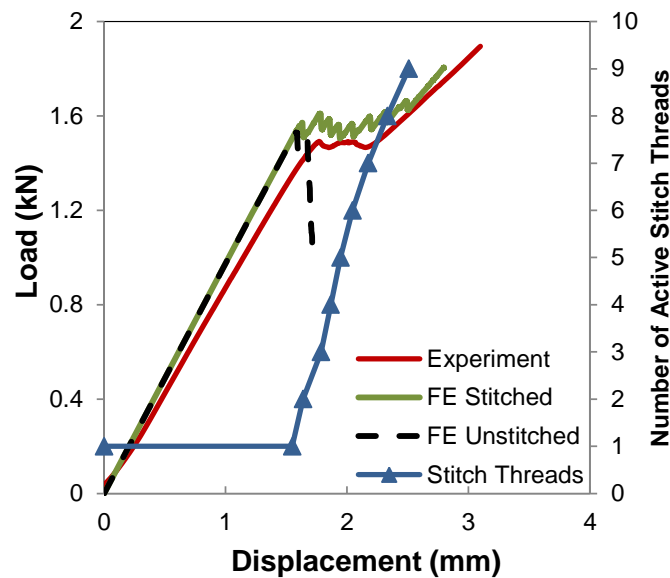


Figure 3.21: Load displacement curve with number of active stitch thread at crack region

The delamination interface at crack length of 38 mm and 50 mm are depicted in Figure 3.23. It also shows that at stitch thread position, the delamination (the red area) is suppressed significantly due to the full effect of reducing crack sliding displacement by the stitch threads.

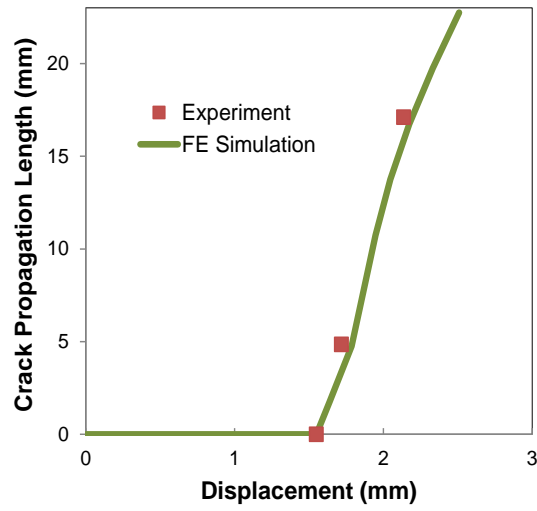


Figure 3.22: Crack propagation length vs. displacement

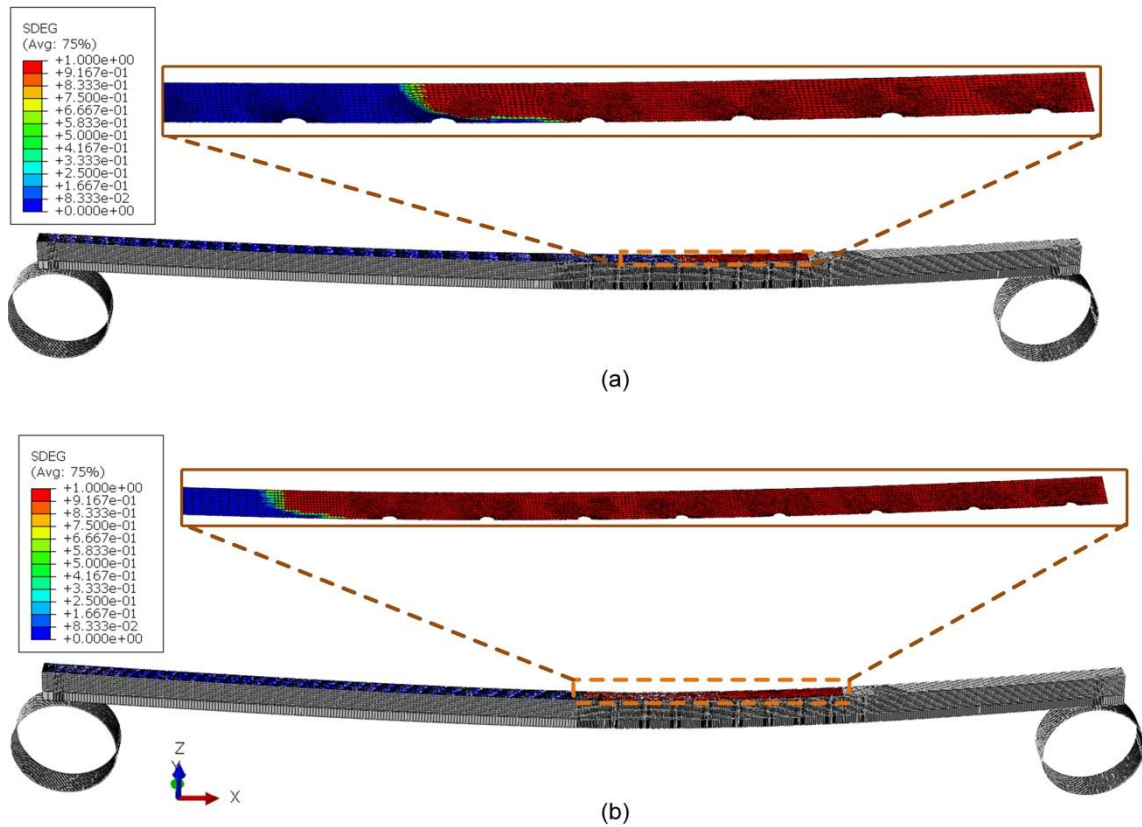


Figure 3.23: Delamination indicator (a) At the crack length of 38 mm (b) At the crack length of 50 mm

The possibility of fiber rupture and matrix crack during the simulation is also investigated. Figure 3.24 (b) shows the normal stress (S_{11}) distribution at the entire specimen. The highest stress is at vicinity of stitch threads (delamination region) as shown in zoom area with the maximum stress value about 1542 MPa. Compared to the laminate tensile strength (2950 MPa), the maximum stress is much lower than maximum normal stress (S_{11}). Hence, it is confirmed that there is no fiber rupture during the test.

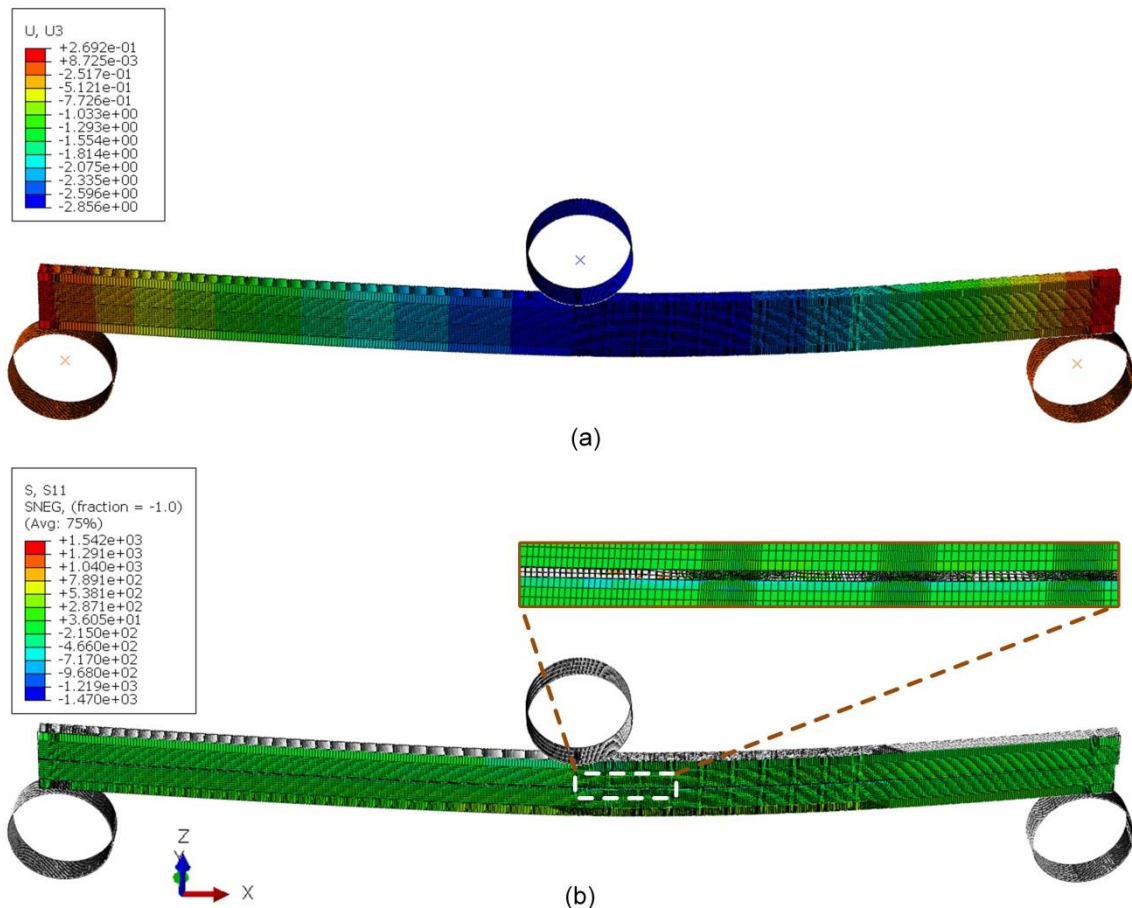


Figure 3.24: Finite element simulation of TENF at the crack length of 50 mm

(a) Deflection- U_3 (b) Normal stress along fiber direction- S_{11}

The possibility of matrix crack is investigated using maximum normal stress perpendicular to fiber direction (S_{22}) and in-plane shear stress (S_{12}) as depicted in Figure 3.25. The maximum value of normal stress (S_{22}) occurred at upper aluminum tab under the loading pin contact region. At the stitched laminate region the normal stress are seem to be lower than matrix tensile strength (50 MPa). Also for in-plane shear stress (S_{12}), the maximum value is lower than matrix shear strength (about 80 MPa). Therefore, it is also confirmed that no matrix crack occurred during the test.

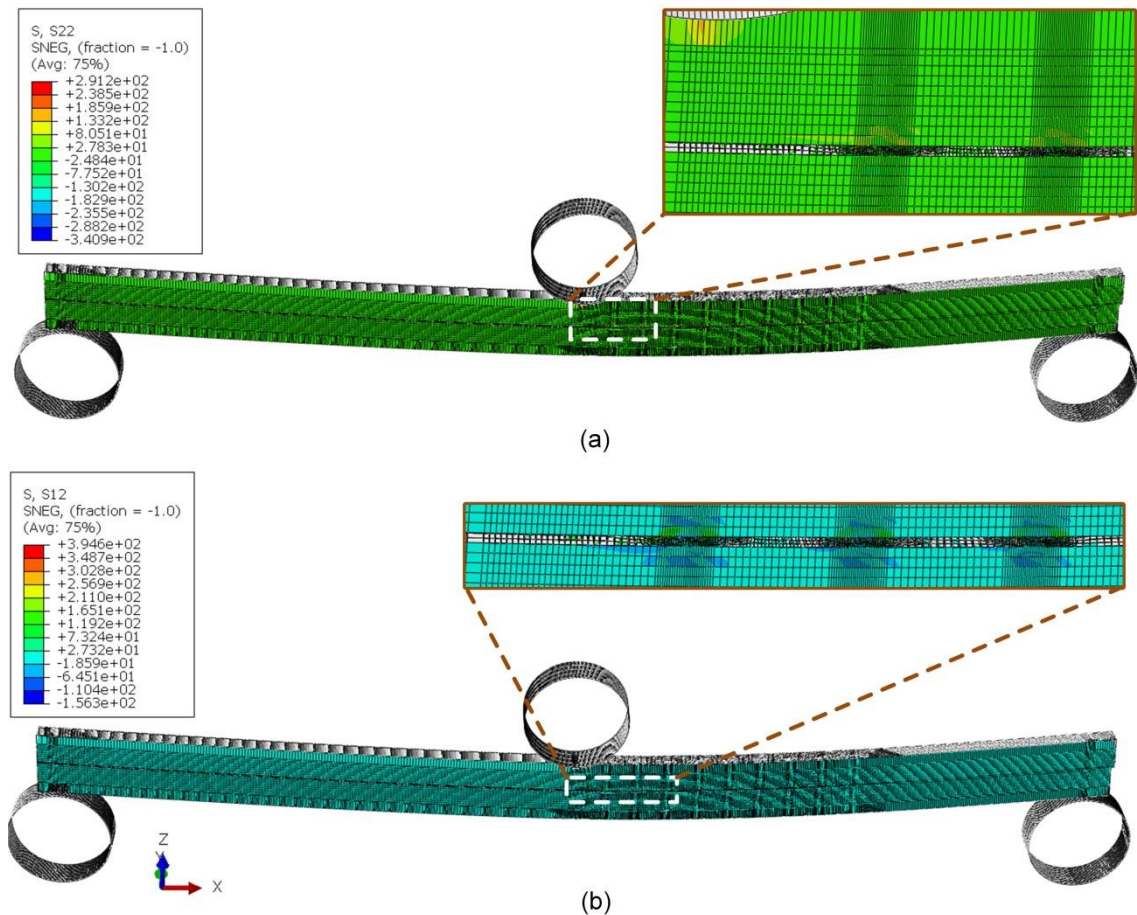


Figure 3.25: Finite element simulation of TENF at the crack length of 50 mm
 (a) Normal stress perpendicular to fiber direction- S_{22} (b) In-plane shear stress- S_{12}

In experimental work, it was reported that there is no stitch thread broken until end of the test for stitched laminate with 500 denier stitch thread thickness. The deformation of each stitch thread at the delaminated region cannot be investigated by experiment. Figure 3.26 shows the predicted deformation of each stitch thread during TENS test. It is important to be noted that the stitch thread will be broken when it reach the expansion of 0.4 mm (considering the maximum load of 180 N and spring connector stiffness of 450 N/mm). Figure 3.26 clearly concludes that the first stitch thread which has the longest expansion (0.16 mm) is still far from broken point.

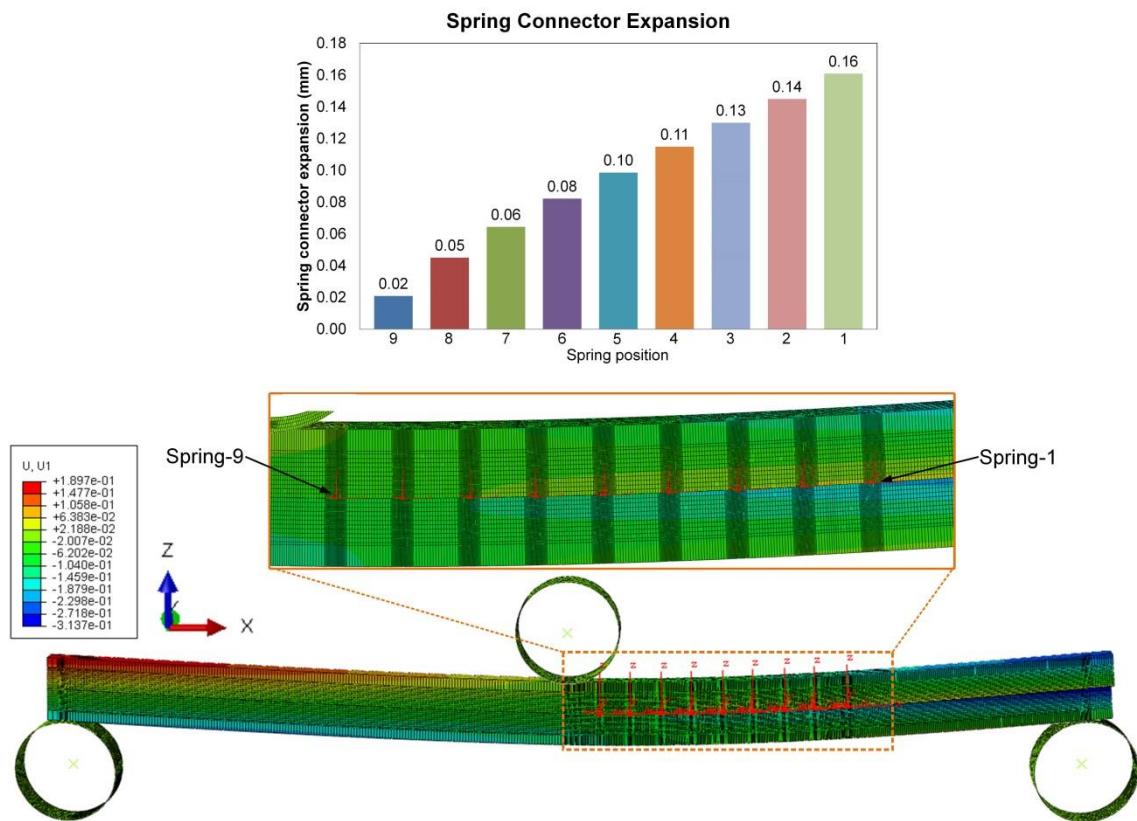


Figure 3.26: Predicting stitch thread deformation during TENS test

3.5 Conclusions

A finite element model of the mode II delamination test has been successfully developed. A single-stitched laminate was modelled under pure shear loading and the results verified by experimental data. TENS models were developed using a cohesive zone element to represent the crack propagation plane and adopting the techniques of single-stitched laminate modelling. A study of the cohesive zone modelling parameters revealed that the interfacial stiffness K_0 and viscosity coefficient μ have significant effects on accuracy and computational time, while the interfacial strength seems to have a negligible effect on the peak load. The appropriate ranges for K_0 and μ are 4.25×10^{14} to $4.5 \times 10^{14} \text{ N m}^{-3}$ and 10^{-5} to 10^{-4} , respectively.

The finite element results showed that the number of stitch rows in the crack region has a strong effect on the peak load before crack propagation. It can also be concluded in general that the stitching technique can suppress propagation of delamination. Even though there is no stitch row in the crack region, the existing stitch threads ahead of the crack tip will immediately suppress the crack propagation once delamination starts to propagate. Furthermore, the finite element simulation also confirms the experimental results that there is no stitched broken during TENS test.

Chapter 4

Feasibility Study of Using Four Point End Notched Flexure (4ENF) Test for Stitched Laminate Application

4.1 Overview

This chapter aims to conduct feasibility study of using four point end notched flexure (4ENF) test as an alternative method for mode II delamination test. Both standard 4ENF and tabbed 4ENF (T4ENF) specimen of stitched composite laminate are investigated numerically. In order to observe whether matrix crack or fiber rupture occurred during the test simulation, maximum normal and shear stresses at each layer are plotted. The matrix crack are then calculated using Hashin`s criteria, while fibers rupture are determined using maximum stress criteria. A parametric study of various matrix strength properties is conducted to understand the limitation of both testing methods. Furthermore, energy release rate of stitched composite are predicted based on compliance calibration method and the error of using T4ENF method are also investigated.

4.2 Modeling Techniques

4.2.1 Finite Element Model

The testing set-up of T4ENF is shown in Figure 4.1 refers to reported work by Davies et.al [99]. It is important to be noted that centre loading pin has capability to be rotated so that the load is kept balanced during the test. Tabs are omitted in case of normal 4ENF test. The laminate consist of 20 layers of carbon fibres

(Torayca-T800SC-24K) with lay-up order of $[+45/90/-45/0/0/+45/90/90/-45/0]_s$. The mechanical properties of laminae are calculated based on homogenization method using in house codes [92] and summarize in Table 4.1. The thickness of each layer is 0.205 mm, and total thickness of specimen is 6.35 mm including aluminium tabs and adhesive bonding. Al 7075T6 (yield strength of 500 MPa) are used for the tab plates.

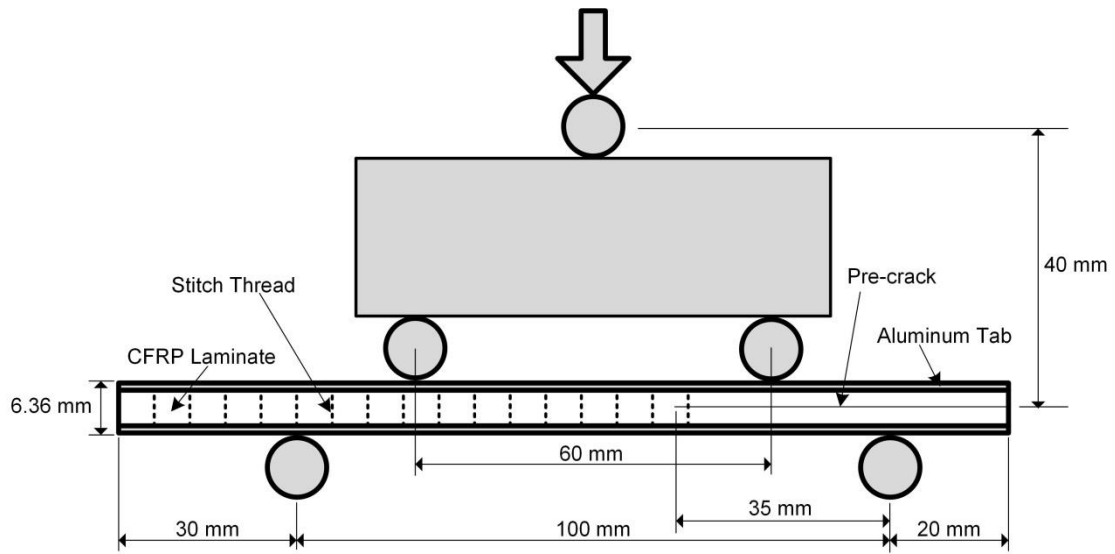


Figure 4.1: Set-up of tabbed 4ENF test

Table 4.1: Mechanical properties of laminae

E_1	E_2	E_3	G_1	G_2	G_3	ν_{12}	ν_{13}	ν_{23}
(GPa)	(GPa)	(GPa)	(GPa)	(GPa)	(GPa)			
158.6	4.7	4.7	3.8	3.8	2.7	0.33	0.33	0.47

Finite element model of tabbed 4ENF test are depicted in Figure 4.2. The fixture is also included in the analysis to investigate the fixture deformation during the test. The same modeling techniques of ENF test in previous chapter are adopted where the stitch threads are modeled by spring connector element and delamination are simulated using

cohesive zone elements as shown in Figure 4.3. All cohesive zone parameters in the previous chapter are also adopted in modeling 4ENF test.

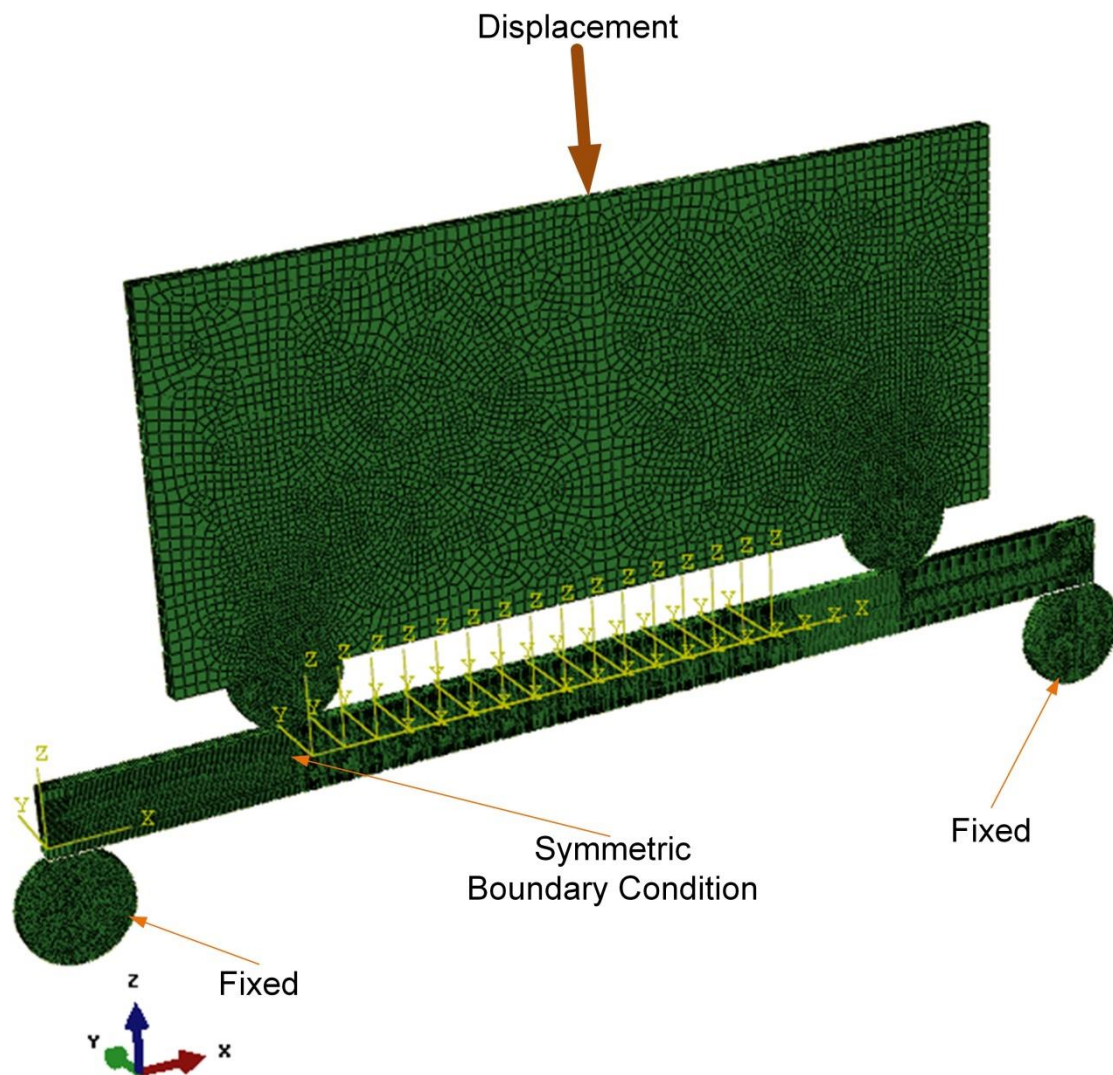


Figure 4.2: Finite element model of Tabbed 4ENF test

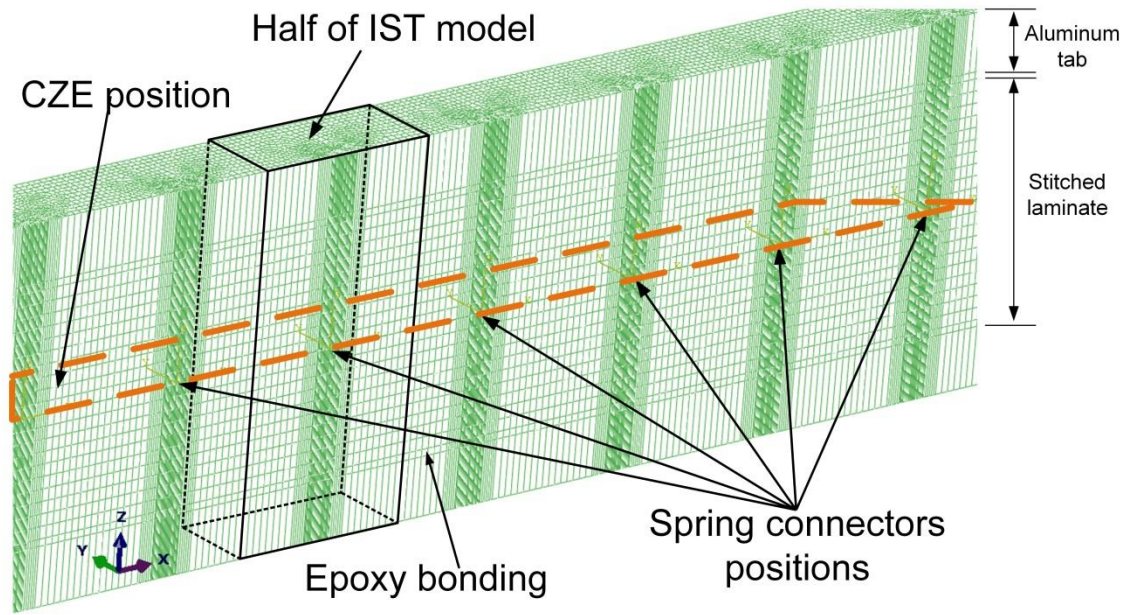


Figure 4.3: Detail modelling techniques of Tabbed 4ENF test

4.2.2 Investigating Laminate Failure during 4ENF Test

It is important to be noted that there should be no laminate failure except delamination during the 4ENF test. To comply this requirement, the possibility of matrix crack and fiber ruptures are investigated. The matrix crack will be occurred if Equation 4.1 (Hashin`s criteria) is satisfied.

$$\left\{ \frac{\sigma_{22}}{Y_T} \right\}^2 + \left\{ \frac{\sigma_{12}}{S_{xy}} \right\}^2 \geq 1 \quad (4.1)$$

where, σ_{22} and σ_{12} are normal stress perpendicular to fibers orientation and in-plane shear stress, respectively. Y_T is matrix tensile strength, while S_{xy} is matrix shear strength.

Furthermore, fiber ruptures are occurred whenever the maximum stress criterion (Equation 4.2) is satisfied. In this condition, normal stress in fiber direction is equal or more than fiber tensile failure. For carbon fiber T800SC-24K from Toray Inc., fiber tensile failure (X_T) is 2950 MPa [90].

$$\frac{\sigma_{xx}}{X_T} \geq 1 \quad (4.2)$$

Both x and y direction in Equation 4.1 and 4.2 are in local coordinate system. In case of unidirectional laminate, the local coordinate system will be the same with the global one.

4.2.3 Predicting of Energy Release Rates

Energy release rate (G_{IIC}) is calculated from the simulation results using compliance calibration method following Equation 4.3 as proposed by Davies et.al [37].

$$G_{IIC} = \frac{mP^2}{2w} \quad (4.3)$$

where m is the slope of compliance vs. crack length, P is a certain load where delamination start to propagate, and w is the width of the specimen. To obtain the value of m , compliance of the model are simulated at the crack length of 35, 38, 41, and 44 mm. Noted that these crack length involved 1, 2, 3, or 4 active stitch threads at the delaminated area, respectively.

4.3 Results and Discussions

4.3.1 Load-displacement Curves

Predicted load vs. displacement curves, deformations and delamination regions are presented in Figures 4.4-11. The simulation results of unstitched unidirectional and multidirectional laminate are also presented (Figure 4.4-7) as references. Relatively constant load after crack propagations are depicted that indicate stable crack propagation, even for unstitched laminate. It is worth to be noted that stable crack propagations is a typical characteristic of 4ENF test [38, 99-101].

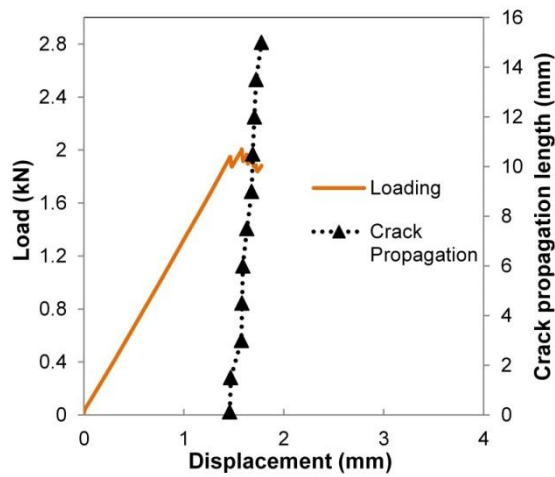


Figure 4.4: Predicted load-displacement curve of unstitched unidirectional laminate under 4ENF test

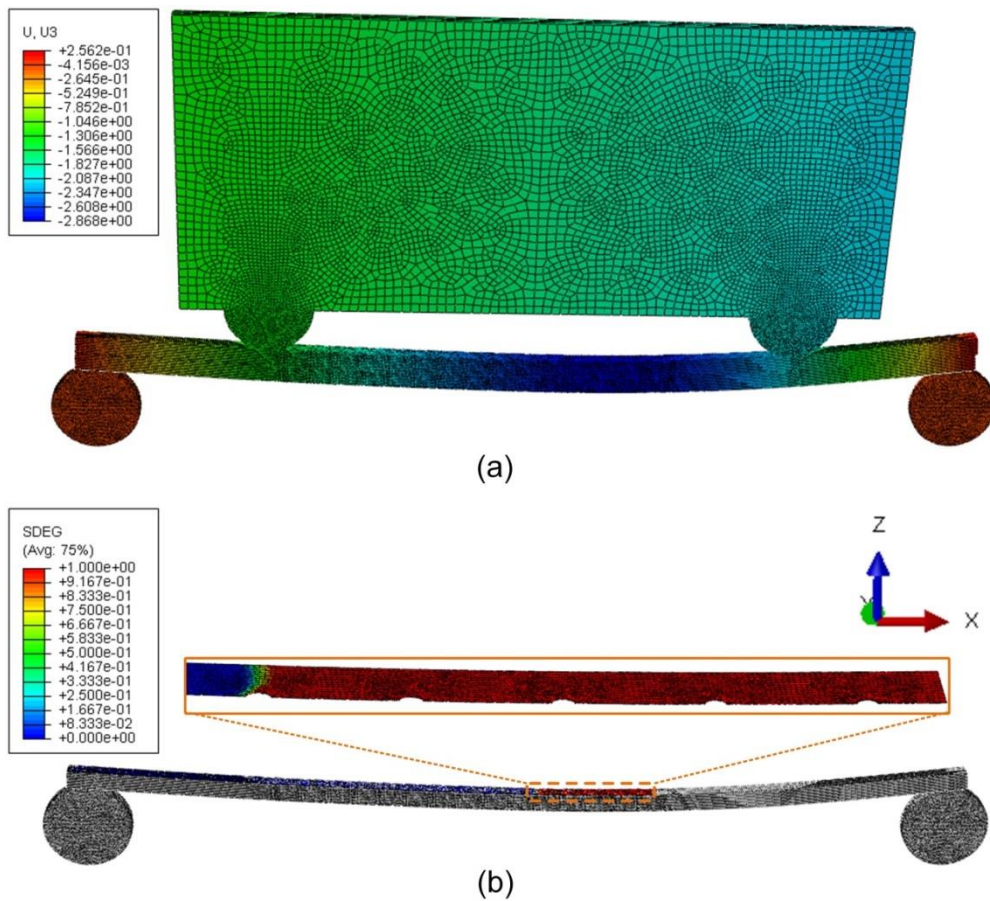


Figure 4.5: Simulation results of unstitched unidirectional laminate under 4ENF test
 (a) Deformation (b) Delamination propagated till 48.5 mm length

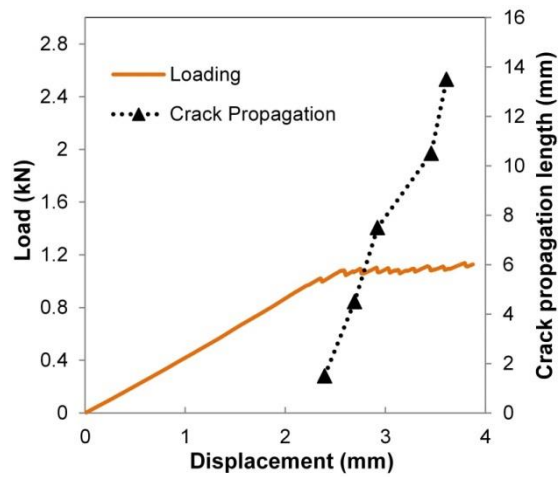


Figure 4.6: Predicted load-displacement curve of unstitched multidirectional laminate under 4ENF test

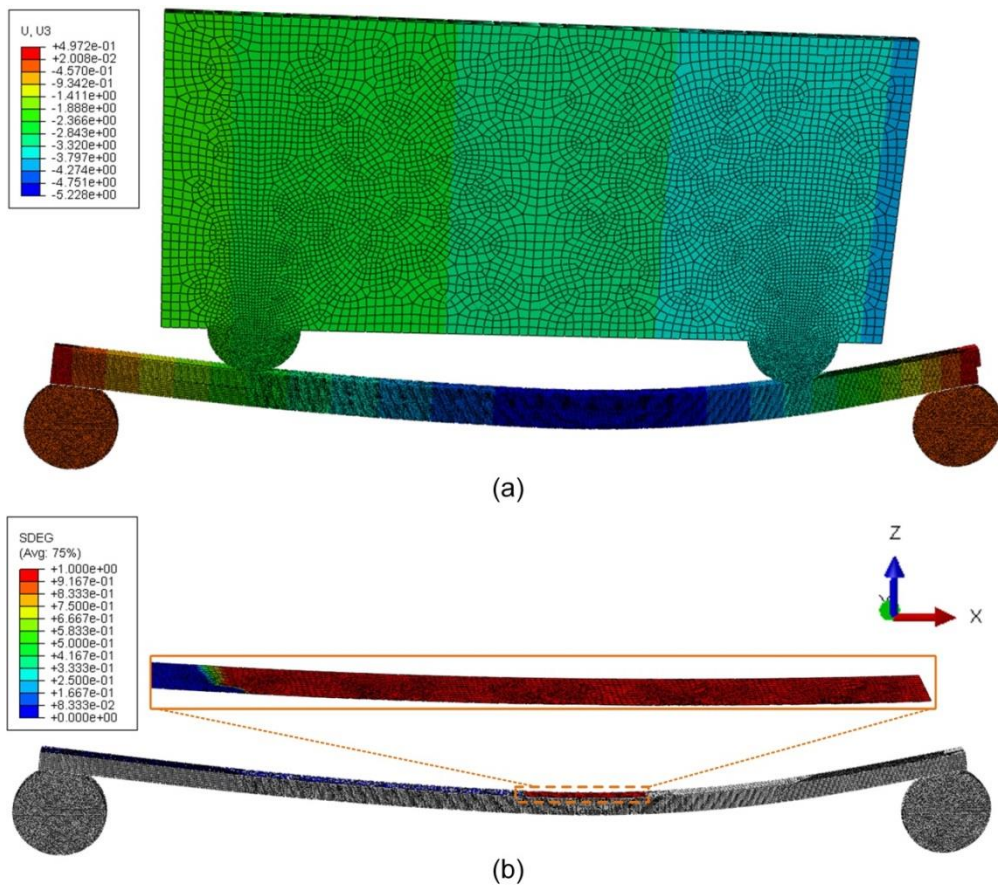


Figure 4.7: Simulation results of unstitched multidirectional laminate under 4ENF test

(a) Deformation (b) Delamination propagated till 48.5 mm length

Figure 4.8 shows simultaneously the load-displacement curve of stitched laminate under 4ENF test (without tabs) with respective crack propagation length. The loads are kept increasing after crack propagation that indicate the load bridging by stitch threads at delaminated region. Figure 4.9 (a) depicted the fixture is not in horizontal condition due to the rotation at the loading point to balance the load at both contact points with the specimen. The figure is also indicated that there is no deflection at the fixture due to relative high load during the test. Figure 4.9 shows the delamination pattern of stitched laminate which is different with the pattern of unstitched laminate shown previously (Figure 4.5 and 4.7). The areas closed to the stitched thread are retained from delamination due to suppressed sliding displacement by the stitch thread. Furthermore, stitch threads deformation are depicted in Figure 4.10, the maximum stitch thread extension is 0.16 mm which shown by the first stitch thread (spring-1 in the finite element simulation). It confirm that there is no stitched broken during the test simulation.

The load-displacement curve of stitched laminate under tabbed 4ENF test is depicted in Figure 4.11. The effect of tabs plates are clearly shown by highest slope of the curve compared to specimen without tabs (Figure 4.8). Although higher load occurred during the test, the fixture still kept un-deformed as shown in Figure 4.12 (a). It is worth noted that the deformation at loading point on the upper side of the fixture does not show any concentrated deformation, hence confirmed no deflection of the fixture. Moreover, the delamination pattern (Figure 4.12 (b)), also shows the effect of sliding displacement suppression by stitch threads at the delaminated region. Figure 4.13 shows the deformation of each stitch threads at delaminated region. The maximum extension is 0.12 mm which shorter than the maximum extension in 4ENF simulation.

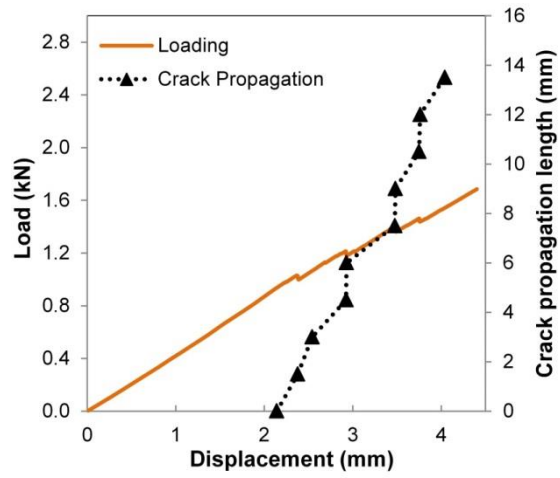


Figure 4.8: Predicted load-displacement curve of stitched laminate under 4ENF test

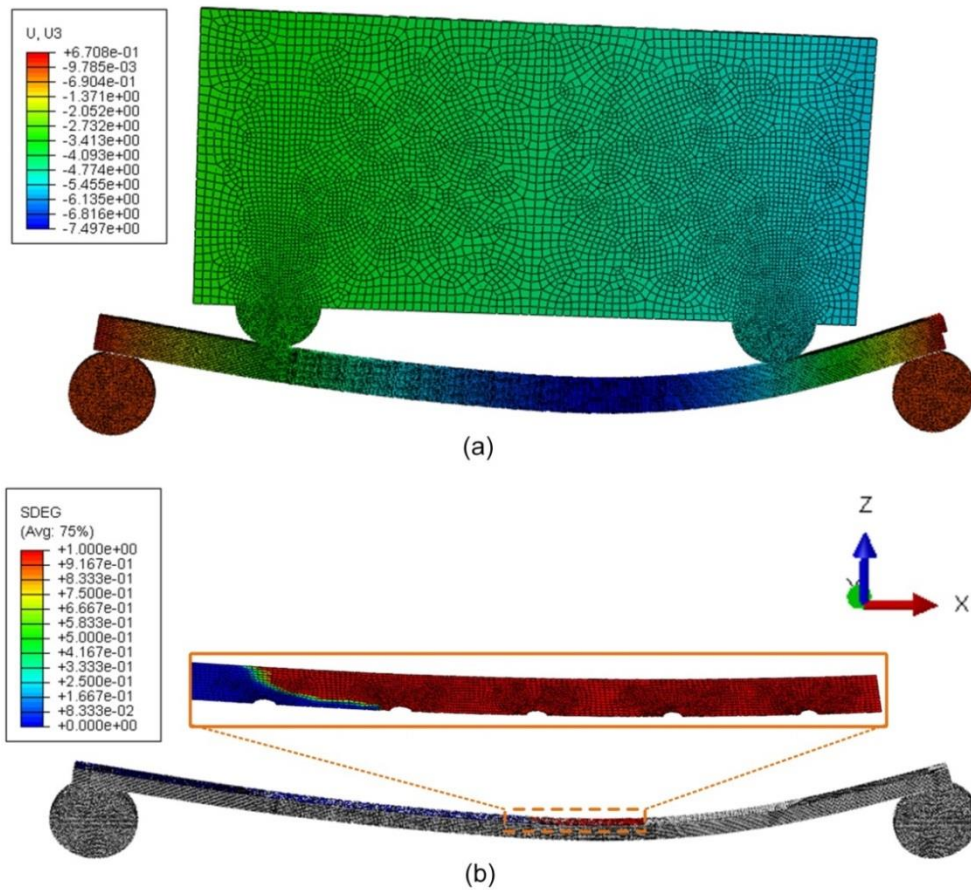


Figure 4.9: Simulation results of stitched multidirectional laminate under 4ENF test

(a) Deformation (b) Delamination propagated till 48.5 mm length

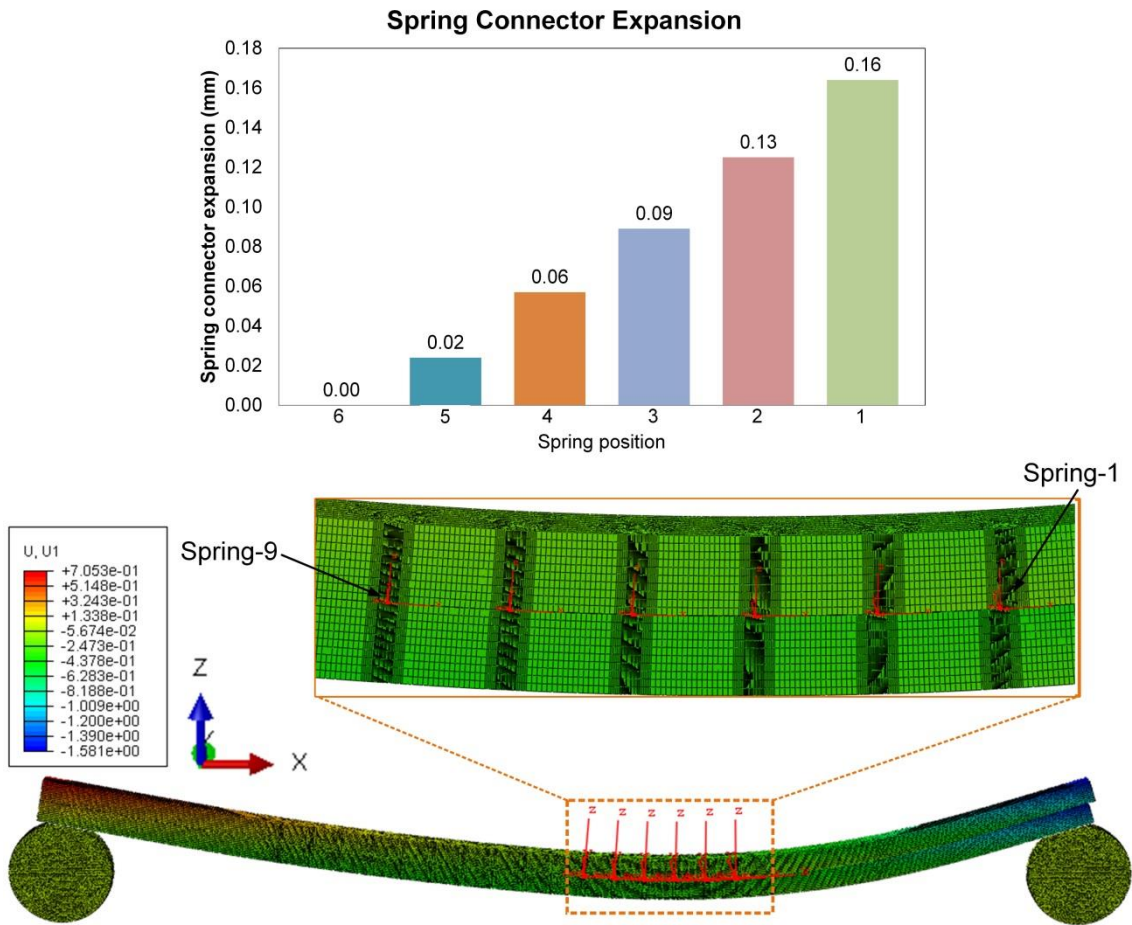


Figure 4.10: Predicting stitch thread deformation during 4ENF test

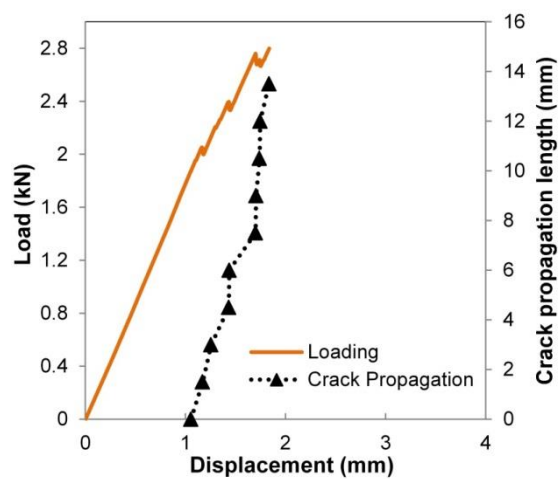


Figure 4.11: Predicted load-displacement curve of stitched laminate under Tabbed 4ENF

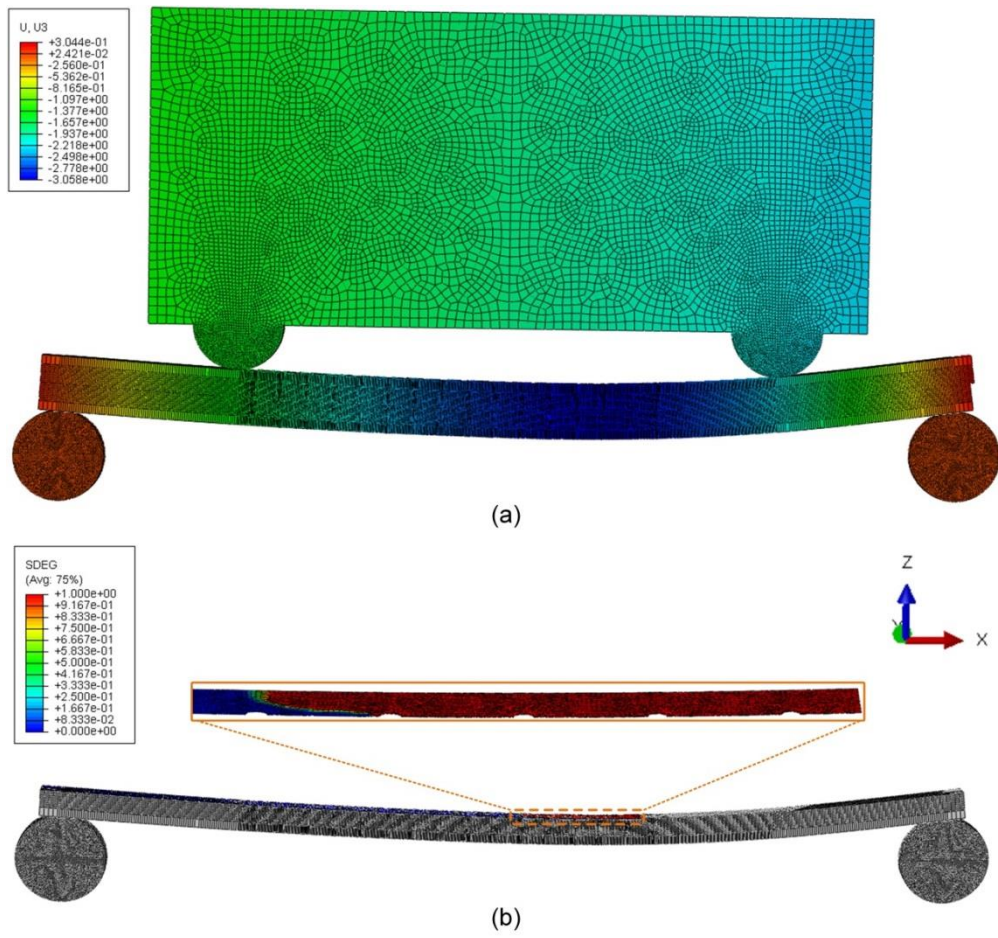


Figure 4.12: Simulation results of stitched multidirectional laminate under T4ENF test

(a) Deformation (b) Delamination propagated till 48.5 mm length

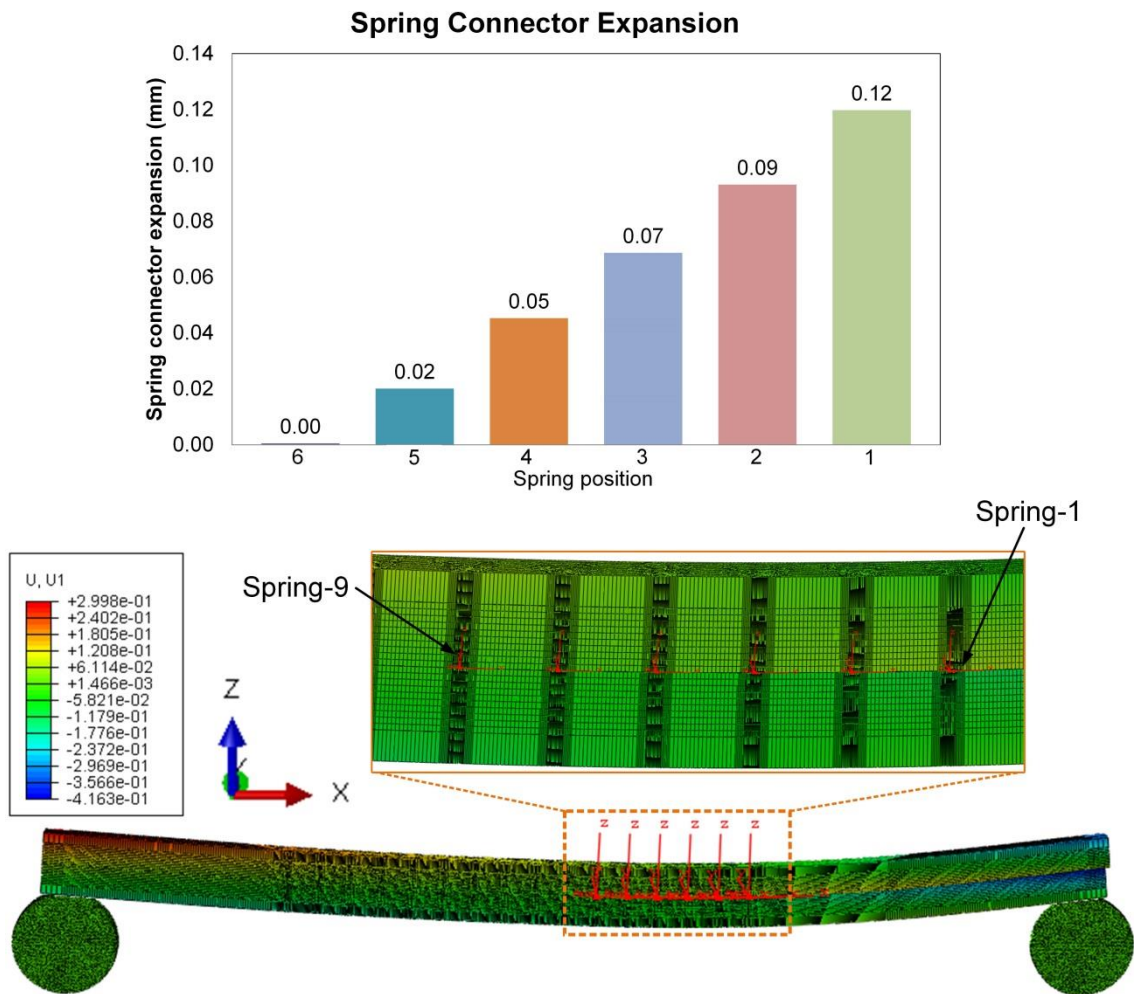


Figure 4.13: Predicting stitch thread deformation during T4ENF test

4.3.2 Laminate Failure Possibility during 4ENF Test

In order to investigate the possibility of premature failure during 4ENF test, stresses analysis at each layer of laminate are conducted, particularly on the stress components (σ_{xx} , σ_{xy} , σ_{yy}) in Equation 4.1 and 4.2. The stresses were measured at the middle span loading pins which are the highest stresses at each layer.

Considering all of required stresses components are in local coordinate, the stresses in unstitched unidirectional laminate are presented first (Figures 4.14-16). The local coordinate of unidirectional laminate is the same with global coordinate system.

Figure 4.14 shows normal stresses along fiber direction (σ_{xx}) at each layer of unidirectional laminate at various crack propagation length (Δa) during 4ENF simulation. At initial state of loading where the crack (delamination) has not been propagated yet, the stresses along the thickness are in one linear line. By increasing the displacement, the crack starts to propagate toward the middle span. At position where the crack tip close to middle span ($\Delta a = 14$ mm) the stresses plot starts to form two linear lines.

Figure 4.15-16 exhibit the normal stresses perpendicular to fiber direction (σ_{yy}) and in plane shear stresses (σ_{xy}) which are the main stress components to determine matrix crack. In case of unidirectional laminate, both of stresses are almost zero, a small increment appears (below 3 MPa) when the crack tip is closed to measured position.

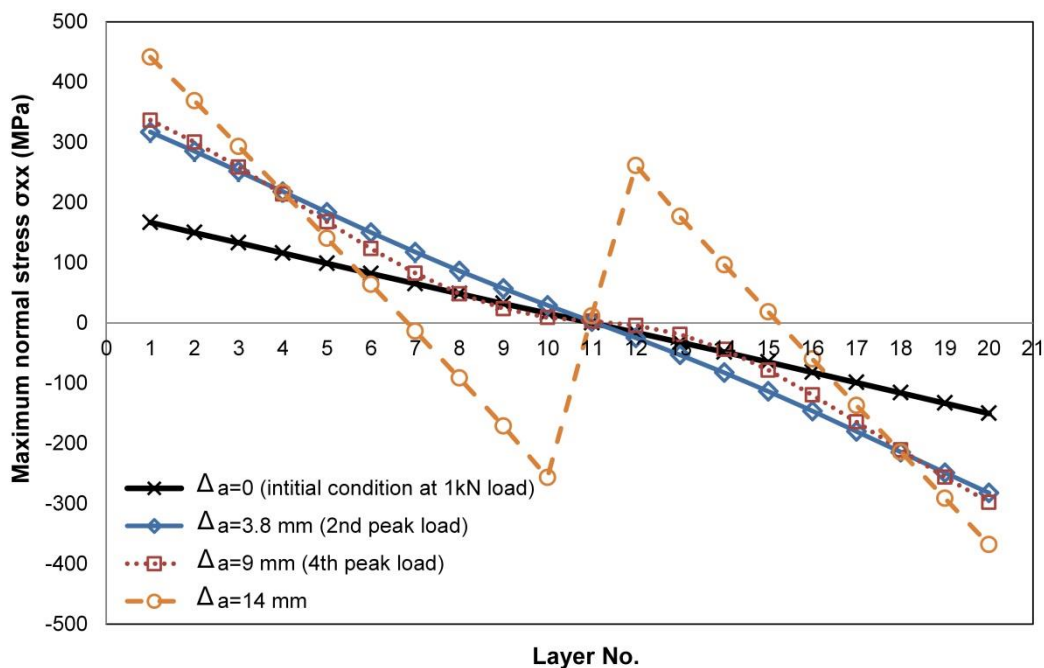


Figure 4.14: Normal stress along fiber direction (σ_{xx}) of unstitched unidirectional laminate

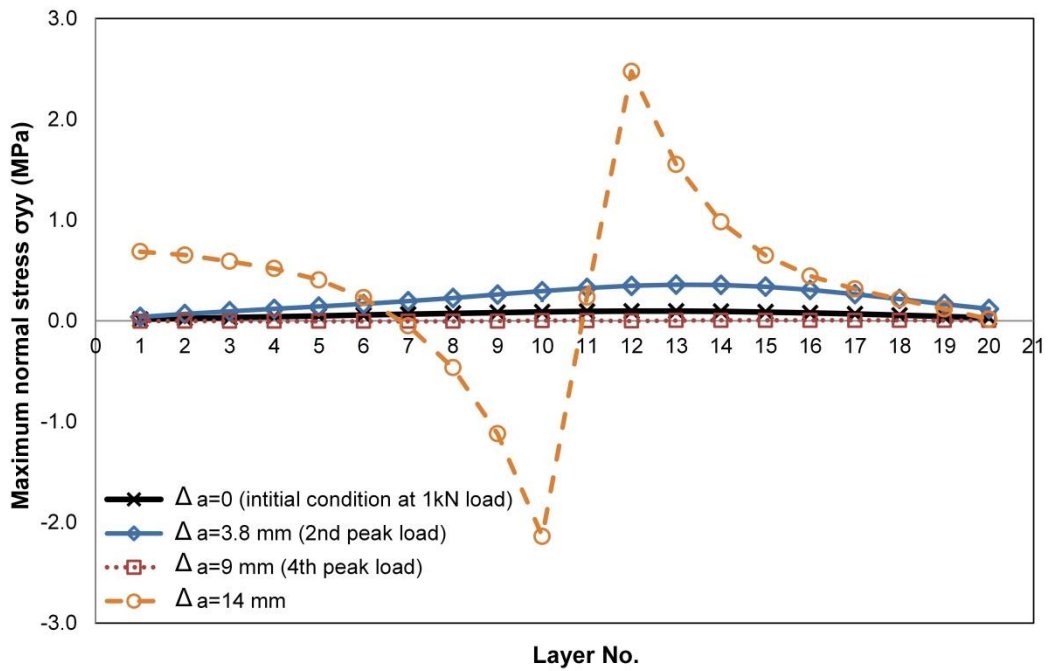


Figure 4.15: Normal stress perpendicular to fiber direction (σ_{yy}) of unstitched unidirectional laminate

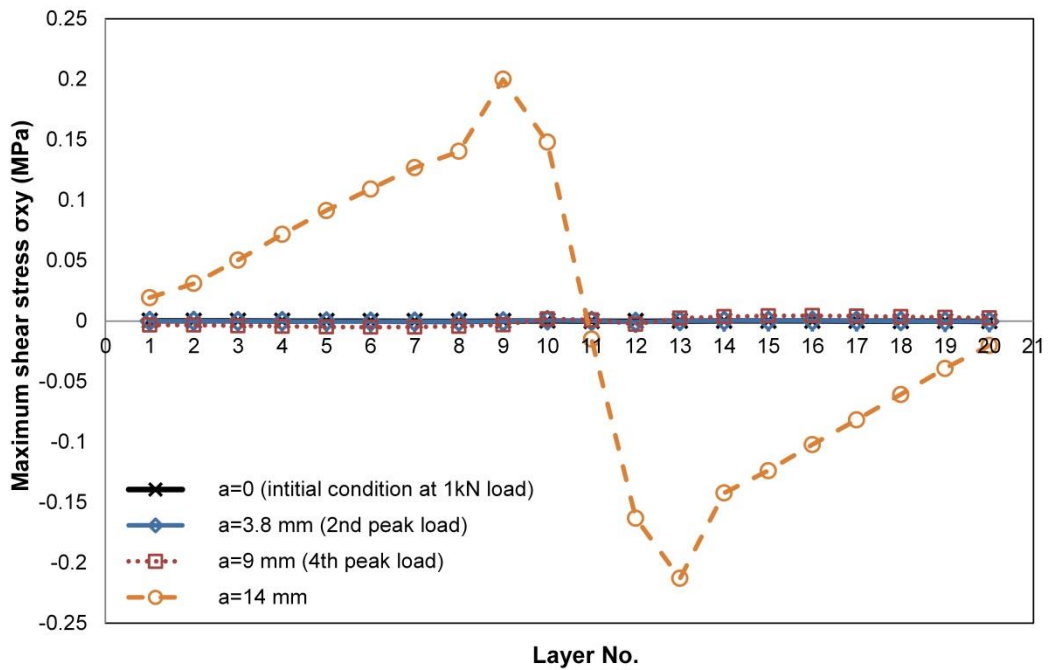


Figure 4.16: In plane shear stress (σ_{xy}) of unstitched unidirectional laminate

In order to investigate the possibility of matrix crack during 4ENF and T4ENF test of stitched laminate, normal stress perpendicular to fiber direction (S_{22}) and in-plane shear stress of stitched laminate (S_{12}) are depicted in Figures 4.17-20. The maximum stresses (for both S_{22} and S_{12}) are occurred at interface between stitch area and surrounding laminate which has been discussed previously in IST simulation. However, the energy dissipated by damages occurred at stitch area (due to stitch bridging) are considered in mode II energy release rate. However, the damages (matrix crack) occurred in other positions are not consider in mode II energy release rate, thus prohibited during the test. To address this restriction, the stresses (S_{22} and S_{12}) at the middle of loading span are plotted in Figure 4.18 and 4.20. It is important to be noted that the stress value are taken at the end of simulation, where the crack propagation length reached 13.5 mm. From the figures, it is clearly shown that the maximum value occurs at the lowest layer (45°), from which couple effect of both stresses on matrix crack are calculated (using Equation 4.1). The possibility of matrix crack is highly depends on type of the matrix. To evaluate the effect of matrix tensile strength on matrix crack, a parametric study is reported in Table 4.2. In this parametric study, matrix shear strengths are assumed to be the same (80 MPa) because its contribution to initiate matrix crack is relatively small. Table 4.2 shows that using a typical matrix with tensile strength lower than 40 MPa, 4ENF has a problem due matrix crack which occurred during the test. On the other hand, T4ENF test is suitable for any type of matrix because it reduces the maximum stresses as shown in Figure 4.18 and 4.20.

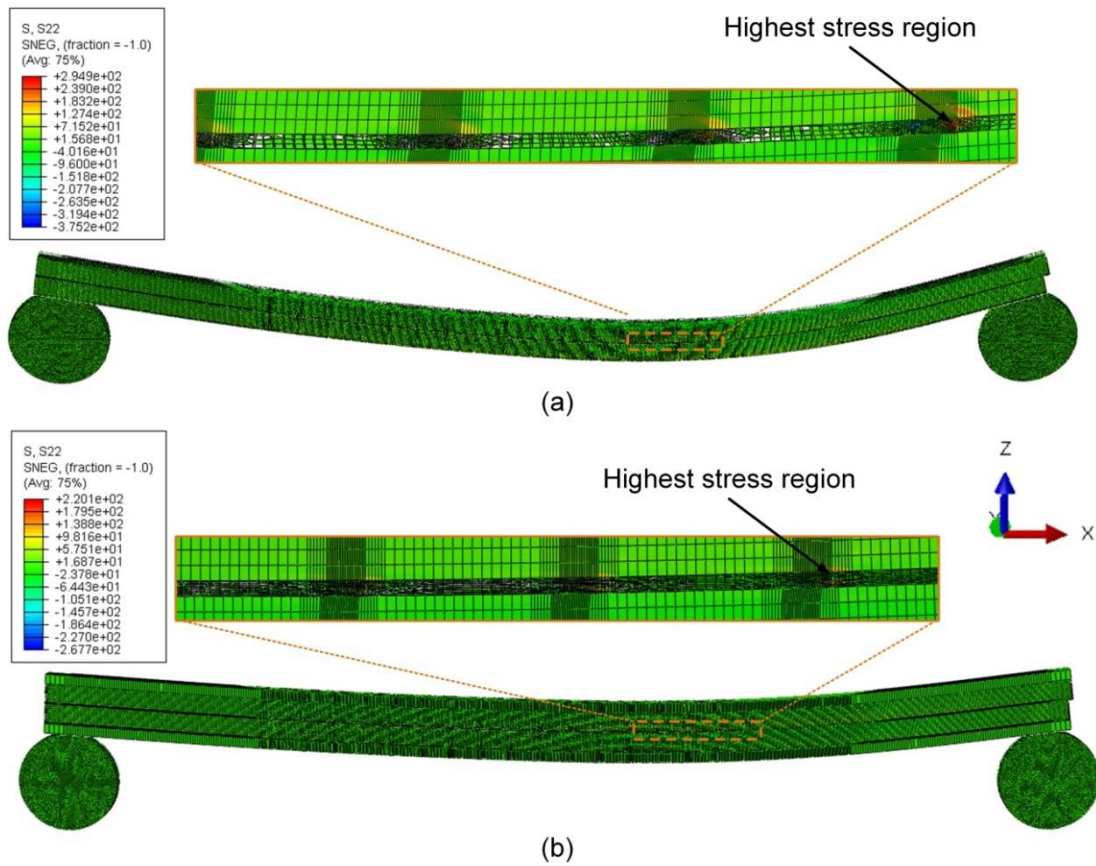


Figure 4.17: Normal stresses perpendicular to fibers direction- S_{22} (a) Stitched laminate without tabs (b) Stitched laminate with tabs

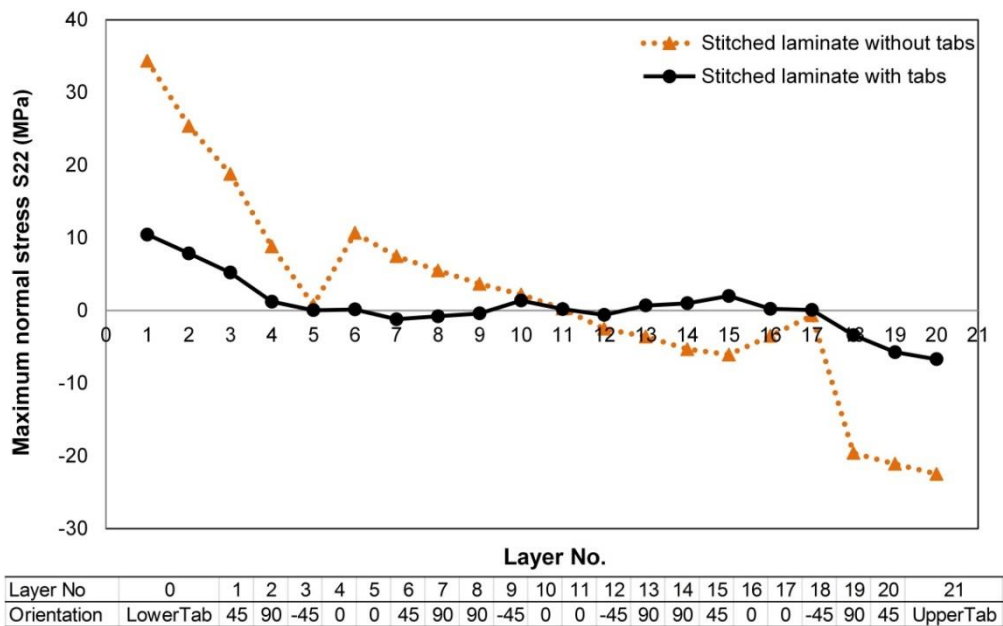


Figure 4.18: Normal stress perpendicular to fiber direction at each layer

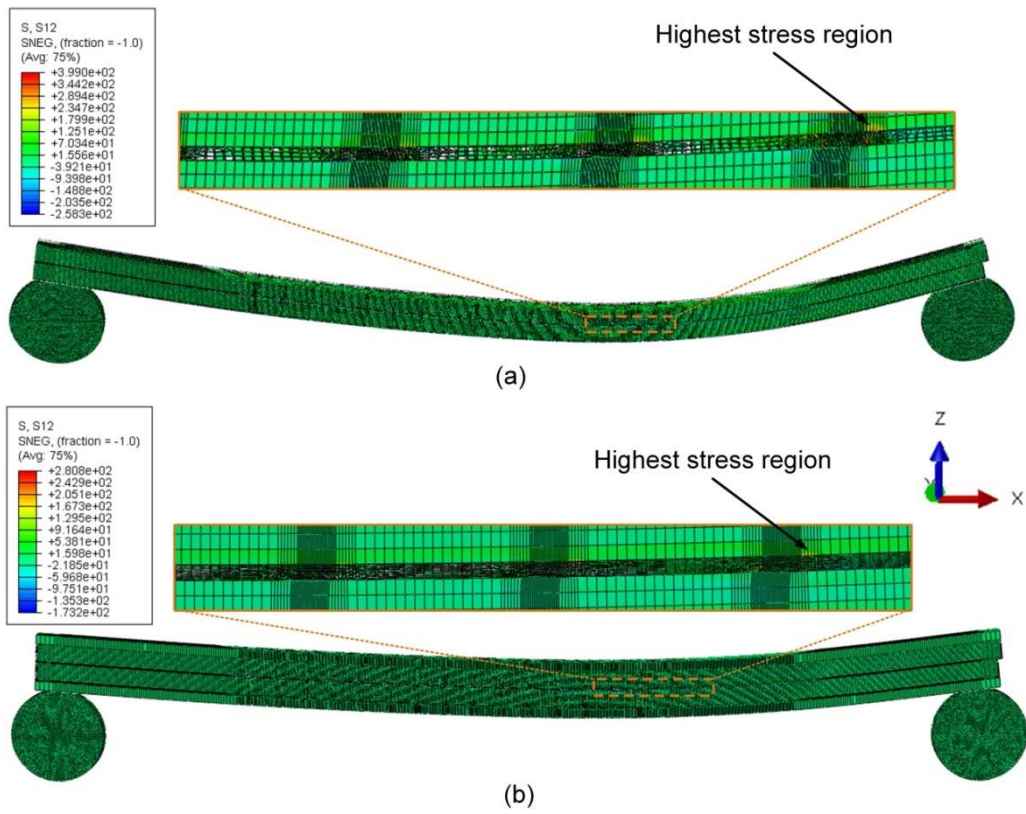


Figure 4.19: In-plane shear stresses- S_{12} (a) Stitched laminate without tabs (b) Stitched laminate with tabs

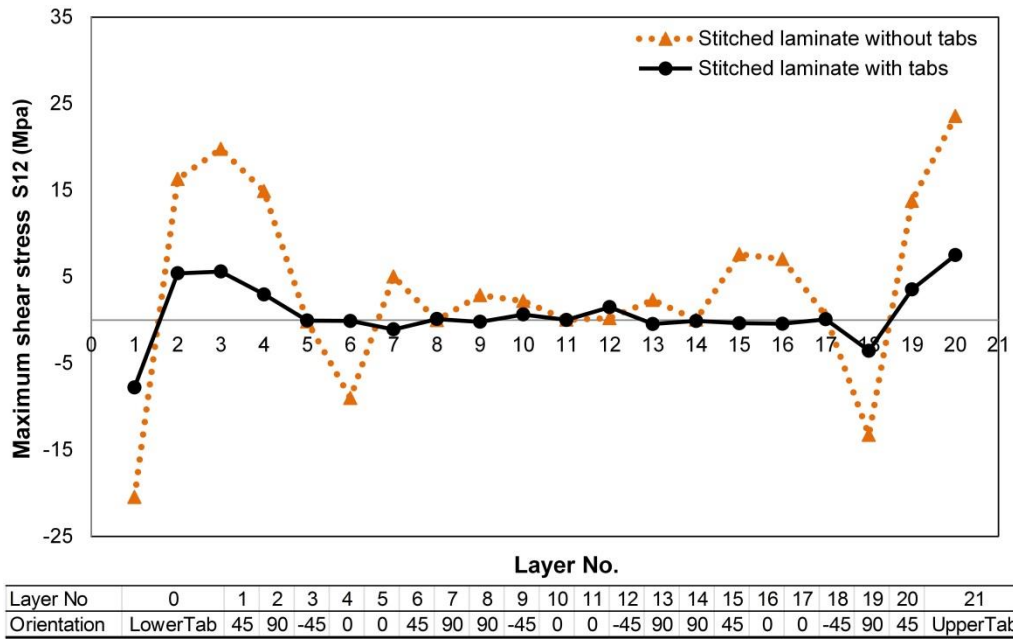


Figure 4.20: In-plane shear stress at each layer

Table 4.2: Parametric study of matrix crack

Method	σ_{yy} (MPa)	σ_{xy} (MPa)	Matrix crack (Equation 4.1) varied by Y_T (MPa)			
			30	40	50	60
4ENF	34.35	-20.45	1.38	0.80	0.54	0.39
T4ENF	10.46	-7.80	0.13	0.08	0.05	0.04

Furthermore, the fiber rupture is not occurred because the maximum normal stress along fiber direction (Figure 4.21 and 4.22) are much lower than fiber tensile strength (2950 MPa). Figure 4.21 also shows the normal stress at aluminum tabs (268.1 MPa) which is lower than the yield strength of Al 7075T6 (500 MPa). Hence, it is confirmed that the tab plates are still far away from plastic deformation.

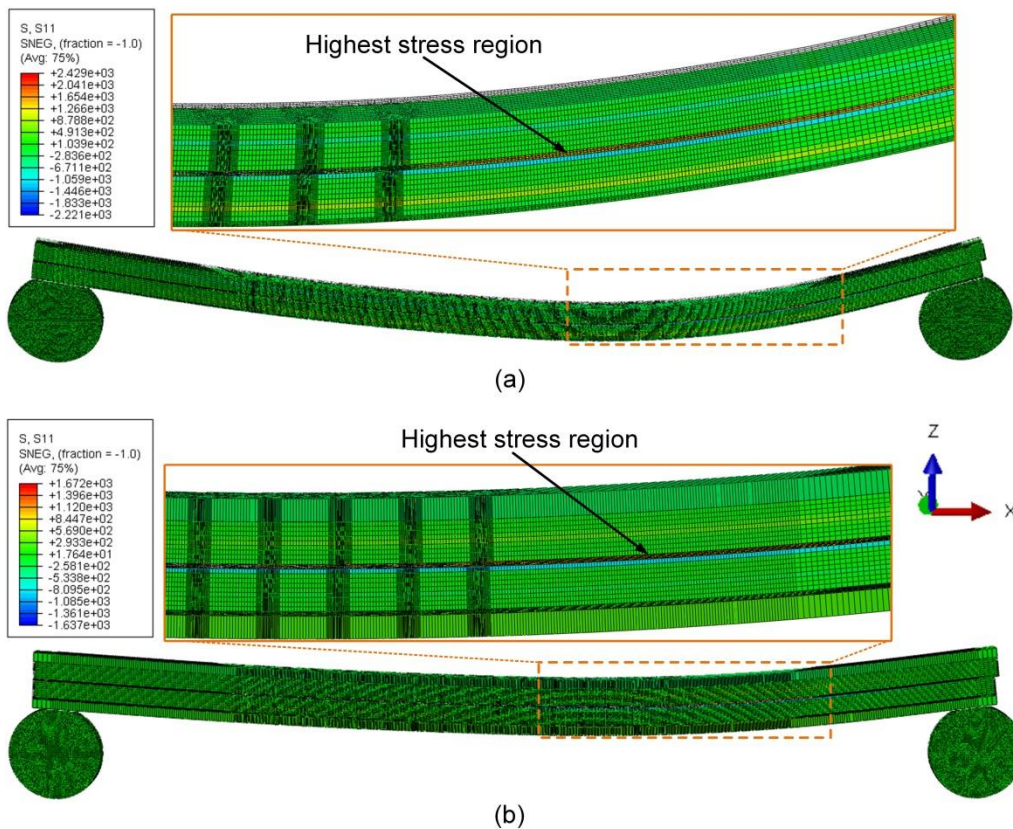


Figure 4.21: Normal stresses along fibers direction- S_{11} (a) Stitched laminate without tabs (b) Stitched laminate with tabs

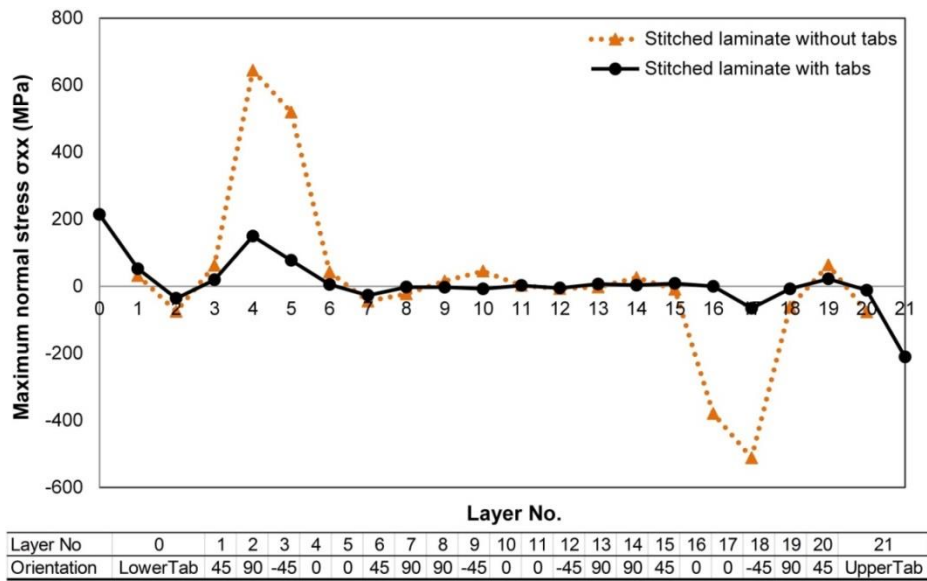


Figure 4.22: Normal stress in fiber direction

4.3.3 Energy Release Rates Prediction

Energy release rates (G_{IIC}) are calculated using Equation 4.3. The slopes (m) are obtained from compliance vs crack length as shown in Figure 4.23. Compliances of T4ENF are lower than those of 4ENF due to the existence of the tabs. The slopes (m) for 4ENF and T4ENF are $4e-05$ and $1e-05$, respectively. The loads (P) are recorded at several points where the delamination starts to propagate. Energy release rates (G_{IIC}) obtained using 4ENF and T4ENF are compared in Table 4.2. The errors of using T4ENF compared with 4ENF are less than three percent.

Considering specimen damage possibility and results accuracy, T4ENF exhibits the best choice. It could be used to some extent where delamination propagates passing through the center of loading span, so that higher G_{IIC} could be measured. In this case, one should be aware with aluminum tabs plastic deformation while increasing the displacement extremely.

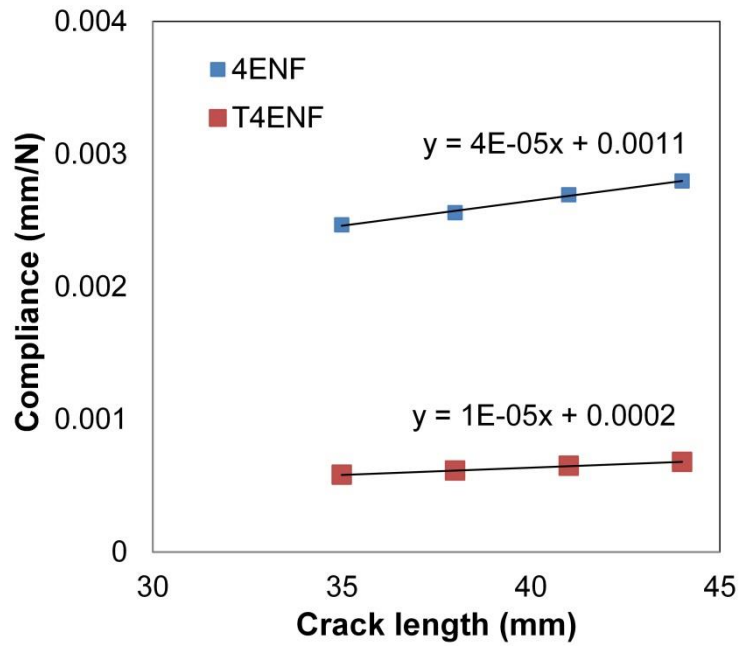


Figure 4.23: Compliance vs. crack length

Table 4.3: Energy release rate prediction

Crack Length (mm)	Load (kN)		G_{II} (kJ/m ²)		Error (%)
	4ENF	T4ENF	4ENF	T4ENF	
35	0.94	1.87	0.83	0.84	0.44
36.5	1.02	2.03	0.99	0.98	-0.79
38	1.07	2.13	1.08	1.08	0.38
39.5	1.21	2.40	1.39	1.37	-1.93
41	1.18	2.34	1.33	1.30	-1.84
42.5	1.40	2.76	1.86	1.81	-2.71
44	1.37	2.70	1.78	1.74	-2.63

4.4 Conclusions

Specimen preparation for standard 4ENF test is simpler than T4ENF test. Therefore, prior to experimental testing, it is better to check whether 4ENF test is quite enough to evaluate mode II delamination properties of typical stitched composites. The

numerical results of this study could be used as a general guideline that the laminate with relatively higher matrix tensile strength (above 40 MPa for the typical lay-up in this study) could be tested using standard 4ENF test, otherwise T4ENF test has to be used. T4ENF provide a wider capability because it reduces the critical normal and shear stress at each layers. It has also been proved numerically that T4ENF possesses quite similar results with standard 4ENF, with the error of less than three percent.

Chapter 5

Conclusions and Recommendations

5.1 Conclusion

This dissertation aims to investigate the effectiveness of stitching techniques in improving mode II delamination of composite laminates. Both experimental and numerical works are conducted. Experimental work is focus on evaluating the effect of stitch thread thickness and stitch density on enhancing mode II energy release rates (G_{IIC}) for particular stitch materials namely Vectran. The numerical work is purposed to provide a general tools that can evaluate any related issue on mode II delamination behavior, including; end notched flexure test (ENF), and four point end notched flexure (4ENF).

The main conclusions are summarized as follows.

First, stitch thread density is the most important parameter in designing the stitched composites. Using tabbed ENF test, it is found that high stitch density (3 x 3 mm) can improve the energy release rate by 2.4 times. However, low stitch density (6 x 6 mm) does not improve the energy release rate which is originally reported in this dissertation. The reason is that stitching process itself increases local fiber volume fraction. Higher fiber volume fraction reduced the energy released rate because it creates higher interface stress between fibers and matrix, thus the delamination occur easier. Therefore, in low stitched density, G_{IIC} improvement by stitch thread bridging is covered by G_{IIC} reduction due to higher local fiber volume fraction.

Second, stitch thread thickness is the next parameter to be considered. The

results explain that its effect on improvement G_{IIC} is not as higher as stitch density. Furthermore, it is important to be noted that using thicker stitch thread thickness will create bigger resin rich region and higher in-plane fiber waviness which can reduce the in-plane properties of stitched composites. So, it is better to increase stitch density rather than stitch thread thickness to optimize the mechanical properties.

Third, a novel interlaminar shear test (IST) is performed to understand the bridging mechanism of single stitched laminate. Based on force-displacement curve, micro-CT image and fracture surface of IST specimens, it could be summarized that stitch thread dissipates the energy by de-bonding from surrounding laminate, penetrating the laminate, followed by stitch deformation and fracture. It is also important to be noted that the stitch thread broken at delaminated surface, so that the friction force between stitch and laminate could be ignored.

Four, using cohesive zone element and spring connector to represent the stitch thread bridging, finite element model of ENF and 4ENF test are successfully modeled. The simulation results show good agreement with the experimental one. Furthermore, using developed FE model, the feasibility study of using 4ENF test is investigated. The simulation results show that 4ENF specimen without tab can be used if the matrix tension strength is relatively high (above 40 MPa in this study), otherwise tabbed 4ENF specimen has to be used.

Generally, the main conclusions in this thesis fit up the results of long term research on stitched composites manufactured by sophisticated stitching techniques [11] and utilizing Vectran as the stitch threads material. Using this stitching technique, the delamination propagation is suppressed significantly in case of mode I [102], mode II (this study) and low velocity impact testing [102], as discussed in literature review.

In-plane properties, the most reported drawback of 3-dimensional composites, have also been investigated [103]. Some issue such as tensile strength and failure strain are even increase by 10%. Only compression strength still show a small decreasing about 16% which actually could be solved by minimizing fiber waviness and utilizing thinner stitched thread to reduce resin rich region [103]. Finally, considering the tremendous improvement on delamination behavior and minimum change on in-plane properties, stitching techniques in this study seems to be applicable for solving the delamination issue of composites laminate for the next generation of aircraft structures.

5.2 Recommendations

Recommendations for future works are listed below:

1. It is interesting to evaluate shear mode delamination behavior of higher stitch density such as 1.5 x 1.5 mm or 1 mm x 1 mm, so that a correlation between the stitch-threads density and G_{IIC} can be fully described.
2. Experimental work in 4ENF will be most valuable in order to verify the possibility of using 4ENF test without tabs.
3. It is important to check the effect of neglecting stitch thread area and its surrounding area in FE modeling because it has to be modelled with very fine mesh, thus time consuming. It worse to be investigated whether multi point constraints (in shear direction) could be applied to entire surface without affecting the results.
4. It is also interesting to investigate experimentally the matrix crack and materials degradation rule for stitched composite using open-hole tension. The results will be important to obtain more accurate results of quasi static indentation and low velocity impact test simulation.

References

- [1] Tong L, Mouritz AP, Bannister MK. 3D Fibre Reinforced Polymer Composites. Elsevier. 2002:1-241.
- [2] Mouritz AP, Bannister MK, Falzon PJ, Leong KH. Review of applications for advanced three-dimensional fibre textile composites. *Composites Part A*. 1999;30:1445-1461.
- [3] Bilisik K. Three-dimensional braiding for composites: A review. *Textile Research Journal*. 2013;83:1414–1436.
- [4] Leong KH, Ramakrishna S, Huang ZM, Bibo GA. The potential of knitting for engineering composites—a review. *Composites Part A*. 2000;31:197-220.
- [5] Mouritz AP, Leong KH, Herszberg I. A review of the effect of stitching on the in-plane mechanical properties of fibre-reinforced polymer composites. *Composites Part A*. 1997;28:979-991.
- [6] Mouritz AP, Cox BN. A mechanistic interpretation of the comparative in-plane mechanical properties of 3D woven, stitched and pinned composites. *Composites Part A: Applied Science and Manufacturing*. 2010;41(6):709-728.
- [7] Mouritz AP, Cox BN. A mechanistic approach to the properties of stitched laminates. *Composites Part A*. 2000;31(1):1-7.
- [8] Mouritz AP. Review of z-pinned composite laminates. *Composites Part A: Applied Science and Manufacturing*. 2007;38:2383–2397.
- [9] Mouritz AP. Design dilemma for Z-pinned composites structures. 27th International Congress of the Aeronautical Sciences. 2010:1-11.
- [10] Scarponi C, Perillo AM, Cutillo L, Foglio C. Advanced TTT composite materials

for aeronautical purposes: Compression after impact (CAI) behaviour. *Composites Part B: Engineering*. 2007;38(2):258-264.

[11] Yasui Y, Hori F, Amano M, Takeuchi J. Method and apparatus for production of a three-dimensional fabric. US Patent 5833802. 1998:1–12.

[12] Dransfield KA, Jain LK, Mai Y-W. On the effects of stitching in CFRPs—I. Mode I delamination toughness. *Composites Science and Technology*. 1998;58:815–827.

[13] Wood MDK, Sun X, Tong L, Katzos A, Rispler AR, Mai Y-W. The effect of stitch distribution on Mode I delamination toughness of stitched laminated composites – experimental results and FEA simulation. *Composites Science and Technology*. 2007;67:1058–1072.

[14] Solaimurugan S, Velmurugan R. Influence of in-plane fibre orientation on mode I interlaminar fracture toughness of stitched glass/polyester composites. *Composites Science and Technology*. 2008;68:1742–1752.

[15] Tan KT, Watanabe N, Sano M, Iwahori Y, Hoshi H. Interlaminar Fracture Toughness of Vectran-stitched Composites - Experimental and Computational Analysis. *Journal of Composite Materials*. 2010;44(26):3203–3229.

[16] Jain LK, Mai Y-W. Mode I Delamination Toughness of Laminated Composites with Through-Thickness Reinforcement. *Applied Composite Materials*. 1994;1:1–17.

[17] Tan KT, Watanabe N, Iwahori Y. Experimental investigation of bridging law for single stitch fibre using Interlaminar tension test. *Composite Structures*. 2010;92(6):1399-1409.

[18] Cox BN, Massabo R, Kedward K. Suppression of delaminations in curved structures by stitching. *Composites Part A*. 1996;27:1133-1138.

[19] Jain LK, Mai Y-W. Analysis of stitched laminated ENF specimens for interlaminar

- mode II fracture toughness. *International Journal of Fracture* 1994; 68:219–244.
- [20] Jain LK, Mai Y-W. Determination of mode II delamination toughness of stitched laminated composites. *Composites Science and Technology*. 1995;55:241–253.
- [21] Sankar BV, Sharma SK. Mode II delamination toughness of stitched graphite/epoxy textile composites. *Composites Science and Technology*. 1997;57:729–737.
- [22] Jain LK, Dransfield KA, Mai Y-W. On the effect of stitching in CFRPs-II. mode II delamination toughness. *Composites Science and Technology* 1998;58:829–837.
- [23] Mouritz AP, Jain LK. Further validation of the Jain and Mai models for interlaminar fracture of stitched composites. *Composites Science and Technology*. 1999;59:1653–1662.
- [24] Wood MDK, Sun X, Tong L, Luo Q, Katzos A, Rispler A. A New ENF Test Specimen for the Mode II Delamination Toughness Testing of Stitched Woven CFRP Laminates. *Journal of Composite Materials*. 2007;41(14):1743–1772.
- [25] Plain KP, Tong L. An experimental study on mode I and II fracture toughness of laminates stitched with a one-sided stitching technique. *Composites Part A: Applied Science and Manufacturing*. 2011;42(2):203–210.
- [26] Cox BN, Sridhar N. A traction law for inclined fiber tows bridging mixed-mode cracks. *Mechanics of Advanced Materials and Structures*. 2002;9:299–331.
- [27] Rys T, Sankar BV, Ifju PG. Investigation of Fracture Toughness of Laminated Stitched Composites Subjected to Mixed Mode Loading. *Journal of Reinforced Plastics and Composites*. 2010;29:422-430.
- [28] Trabelsi W, Michel L, Othomene R. Effects of Stitching on Delamination of Satin Weave Carbon-Epoxy Laminates Under Mode I, Mode II and Mixed-Mode I/II

Loadings. *Applied Composite Materials*. 2010;17(6):575-595.

[29] Yudhanto A, Watanabe N, Iwahori Y, Hoshi H. Compression properties and damage mechanisms of stitched carbon/epoxy composites. *Composites Science and Technology*. 2013;86:52–60.

[30] Stickler PB, Ramulu M. Experimental and numerical analysis of transverse stitched T-joints in bending. *Composite Structures*. 2000;50:91-100.

[31] Stickler PB, Ramulu M. Investigation of mechanical behavior of transverse stitched T-joints with PR520 resin in flexure and tension. *Composite Structures*. 2001;52:307-314.

[32] Stickler PB, Ramulu M. Parametric analyses of stitched composite T-joints by the finite element method. *Materials & Design*. 2002;23:751-758.

[33] Aymerich F, Onnis R, Priolo P. Analysis of the fracture behaviour of a stitched single-lap joint. *Composites Part A: Applied Science and Manufacturing*. 2005;36(5):603-614.

[34] Ghasemnejad H, Argentiero Y, Tez TA, Barrington PE. Impact damage response of natural stitched single lap-joint in composite structures. *Materials & Design*. 2013;51:552-560.

[35] Tong L, Jain LK, Leong D, Kelly, Herszberg I. Failure of transversely stitched RTM lap joints. *Composites Science and Technology*. 1998;58:221-227.

[36] Tong L, Steven GP. A numerical study on stresses in resin transfer moulding lap joints reinforced with transverse stitching. *Composite Structures*. 1996;36:91-100.

[37] Davies P, Sims GD, Blackman BRK, Brunner AJ, Kageyama K, Hojo M, et al. Comparison of test configurations for determination of mode II interlaminar fracture toughness results from international collaborative test programme. *Plastics, Rubber and*

Composites. 1999;28(9):432–437.

[38] Martin RH, Davidson BD. Mode II fracture toughness evaluation using four point bend, end notched flexural test. *Plastics, Rubber and Composites*. 1999;28(8):401-406.

[39] Brunner AJ, Blackman BRK, Davies P. A status report on delamination resistance testing of polymer–matrix composites. *Engineering Fracture Mechanics*. 2008;75:2779–2794.

[40] K7086 J. Testing methods for interlaminar fracture toughness of carbon fibre reinforced plastics. Japan Standard Association (in Japanese) 1993.

[41] Chen L, Ifju PG, Sankar BV. Analysis of Mode I and Mode II Tests for Composites with Translaminar Reinforcements. *Journal of Composite Materials*. 2005;39:1311–1333.

[42] Zhao L, Gong Y, Zhang J, Chen Y, Fei B. Simulation of delamination growth in multidirectional laminates under mode I and mixed mode I/II loadings using cohesive elements. *Composite Structures*. 2014;116:509-522.

[43] Bianchi F, Zhang X. A cohesive zone model for predicting delamination suppression in z-pinned laminates. *Composites Science and Technology*. 2011;71(10):1898–1907.

[44] Bianchi F, Zhang X. Predicting mode-II delamination suppression in z-pinned laminates. *Composites Science and Technology*. 2012;72(8):924-932.

[45] Zhao L, Gong Y, Qin T, Mehmood S, Zhang J. Failure prediction of out-of-plane woven composite joints using cohesive element. *Composite Structures*. 2013;106:407-416.

[46] Wang Y, Soutis C, Hajdaei A, Hogg PJ. Finite element analysis of composite

T-joints used in wind turbine blades. *Plastics, Rubber and Composites*. 2015;44(3):87-97.

[47] Soutis C, Fleck NA, Smith PA. Failure prediction technique for compression loaded carbon fibre-epoxy laminate with open holes. *Journal of Composite Materials*. 1991;25(11):1476-1498.

[48] Ahmad H, Crocombe AD, Smith PA. Physically based finite element strength prediction in notched woven laminates under quasi-static loading. *Plastics, Rubber and Composites*. 2013;42(3):93-100.

[49] Abrate S. *Impact engineering of composite structures*. Book, Springer. 2011:1-411.

[50] Tan KT, Watanabe N, Iwahori Y. Effect of stitch density and stitch thread thickness on low-velocity impact damage of stitched composites. *Composites: Part A*. 2010;41:1857–1868.

[51] Tan KT, Watanabe N, Iwahori Y. X-ray radiography and micro-computed tomography examination of damage characteristics in stitched composites subjected to impact loading. *Composites: Part B*. 2011;42:874–884.

[52] Tan KT, Watanabe N, Iwahori Y, Ishikawa T. Understanding effectiveness of stitching in suppression of impact damage: An empirical delamination reduction trend for stitched composites. *Composites: Part A*. 2012;43:823–832.

[53] Tan KT, Yoshimura A, Watanabe N, Iwahori Y, Ishikawa T. Effect of stitch density and stitch thread thickness on damage progression and failure characteristics of stitched composites under out-of-plane loading. *Composites Science and Technology*. 2013;74:194–204.

[54] Tan KT, Yoshimura A, Watanabe N, Iwahori Y, Ishikawa T. Further investigation of Delamination Reduction Trend for stitched composites. *Composites Science and*

Technology. 2015;118:141-153.

[55] Yoshimura A, Nakao T, Takeda N. Improvement of Out-of-Plane Impact Damage Resistance of CFRP Due to Through-the-Thickness Stitching. *Advanced Composite Materials*. 2009;18(2):121-134.

[56] Lopresto V, Melito V, Leone C, Caprino G. Effect of stitches on the impact behaviour of graphite/epoxy composites. *Composites Science and Technology*. 2006;66(2):206-214.

[57] Aymerich F, Priolo P. Characterization of fracture modes in stitched and unstitched cross-ply laminates subjected to low-velocity impact and compression after impact loading. *International Journal of Impact Engineering*. 2008;35(7):591-608.

[58] Aymerich F, Francesconi L. Damage Mechanisms in Thin Stitched Laminates Subjected to Low-velocity Impact. *Procedia Engineering*. 2014;88:133-140.

[59] Francesconi L, Aymerich F. Impact damage resistance of thin stitched carbon/epoxy laminates. *Journal of Physics: Conference Series*. 2015;628:012099.

[60] Aymerich F, Pani C, Priolo P. Damage response of stitched cross-ply laminates under impact loadings. *Engineering Fracture Mechanics*. 2007;74(4):500-514.

[61] Aymerich F, Dore F, Priolo P. Simulation of multiple delaminations in impacted cross-ply laminates using a finite element model based on cohesive interface elements. *Composites Science and Technology*. 2009;69(11-12):1699-1709.

[62] Bouvet C, Castanié B, Bizeul M, Barrau J-J. Low velocity impact modelling in laminate composite panels with discrete interface elements. *International Journal of Solids and Structures*. 2009;46(14-15):2809-2821.

[63] Bouvet C, Rivallant S, Barrau JJ. Low velocity impact modeling in composite laminates capturing permanent indentation. *Composites Science and Technology*.

2012;72(16):1977-1988.

[64] González EV, Maimí P, Camanho PP, Turon A, Mayugo JA. Simulation of drop-weight impact and compression after impact tests on composite laminates. *Composite Structures*. 2012;94(11):3364-3378.

[65] Hongkarnjanakul N, Bouvet C, Rivallant S. Validation of low velocity impact modelling on different stacking sequences of CFRP laminates and influence of fibre failure. *Composite Structures*. 2013;106:549-559.

[66] Hongkarnjanakul N, Rivallant S, Bouvet C, Miranda A. Permanent indentation characterization for low-velocity impact modelling using three-point bending test. *Journal of Composite Materials*. 2013;48(20):2441-2454.

[67] Rivallant S, Bouvet C, Hongkarnjanakul N. Failure analysis of CFRP laminates subjected to compression after impact: FE simulation using discrete interface elements. *Composites Part A: Applied Science and Manufacturing*. 2013;55:83-93.

[68] Zhang J, Zhang X. An efficient approach for predicting low-velocity impact force and damage in composite laminates. *Composite Structures*. 2015;130:85-94.

[69] Zhang J, Zhang X. Simulating low-velocity impact induced delamination in composites by a quasi-static load model with surface-based cohesive contact. *Composite Structures*. 2015;125:51-57.

[70] Hufenbach W, Hornig A, Gude M, Böhm R, Zahneisen F. Influence of interface waviness on delamination characteristics and correlation of through-thickness tensile failure with mode I energy release rates in carbon fibre textile composites. *Materials & Design*. 2013;50:839–845.

[71] Hysol. Hysol® EA 9309.3NA, Technical Data Sheet. Henkel Corporation; available at <http://wwwhenkelnacom/product-search-1554htm?nodeid=8797799809025>

(accessed January 2014).

[72] Carlsson LA, Gillespie JW. Mode-II interlaminar fracture of composites. In: K. Friedrich, editor. Application of fracture mechanics to composite materials. Elsevier Science Publisher. 1989:113–157.

[73] Blackman BRK, Brunner AJ, Williams JG. Mode II fracture testing of composites: a new look at an old problem. *Engineering Fracture Mechanics*. 2006;73:2443–2455.

[74] Carlsson LA, Gillespie JW, Trethewey BR. Mode II Interlaminar Fracture of Graphite/Epoxy and Graphite/PEEK. *Reinforced Plastics and Composites*. 1986;5:170–187.

[75] Reeder JR, Demarco K, Whitley KS. The use of doubler reinforcement in delamination toughness testing. *Composites Part A: Applied Science and Manufacturing*. 2004;35:1337–1344.

[76] Gill AF, Robinson P, Pinho S. Effect of variation in fibre volume fraction on modes I and II delamination behaviour of 5HS woven composites manufactured by RTM. *Composites Science and Technology*. 2009;69:2368–2375.

[77] Feret V, Ghiasi H, Hubert P. Effect of fibre volume fraction on mixed-mode fracture of a fabric carbon/epoxy composite. *Applied Composite Materials*. 2013;20:415–429.

[78] Yudhanto A, Watanabe N, Iwahori Y, Hoshi H. Effect of stitch density on tensile properties and damage mechanisms of stitched carbon/epoxy composites. *Composites: Part B* 2013;46:151–165.

[79] Mouritz AP, Cox BN. A mechanistic approach to the properties of stitched laminates. *Composites Part A: Applied Science and Manufacturing*. 2000;31:1–27.

[80] Hojo M, Matsuda S, Ochiai S, Tsujioka N, Nakanishi Y, Maekawa Z, et al. Mode II

interlaminar properties under static and fatigue loadings for CF/epoxy laminates with different fiber-surface treatment. *Advanced Composites Materials*. 2001;10(2,3):237–246.

[81] Lee SM. Mode II delamination failure mechanisms of polymer matrix composites. *Materials Science*. 1997;32:1287–1295.

[82] Fu S-Y, Yuea C-Y, Hua X, Mai Y-W. Analyses of the micromechanics of stress transfer in single- and multi-fiber pull-out tests. *Composites Science and Technology*. 2000;60(4):569–579.

[83] K7075 J. Testing methods for carbon fiber content and void content of carbon fiber reinforced plastics. Japan Standard Association (in Japanese). 1991.

[84] Pereira AB, De Morais AB, Marques AT, De Castro PT. Mode II interlaminar fracture of carbon/epoxy multidirectional laminates. *Composites Science and Technology*. 2004;64:1653-1659.

[85] Chou I, Kimpara I, Kageyama K, Ohsawa I. Mode I and mode II fracture toughness measured between differently oriented plies in graphite/epoxy composites. In: *Composite Materials: Fatigue and Fracture – 5th volume*. ASTM STP 1230 Philadelphia: American Society for Testing and Materials. 1995:132–151.

[86] Polaha JJ, Davidson BD, Hudson RC, Pieracci A. Effects of mode ratio, ply orientation and precracking on the delamination toughness of a laminated composite. *Journal of Reinforced Plastics and Composites*. 1996;15:141–173.

[87] De Morais AB. Analysis of mode II interlaminar fracture of multidirectional laminates. *Composites Part A: Applied Science and Manufacturing*. 2004;35:51–57.

[88] Mollón V, Bonhomme J, Argüelles A, Viña J. Influence of the crack plane asymmetry over GII results in carbon epoxy ENF specimens. *Composite Structures*.

2012;94:1187–1191.

[89] Resin DXE. Denatite XNR6813 Epoxy Resin, Technical Information Sheet. Nagase Chemtex Corp.

[90] T800S. Torayca-T800S, Technical Data Sheet. Toray Carbon Fibers America Inc.

[91] Iwahori Y, Nakane K, Watanabe N. DCB test simulation of stitched CFRP laminates using interlaminar tension test results. *Composites Science and Technology*. 2009;69:2315-2322.

[92] Nasution MRE, Watanabe N, Kondo A, Yudhanto A. Thermomechanical properties and stress analysis of 3-D textile composites by asymptotic expansion homogenization method. *Composites Part B: Engineering*. 2014;60:387-391.

[93] Alfano G, Crisfield MA. Finite element interface models for the delamination analysis of laminated composites: mechanical and computational issues. *International Journal for Numerical Methods in Engineering*. 2001(50):1701-1736.

[94] Krueger R. Development and Application of Benchmark Examples for Mode II Static Delamination Propagation and Fatigue Growth Predictions. NASA/CR–2011-217305 NIA Report No 2011-02. 2011.

[95] Hamitouche L, Tarfaoui M, Vautrin A. An interface debonding law subject to viscous regularization for avoiding instability: Application to the delamination problems. *Engineering Fracture Mechanics*. 2008;75(10):3084-3100.

[96] Cox BN, Massabo R, Mumm DR, Turrettini A, Kedward K. Delamination fracture in the presence of through-thickness reinforcement. *Proceeding of ICCM-11, Gold Coast, Australia*. 1997.

[97] Iwahori Y, Nakane K, Watanabe N. DCB test simulation of stitched CFRP laminates using interlaminar tension test results. *Composites Science and Technology*.

2009;69(14):2315–2322.

[98] Herwan J, Kondo A, Morooka S, Watanabe N. Effects of stitch density and stitch thread thickness on mode II delamination properties of Vectran stitched composites. *Plastics, Rubber and Composites*. 2014;43(9):300-308.

[99] Davies P, Casari P, Carlsson LA. Influence of fibre volume fraction on mode II interlaminar fracture toughness of glass/epoxy using the 4ENF specimen. *Composites Science and Technology*. 2005;65(2):295-300.

[100] Zile E, Tamuzs V. Mode II Delamination of a Unidirectional Carbon Fiber/Epoxy Composite in Four-Point Bend End-Notched Flexure Tests. *Mechanics of Composite Materials*. 2005;41(5):383-390.

[101] Wang W-X, Nakata M, Takao Y, Matsubara T. Experimental investigation on test methods for mode II interlaminar fracture testing of carbon fiber reinforced composites. *Composites Part A: Applied Science and Manufacturing*. 2009;40(9):1447-1455.

[102] Tan KT. Characterization of impact damage tolerance and performance of stitched CFRP laminate. *Doctoral Thesis*. 2011:1-206.

[103] Yudhanto A. Mechanical characteristics and damage mechanisms of stitched carbon/epoxy composites under static and fatigue loads. *Doctoral Thesis*. 2013:1-169.

[104] Aoki Y, Suemasu H, Ishikawa T. Damage propagation in CFRP laminates subjected to low velocity impact and static indentation. *Advanced Composite Materials*. 2007;16(1):45-61.

[105] Bull DJ, Spearing SM, Sinclair I. Investigation of the response to low velocity impact and quasi-static indentation loading of particle-toughened carbon-fibre composite materials. *Composites Part A: Applied Science and Manufacturing*. 2015;74:38-46.

- [106] Chuo I, Inutake T, Namba K. Correlation of damage resistance under low velocity impact and Mode II delamination resistance in CFRP laminates. *Advanced Composite Materials*. 1999;8(2):167-176.
- [107] Tan KT, Watanabe N, Iwahori Y, Ishikawa T. Effect of stitch density and stitch thread thickness on compression after impact strength and response of stitched composites. *Composites Science and Technology*. 2012;72:587–598.
- [108] Seal. Seal Texipreg - Graphite/Epoxy Prepreg. Technical Data Sheet. Seal Corp. 2016:1-3.
- [109] Hibbeler RC. *Mechanics of materials*. Pearson Education South Asia. 2011:359-403.

Appendix A. Predicting Damage in Stitched Composites under Quasi Static Indentation Test

A.1 Overview

A general design tools is definitely needed to predict damage initiation and propagation during low velocity impact loading. To understand damage mechanism of low velocity impact (LVI), quasi static indentation (QSI) test is usually used [53, 104, 105]. Both of LVI and QSI are strongly related to mode II delamination properties [106] which is the main topic of this thesis. Finite element model of quasi static indentation is developed by considering both of possible damages which are delamination and matrix crack. As an initial work, a relatively simple laminate orientation of $[90_3/0_3]_s$ is modeled and surface based cohesive element is employed to simulate the delamination. Moreover, to capture the matrix crack, Hashin's criteria is introduced to the model using user subroutine in ABAQUS package. The simulation results, such as delamination area and load-displacement curve are verified with the experimental data from literature.

A.2 Modelling Techniques

A.2.1 Finite Element Model

The experimental work on quasi static indentation (QSI) and low velocity impact (LVI) of stitched composites has been conducted by many researchers [50-56, 107]. Particularly in QSI experiment, our group member has been conducted the test [53] using 20 plies carbon fibers T800SC-24K (Toray Industries) with in-plane fiber orientation of $[+45/90/-45/0/0/+45/90/90/-45/0]_s$. This ply orientation creates a complicated failure mechanism where the delamination occurred at almost all

interlaminars. Therefore, modelling such cases will need an extraordinary computational capability (hardware) and longer computational time. In order to develop a numerical model for stitched composites under QSI test, it is better to start working from a simple case. Thus work reported by Aymerich et al. [61] which used 12 ply $[90_3/0_3]_s$ is selected in this study. The laminates are manufactured from unidirectional prepreg tapes of graphite/epoxy HS160/REM. The mechanical properties of laminae shown in Table A.1, where E_{11} , E_{22} , E_{33} are Young`s modulus in the fiber, perpendicular to fiber and thickness directions, respectively. Y_T is the matrix tensile strength, and S_{xy} , S_{yz} are matrix shear strength. The specimen size is 65 x 87.5 mm with average thickness of 2 mm. Low velocity impact tests were conducted using a drop-weight impact testing machine with hemispherical nose steel impactor of 12.5 mm diameter. The samples were simply supported on a steel plate with a 45 x 67.5 mm rectangular opening-hole.

Table A.1: Mechanical properties of lamina [108]

Elastic Modulus (GPa)		Shear Modulus (GPa)	Poisson`s Ratio	Matrix Strength (MPa)	
E_{11}	$E_{22} = E_{33}$	$G_{12} = G_{13} = G_{23}$	$\nu_{12} = \nu_{13} = \nu_{23}$	Y_T	$S_{xy} = S_{yz}$
125	7.45	3.97	0.261	30.0	80.0

The finite element model is developed using the commercial software ABAQUS package. To reduce computational time, only a quarter of specimen is modelled with symmetric boundary condition. The size of laminate model is 38.75 x 22.5 x 2 mm as shown in Figure 5.1. Solid elements (C3D8) are used with element size of 0.23 x 0.27 mm and each layer is modelled by one element in thickness direction [69]. At stitch threads region, much smaller element size is used (0.05 x 0.05 mm) and the indenter is modeled as a rigid shell.

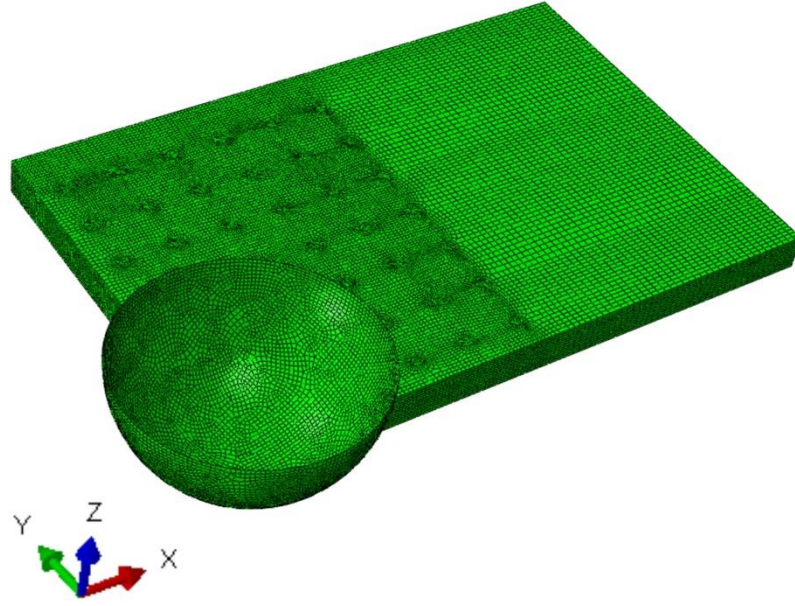


Figure A.1: Finite element model of quasi static indentation

A.2.2 Damage Modelling

Finite element model of ENF and 4ENF tests in the previous chapter considered only one type of damage which was delamination. In QSI model, initiation of matrix cracks is introduced using Hashin`s criterion as shown in equation (A.1).

$$\left\{ \frac{\sigma_{yy}}{Y_T} \right\}^2 + \left\{ \frac{\sigma_{xy}}{S_{xy}} \right\}^2 + \left\{ \frac{\sigma_{yz}}{S_{yz}} \right\}^2 \geq 1 \quad (\text{A.1})$$

This criterion is attached to the model using user subroutine called USDFLD in ABAQUS package. During damage propagation, the material degradations are considered to be 0.2 of those initial values, for E_{22} , G_{xy} , and G_{yz} , Prior to applying in quasi static indentation model, the user subroutine is verified first in a simple model of laminate 0_4 and 90_4 with open hole under tension as described in Figure A.2.

Since the compressive through thickness stress in low velocity impact is considerably high, the delamination is modeled using surface-based cohesive contact

[69]. It can incorporate friction at the same surface, to take into account the effect of compressive through thickness stress. The delamination initiation and propagation follows stress-based quadratic criterion and mixed mode energy as describe in equation 3.1-2). The cohesive parameters are listed in Table A.2.



Figure A.2: Finite element model of open-hole tension test

Table A.2: Cohesive contact parameters [69]

Stiffness (MPa/mm)		Strength (MPa)		ERR (J/mm ³)		Friction
K_I	$K_{II} = K_{III}$	σ_I^0	$\sigma_{II}^0 = \sigma_{III}^0$	G_n^c	$G_s^c = G_t^c$	Coefficient
120,000	43,000	30	80	0.52	0.97	0.6

A.3 Results and Discussions

A.3.1 Verification of User Subroutine for Matrix Crack

The red region in Figure A.3 (c) and A.4 (d) indicates the matrix crack which occurred on the simple laminate 0_4 and 90_4 of open-hole tension simulation at a certain displacement. Corresponding stress in fiber and perpendicular to fiber direction are plotted in Figure A.3 (a, b) and A.4 (a, b). It is confirmed that the matrix cracks

occurred parallel to the in-plane fiber direction. These results ensure that the user subroutine has worked properly to simulate matrix crack.

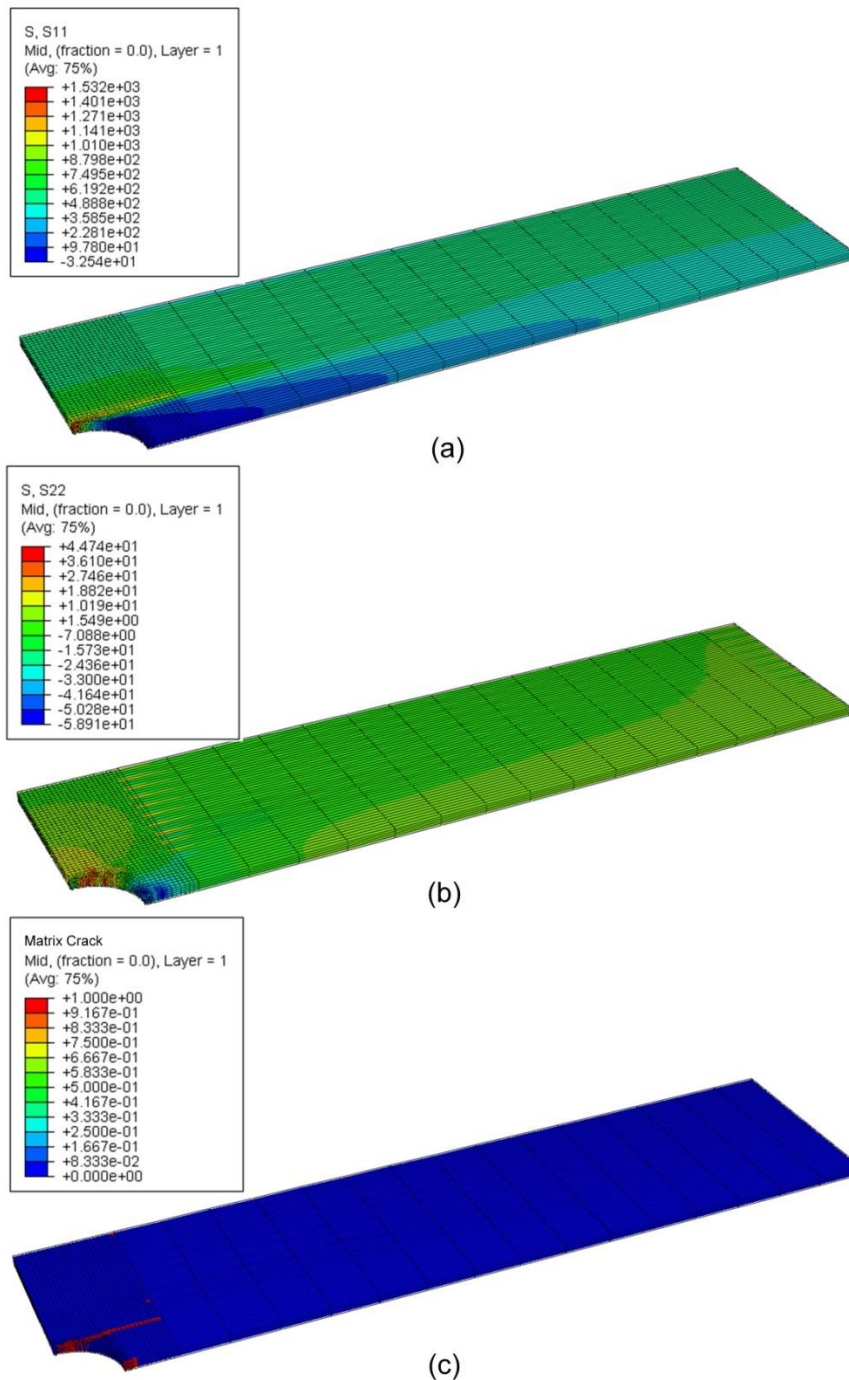


Figure A.3: Open hole simulation of unidirectional 0° laminate (a) Normal stress along fibers direction (b) Normal stress perpendicular to fibers direction (c) Matrix crack

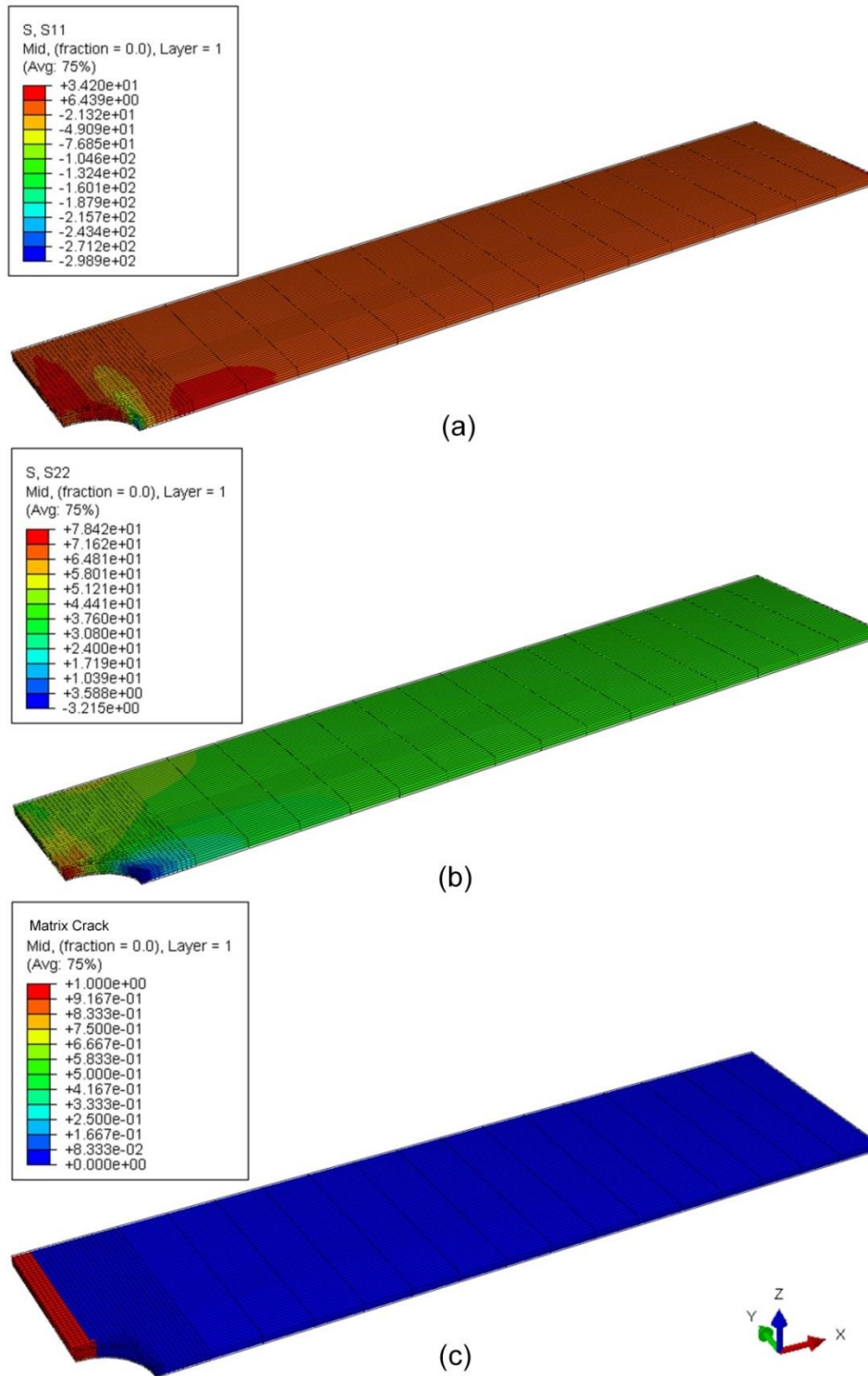


Figure A.4: Open hole simulation of unidirectional 90° laminate (a) Normal stress along fibers direction (b) Normal stress perpendicular to fibers direction (c) Matrix crack

A.3.2 Finite Element Results of Quasi Static Indentation

Deformation shape and stresses distribution from QSI simulation at 1.8 mm displacement are shown in Figure A.5-6. Related load-displacement curves and predicted delamination area are depicted in Figure A.7-8. Both of unstitched and stitched laminates show almost similar deformation shapes and load displacement curves. It can be understood that the stitching effects have not appeared yet due to the small damage and delamination, hence there are only a few active stitch threads at delaminated area (Figure A.8). The load bridged by the stitched threads seems negligible until this point of loading.

Concerning the stress distribution, particularly normal stress perpendicular to fiber direction (S_{22}), the matrix crack should be occurred at vicinity of indentation region due to the high normal compressive stress and due to high normal tensile stress at the back side of indentation surface. It is important to be noted that the tensile matrix and shear matrix strength in this study are 30 MPa and 80 MPa respectively. Furthermore, the in-plane shear stress (S_{12}) also contributes to the matrix crack (following equation A.1) even the maximum value of S_{12} (67.8 MPa) is still under the shear matrix strength.

The maximum normal stress along fibers direction (S_{11}) is very close to fiber tensile strength which is about 2950 MPa for a typical carbon fiber. Therefore, further simulation with higher loading or displacement should consider the fiber breaking in damage modeling.

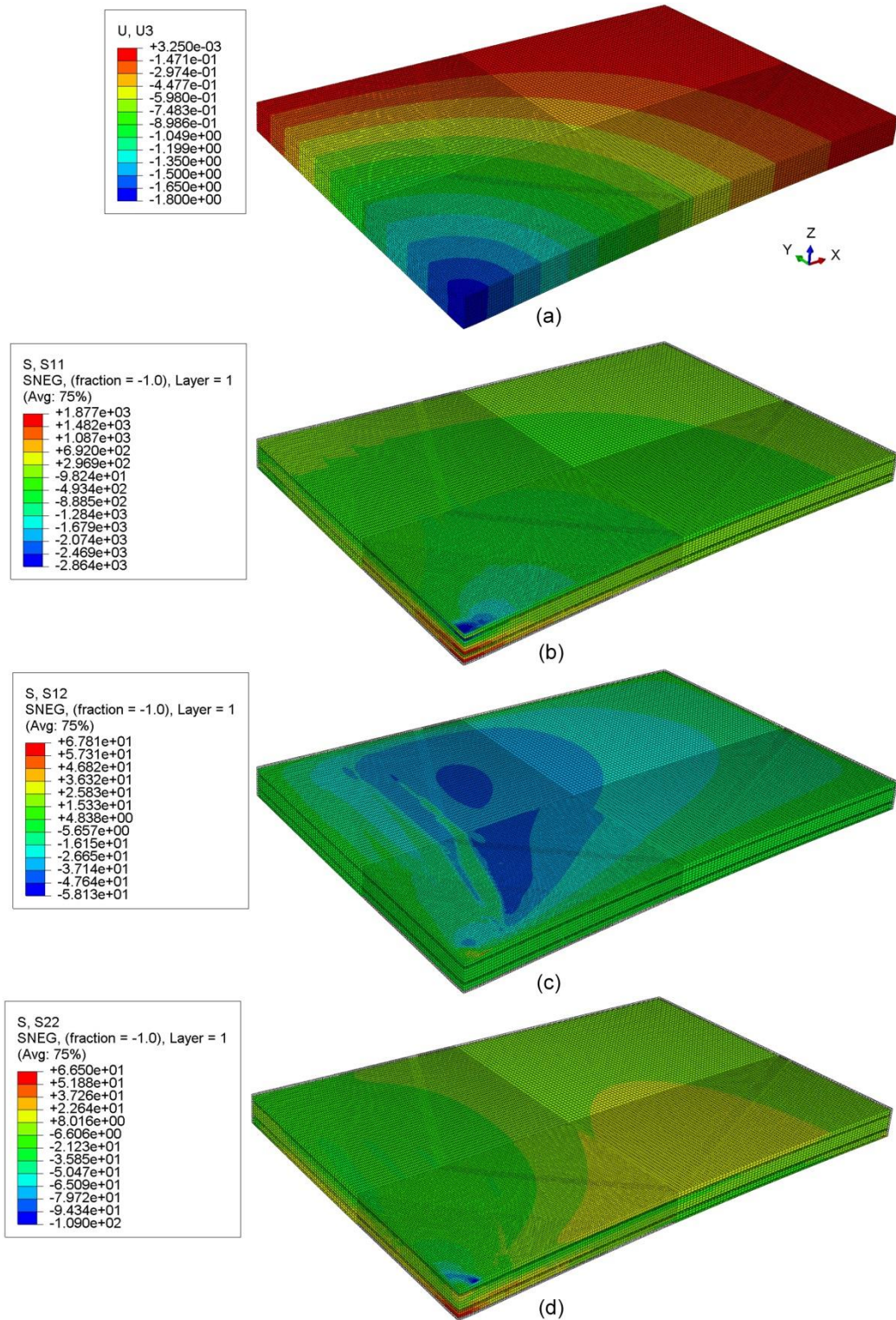


Figure A.5: QSI simulation results of unstitched laminate (a) Deformation (b) Normal stress along fibers direction (c) In-plane shear stress (d) Normal stress perpendicular to fiber direction

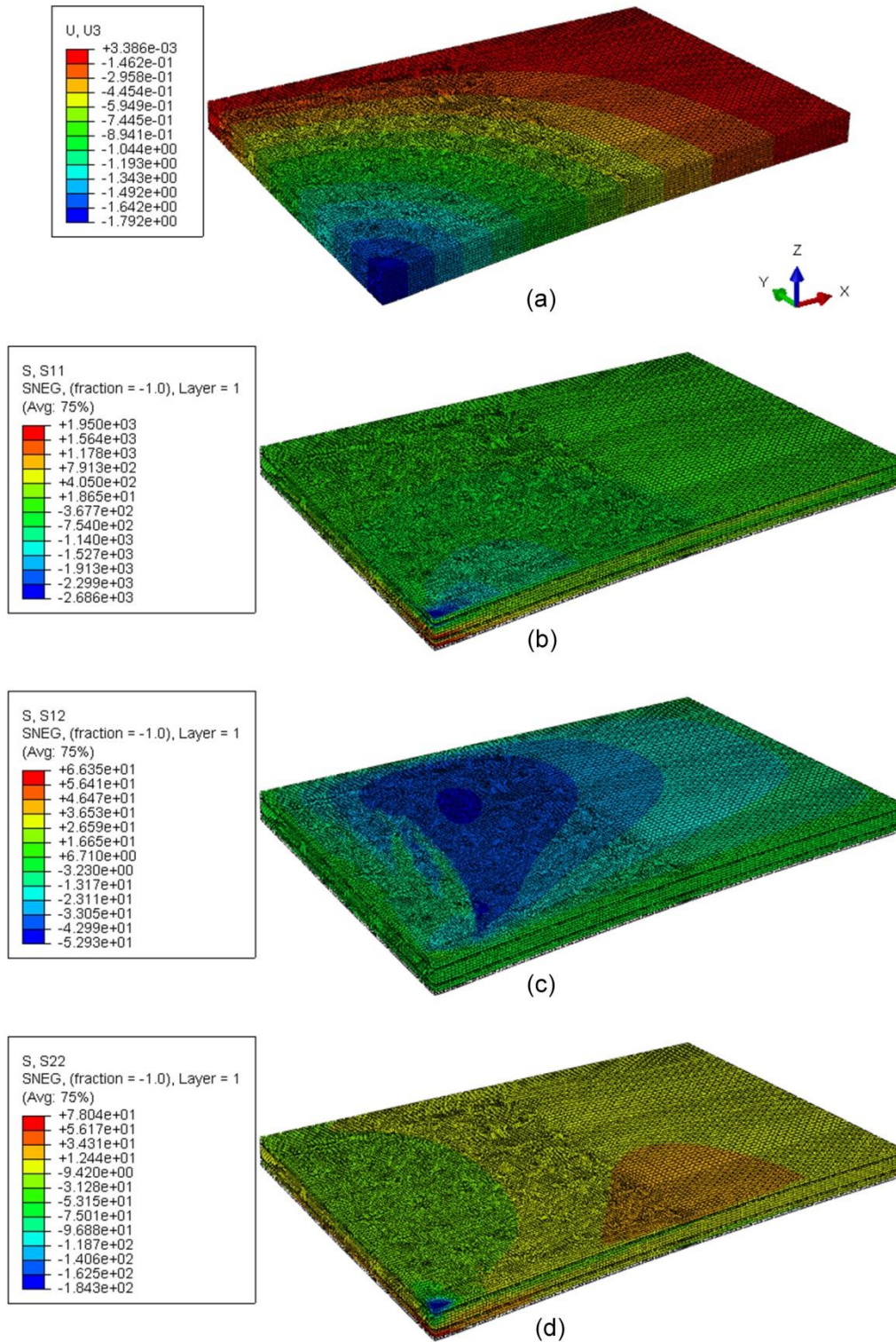


Figure A.6: QSI simulation results of stitched laminate (a) Deformation (b) Normal stress along fibers direction (c) In-plane shear stress (d) Normal stress perpendicular to fiber direction

Figure A.7 shows the load displacement curve obtained by finite element simulation. The slopes of both finite element results are reduced earlier than the experimental one. To address this issue, a parametric study of matrix tensile strength and materials degradation rules after damage initiation are investigated in next section.

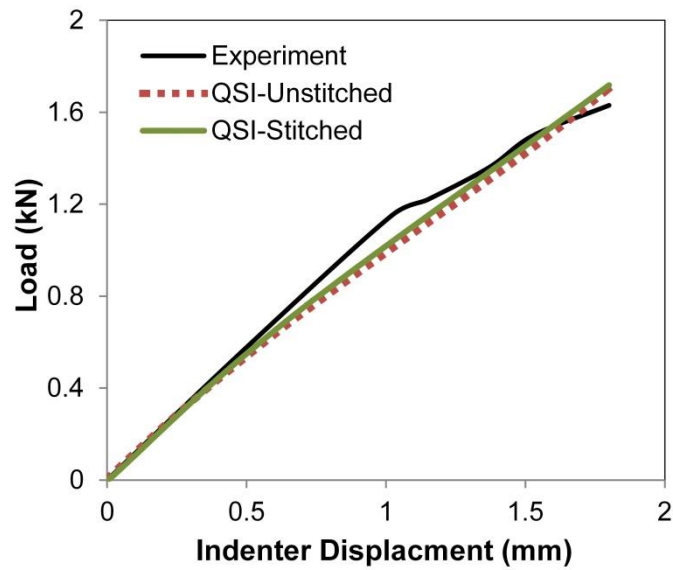


Figure A.7: Load-displacement of quasi static indentation results

Predicted delamination areas of unstitched and stitched laminate at 1.8 mm displacement are depicted in Figure A.8. The delamination area of stitched laminate is a bit smaller than unstitched one. However, predicted delamination shape and area of unstitched laminate is not similar with the experimental results [61]. Further study is needed to improve the results such as determining more accurate cohesive contact properties, materials degradation rules, etc.

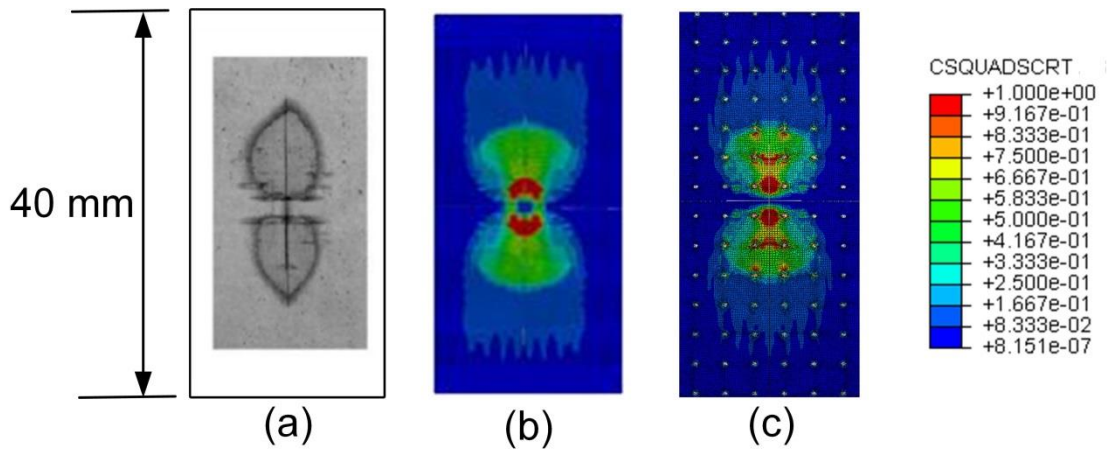


Figure A.8: Delamination area at indentation depth of 1.8 mm (a) Experiment [61], (b) FE results for unstitched laminate, (c) FE results for stitched laminate

A.3.3 Effect of damage parameters

In order to obtain a reasonable prediction of load-displacement curve of QSI test, parametric study on damage criterion are conducted, particularly on matrix tensile strength and materials degradation rules. Figure A.9 shows the effect of matrix tensile strength on the slope of load displacement curve. All of predicted curves with considering matrix crack in damage modeling show the same point where the slope start to be changed (about 0.4 mm of indenter displacement). After this point, the parametric model with 70 MPa of matrix tensile strength exhibits higher slope, even the different with other models is almost negligible. In addition, the simulation result without introducing matrix crack in the damage modeling is also plotted and show a closer slope with experimental one till a point where the slope of experimental curve changed significantly.

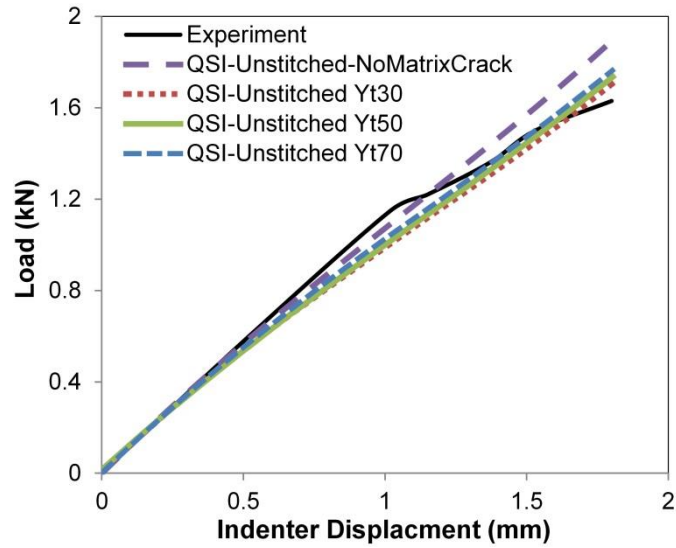


Figure A.9: Effect of matrix tensile strength on QSI results

Figure A.10 exhibits effect of materials degradation rule on load-displacement curve of QSI simulation of unstitched laminate where modulus elasticity in y-direction (E_{22}) and shear modulus (G_{xy} , G_{yz}) are remained 0.2, 0.3, 0.4, or 0.5 after matrix crack occurred at certain elements. The results show that there is a small effect of the materials degradation rules on the slope of load displacement curve. Considering the slope after damage initiation of experimental results, it is recommended to choose 0.2 or less for materials degradation rules. However, the problem remained unsolved for the point where the slope changed, because all of degradation rules show the slope changed at the same point (about 0.4 mm of indentation).

In addition to further investigation on cohesive contacts properties as mentioned above, more experimental results are also needed to understand the range of data that could be compared with finite element simulation results.

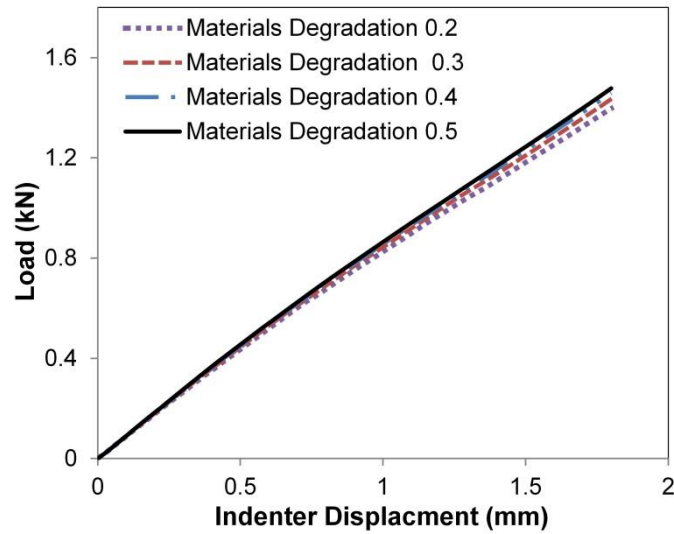


Figure A.10: Effect of materials degradation rule on QSI results

A.4 Conclusions

Finite element simulation of quasi static indentation has been conducted and the results are compared with the experimental one in term of load displacement curve, delamination shape and area. In general, the developed finite element simulation can capture a closed result to experimental one, but further studies are needed to improve the accuracy particularly on the point where the slope changed, delamination shape and area. A more accurate cohesive contact properties has to be investigated as well as another method to introduce matrix crack modeling (instead of a simple Hashin's criterion that applied in this study). It is also important to have more experimental data from any references, so that the range of experimental data can be compared with finite element simulation results. Finally, in order to quantify the delamination suppression by stitched threads, more load or displacement should be applied to indenter, hence a larger delamination area are obtained. The larger delamination area, the more active stitch threads work at delaminated area and the bridging effect could be easily evaluated.

Appendix B. User Subroutine for Matrix Crack Simulation

```

SUBROUTINE USDFLD(FIELD,STATEV,PNEWDT,DIRECT,T,CELENT,TIME,DTIME,
  1 CMNAME,ORNAME,NFIELD,NSTATV,NOEL,NPT,LAYER,KSPT,KSTEP,KINC,
  2 NDI,nshr,coord,jmac,jmtyp,matlayo,laccflg)
C
  INCLUDE 'ABA_PARAM.INC'
C
C MATERIAL AND STRENGTH PARAMETERS
  PARAMETER(YT=30.0,SXY=80,SYZ=80)
C
  CHARACTER*80 CMNAME,ORNAME
  CHARACTER*3  FLGRAY(15)
  DIMENSION FIELD(NFIELD),STATEV(NSTATV),DIRECT(3,3),T(3,3),TIME(2),
* coord(*),jmac(*),jmtyp(*)
  DIMENSION ARRAY(15),JARRAY(15)
C
C INITIALIZE FAILURE FLAGS FROM STATEV.
  EM      = STATEV(1)
C
C GET STRESSES FROM PREVIOUS INCREMENT
  CALL GETVRM('S',ARRAY,JARRAY,FLGRAY,jrcd,
$   jmac, jmtyp, matlayo, laccflg)
  S11 = ARRAY(1)
  S22 = ARRAY(2)
  S12 = ARRAY(4)
  S23 = ARRAY(6)
  CALL GETVRM('E',ARRAY,JARRAY,FLGRAY,jrcd,
$   jmac, jmtyp, matlayo, laccflg)
  E12 = ARRAY(4)
C
C MATRIX CRAKING
  IF (EM .LT. 1.D0) THEN
    EM = SQRT((S22/YT)**2+(S12/SXY)**2+(S23/SYZ)**2)
    STATEV(1) = EM
  ENDIF
C
C STATE TRANSITION DIAGRAM
C
C FV1: MATRIX COMPR/TENS FAILURE
C FV1          E1  E2  E3  NU12 NU13 NU23  G12  G13  G23
C
C (0) NO FAILURE 0 ->E1  E2  E3  NU12 NU13 NU23  G12  G13  G23
C (1) MATRIX FAILED 1->
C           E1 0.2*E2  0.2*E3  0  0  0  0.2*G12 0.2*G13 0.2*G23
C
C UPDATE FIELD VARIABLES
C
  FIELD(1) = 0.D0
  IF (EM .GT. 1.D0) FIELD(1) = 1.D0
C
  RETURN
  END

```

Appendix C. Derivation of Equation 2.2

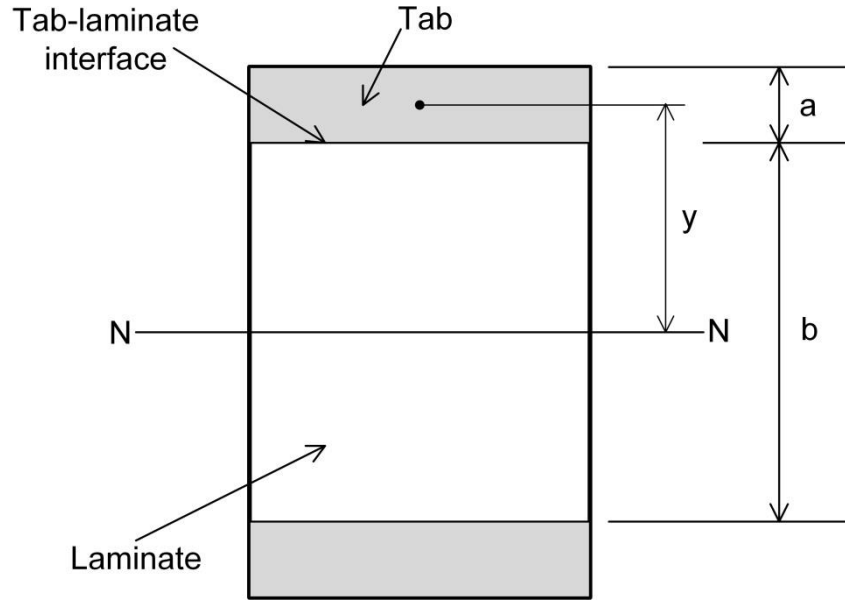


Figure B.1: Cross sectional area of tabbed laminate

The shear stress at tab-laminate interface (τ_{int}) can be calculated by the following equation [109]:

$$\tau_{int} = \frac{VQ}{Iw} \quad (B.2)$$

where V is the internal shear force obtained from equation of equilibrium. I is moment inertia of entire cross-sectional area. Meanwhile w is width of the cross-sectional area, and Q can be calculated from $y A'$ (y is the distance from neutral axis to centroid of tab, and A' is tab cross-sectional area).

Using the symbol in Figure B.1,

$$\tau_{int} = \frac{V[(b/2 + a/2)wa]}{Iw} = \frac{V[a(a+b)]}{2I} \quad (B.3)$$

And shear stress at the middle layer (delamination surface) can also be calculated as follow

$$\tau_{mid} = \frac{V[(b/2+a)w(b/2+a)]}{Iw} = \frac{V(a+b/2)^2}{2I} \quad (\text{B.4})$$

Hence, the ratio of shear stress at tab-laminate interface to shear stress at middle layer can be calculated as:

$$\frac{\tau_{int}}{\tau_{mid}} = \frac{a(a+b)}{(a+b/2)^2} \quad (\text{B.5})$$

To avoid tab de-bonding, it is suggested to consider the ratio in equation (B.5) to be equal to 0.5. Then appropriate tab thickness can be calculated for any laminate thickness.

Acknowledgements

All praise belongs to Allah, Lord of the worlds, the most compassionate and merciful. This dissertation has been completed with the support and encouragement of many people. I would like to express deepest gratitude to my advisor, Prof. Naoyuki Watanabe for his excellent supervision, invaluable supports and useful advice during my PhD research at Tokyo Metropolitan University (TMU). My sincerely thank to Tokyo Metropolitan Government for the generous funding and scholarship under the project of Asian Network of Major Cities 21 (ANMC-21) and Asian Human Resources Fund program. My heartfelt thank goes to Dr. Atsuhiko Kondo (e-Xtream Engineering), the visiting researcher in our laboratory, for his kindness and advice. His constructive comments and suggestion throughout the experimental and numerical work have contributed to the success of this research. I am deeply indebted to Dr. Satoshi Morooka (TMU) and Dr. Hikaru Hoshi (JAXA), who help me a lot to solve many technical problems during the experiment. I would like to acknowledge Prof. Masahito Asai and Prof. Ayumu Inasawa for their relentless support and assistance in the TMU-TMG-JAXA joint project. I would like to extend my gratitude to PhD thesis committee members: Prof. Hiroshi Suemasu (Sophia University), Prof. Koichi Kitazono (TMU), and Prof. Satoshi Kobayashi (TMU), for their review, corrections and comments. My sincere thanks to Ms. Yamada and Ms. Sasaki (International Center TMU) who help and support me and my family since the first day we came to Japan. I greatly appreciate the help and cooperation from former and current members of Watanabe Laboratory, especially Dr. Arief Yudhanto, the late Dr. Agus Trilaksono, Dr. Muhammad Ridlo, Mr. Worawat Parasil, Mr. Prabij Joshi, Mr. Saharat Chantanumataporn, my tutor Mr. Tabuchi Yoshiaki (Kobe Steel), Mr. Yasuhito Mikami, Mr. Norimasa Goto (Hino Motors), Mr. Takuya Yoshida, Mr. Naoto Yamada, Ms. Tomoko Inoue, et al. Many thanks to my friends (Mr. Mohd Fitri, Mr. Bakhtiar Yusuf, Mr. Azhar Aulia Saputra, Ms. Nurjanah, Ms. Ressa Octavianty, et al.) for their kindness. Finally, an honorable mention goes to my family members. I would like to sincerely thank my wife Rifka Juwita for the patience, continuous support, love and prayer, and our children (Rafi, Fitri, Azka, and Zaki) for their encouragement. I am forever indebted to my mother Marianis and my father Rusli (1942-2013) for their unconditional love and endless prayer.